Ultrasonic Field Modeling of Transient Wave Propagation in Homogenous and Non-Homogenous Fluid Media Using Distributed Point Source Method (DPSM)

A Thesis report

Submitted in the partial fulfillment of requirements for the award of the degree of

Master of Engineering
in
CAD/CAM & ROBOTICS

Submitted by

RAGHU RAM TIRUKKAVALLURI

Roll no.**80681016**

Under the guidance of

Dr. ABHIJIT MUKHERJEE
Director
Thapar University, Patiala

Mr. SANDEEP SHARMA
Sr. Lecturer, MED
Thapar University, Patiala

Department of Mechanical Engineering
THAPAR UNIVERSITY
PATIALA (PUNJAB)-147004

JUNE-2008

Certificate

This is to certify that the work which is presented in this thesis report entitled, "**Ultrasonic Field Modeling of Transient Wave Propagation in Homogenous and Non-Homogenous Fluid Media Using Distributed Point Source Method (DPSM)** " being submitted by **Raghu Ram.Tirukkavalluri** in partial fulfillment of requirements for the award of degree of Master of Engineering in CAD/CAM & ROBOTICS, at Mechanical Engineering Department, Thapar University, Patiala, is an authentic record of the initial work carried out by him under the supervision of **Dr. Abhijit Mukherjee , Director,** Thapar University, Patiala and **Mr. Sandeep Sharma,** Sr. Lecturer, Mechanical Engineering Department, Thapar University, Patiala .The matter embodied in this report has not been submitted in part or full to any other university or institute for the award of any degree.

(Dr. Abhijit Mukherjee)
Director
Thapar University, Patiala

(Mr. Sandeep Sharma)
Sr. Lecturer, MED
Thapar University, Patiala

(Dr.S.K.Mohapatra)
Professor & Head, MED
Thapar University,
Patiala.

(Dr.R.K.Sharma)
Dean, Academic Affairs
Thapar University,
Patiala.

Acknowledgement

I take this opportunity to express my sincere gratitude to **Dr. Abhijit Mukherjee, Director**, Thapar University for giving me the opportunity of doing my thesis work under his guidance. I am also thankful to him for his constant supervision and valuable suggestions.

It is my proud privilege to express regards and sincere gratitude to **Mr.Sandeep Sharma, Sr. Lecturer,** Mechanical Engineering Department, Thapar University, Patiala, for his patient listening of my ideas and also suggesting new ways for implementing my ideas by his expert guidance through out my work.

I am also thankful to **Prashant Bhise, Reasearch Student, IIT Bombay,** for sharing his conceptual ideas and guiding me by giving his helping hand in successful completion of my thesis work.

I would like to extend my thanks to **Mrs.Shruti Sharma, Sr. Lecturer, Civil Engineering Department,** Thapar University, Patiala, for her guidance and providing necessary information and facilities for the successful completion of my thesis.

I am also thankful to **Dr.S.K.Mohapatra, Head Mechanical Engineering Department,** Thapar University, Patiala, for the motivation and inspiration that triggered me for my thesis work.

I also take this opportunity to thank to the entire faculty and staff of **Mechanical Engineering Deparment,** Thapar University, Patiala, for their help, inspiration and moral support, which went a long way in successfully completion of this report.

Tirukkavalluri.Raghu Ram

(80681016)

ABSTRACT

In the field of nondestructive evaluation (NDE), the newly developed distributed point source method (DPSM) is gradually gaining popularity. DPSM is a semi-analytical technique used to calculate the ultrasonic fields (pressure, velocity and displacement fields) generated by ultrasonic transducers of finite dimension immersed in homogeneous or non-homogeneous media. In this report the technique is extended to model the propagation of transient wave and its pressure tomo-grams generated both in homogeneous fluid and non-homogeneous fluid having single interface.

Tone burst signal is used as input signal at one end of fluid and reflected as well as transmitted pulse is observed at various points. In the first case DPSM model for homogeneous fluids is developed and results are validated for closed form solutions. In the second case, interface of two fluids is kept perpendicular to wave propagation direction and wave propagation is studied at various points. In both cases, Fast Fourier transformation (FFT) is used convert time domain signal into frequency domain and inverse FFT is used to again transform results in time domain.

Numerical results obtained from DPSM model are compared with experimental results taken from the experimental setup on different fluids and the time-histories are found to be matching with reasonable accuracy.

Keywords: DPSM, FFT, Tomo-grams, Non-Homogeneous fluid, Wave Propagations, Transducer, Interface

CONTENTS

CHAPTER 7 **Experimental Validation**

List of Figures

CHAPTER 1

INTRODUCTION

1.1 NDT AND ITS METHODS

Non Destructive Testing:

The field of Nondestructive testing (NDT) is a very broad, interdisciplinary field that plays a critical role in assuring that structural components and systems perform their function in a reliable and cost effective fashion. The term is generally applied to investigations of material integrity. These tests are performed in a manner that does not affect the future usefulness of the object or material. Because it allows inspection without interfering with a product's final use, NDT provides an excellent balance between quality control and cost-effectiveness.

Non Destructive Evaluation: Nondestructive evaluation (NDE) is a term that is often used interchangeably with NDT. However, technically, NDE is used to describe measurements that are more quantitative in nature. For example, a NDE method would not only locate a defect, but it would also be used to measure something about that defect such as its size, shape, and orientation. NDE may be used to determine material properties such as fracture toughness, formability, and other physical characteristics.

NDT or NDE methods: Although a number of different NDT methods have been developed, but following methods are most commonly used.

- **Visual and Optical Testing-**Visual inspection involves using an inspector's eyes to look for defects. The inspector may also use special tools such as magnifying glasses or mirrors gain access and more closely inspect the subject area.

- **Penetrant Testing-** Test specimens are coated with visible or fluorescent dye solution. Excess dye is then wiped out from the surface, and a developer is applied. The developer acts as blotter, drawing trapped penetrant out of

imperfections open to the surface. With visible dyes, vivid colour contrasts between the penetrant and developer make “bleedout" easy to see.

- **Magnetic Particle Testing (MT)** – In this method a magnetic field in a ferromagnetic material is induced and then dusting the surface with iron particles (either dry or suspended in liquid) is done. Surface and near-surface imperfections distort the magnetic field and concentrate iron particles near imperfections, previewing a visual indication of the flaw.

- **Electromagnetic Testing (ET) or Eddy Current Testing-** Eddy currents are generated in a conductive material by an induced alternating magnetic field and they flow in circles at just below the surface of the material. Interruptions in the flow of eddy currents, caused by imperfections, dimensional changes, or changes in the materials conductive and permeability properties, can be detected with the proper equipment.

- **Radiography (RT) -** Radiography involves the use of penetrating gamma or X-radiation to examine parts and products for imperfections. An X-ray generator or radioactive isotope is used as a source of radiation. The resulting shadowgraph shows the dimensional features of the part. Possible imperfections are indicated as density changes on the film in the same manner as medical X-ray shows broken bones.
- **Ultrasonic Testing (UT) -** ultrasonic testing use transmission of high-frequency sound waves into a material to detect imperfections or to locate changes in material properties. The most commonly used ultrasonic testing technique is pulse echo, wherein sound is introduced into a test object and reflections (echoes) are returned to a receiver from internal imperfections or from the part's geometrical surfaces.

- **Acoustic Emission Testing (AE) -** when a solid material is stressed, imperfections within the material emit short bursts of acoustic energy called "emissions." as in ultrasonic testing; acoustic emissions can be detected by special receivers. Emission sources can be evaluated through the study of their intensity, rate, and location.

- **Leak Testing (LT) -** Several techniques are used to detect and locate leaks in pressure containment parts, pressure vessels, and structures. Leaks can be detected by using electronic listening devices, pressure gauge measurements, liquid and gas Penetrant techniques, and/or a simple soap-bubble test.

Wave propagation provides an efficient means of characterizing defects in structures. For this purpose it is necessary to analyze scattering of waves by such defects. The sudden occurrence of small flaws initiated from damage sites in structural solids generates elastic waves that carry important information on the nature of damage .so next section describes about it.

1.2 BASIC CONCEPTS OF WAVE PROPAGATION

1.2.1 Basic Theory:

Sound Waves*:* - Sound waves are simply organized mechanical vibrations traveling through a medium, which may be a solid, a liquid, or a gas. These waves will travel through a given medium at a specific speed or velocity, in a predictable direction, and when they encounter a boundary with a different medium they will be reflected or transmitted according to simple rules. This is the principle of physics that underlies ultrasonic flaw detection.

- ***Frequency: -*** All sound waves oscillate at a specific frequency, or number of vibrations or cycles per second, which we experience as pitch in the familiar range of audible sound. Human hearing extends to a maximum frequency of about 20,000 cycles per second (20 KHz), while the majority of ultrasonic flaw detection applications utilize frequencies between 500 KHz to 10 MHz. At frequencies in the Megahertz range, sound energy does not travel efficiently through air or other gasses, but it travels freely through most liquids and common engineering materials.

- ***Wave Speed****:* - The speed of a sound wave varies depending on the medium through which it is traveling, affected by the medium's density and elastic properties. Different types of sound waves will travel at different velocities.

- ***Wavelength of a Wave**:* - Wavelength is related to frequency and velocity by the simple equation Wavelength (λ) =velocity (*V*)/frequency (*f*). In ultrasonic flaw detection, the generally accepted lower limit of detection for a small flaw is one-half wavelength, and anything smaller than that will be invisible. In ultrasonic thickness gauging, the theoretical minimum measurable thickness is one wavelength.

- ***Acoustic impedance:*** Sound travels through materials under the influence of sound pressure. Because molecules or atoms of a solid are bound elastically to one another, the excess pressure results in a wave propagating through the solid. The **Acoustic impedance** (**Z**) of a material is defined as the product of its density (ρ) and acoustic velocity (*V*). $Z = \rho V$

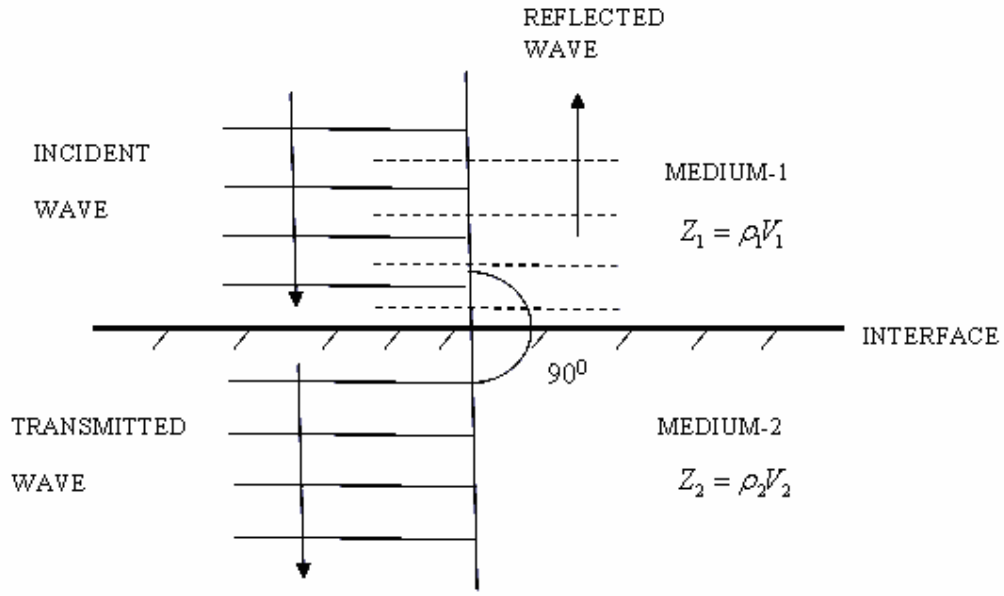

Figure 1.1: Reflection and Transmission of sound wave at normal incidence

$$\text{Reflection coefficient, } R = \left[\frac{Z_2 - Z_1}{Z_2 + Z_1}\right] = \frac{\rho_2 V_2 - \rho_1 V_1}{\rho_2 V_2 + \rho_1 V}$$

$$\text{Transmission coefficient, } T = \frac{2Z_2}{Z_2 + Z_1} = \frac{2\rho_2 V_2}{\rho_2 V_2 + \rho_1 V_1}$$

1.2.2 Modes of Wave Propagation:

The ultrasonic waves propagate in a number of ways in a medium. On the basis of the mode of particle displacement, these waves can be classified as:

a) Longitudinal or Compressional waves(L-waves)

b) Transverse or Shear waves (S-waves)

c) Surface or Rayleigh waves

d) Lamb or Plate waves

- **Longitudinal or Compressional waves**:

In longitudinal waves, the oscillations occur in the longitudinal direction or the direction of wave propagation. Since compressional and dilatational forces are active in these waves, they are also called pressure or compressional waves. Compression waves can be generated in liquids, as well as solids because the energy travels through the atomic structure by a series of comparison and expansion (rarefaction) movements.

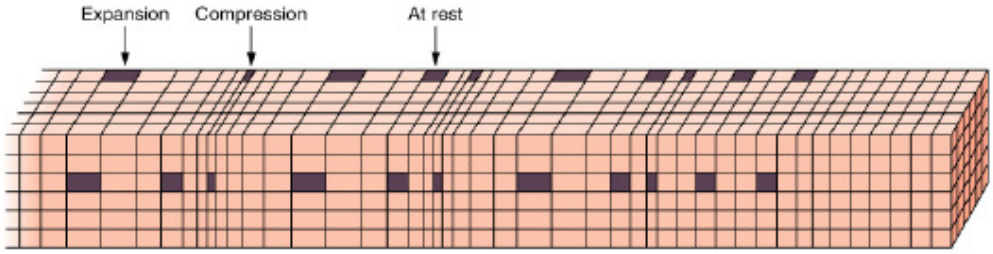

Figure 1.2: Propagation of Longitudinal waves

- **Transverse or Shear waves:**

In the transverse or shear wave, the particles oscillate at a right angle or transverse to the direction of propagation.

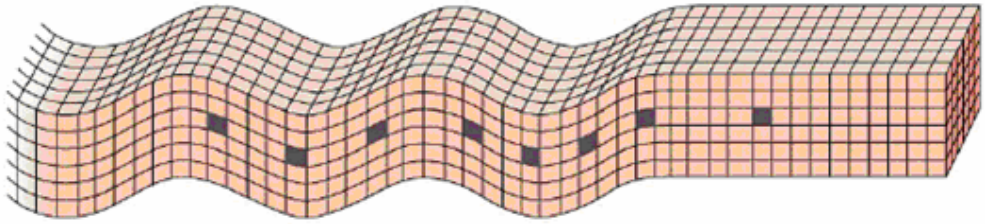

Figure1.3: propagation of Transverse or Shear waves

Shear waves require an acoustically solid material for effective propagation, and therefore, are not effectively propagated in materials such as liquids or gasses. Shear waves are relatively weak when compared to longitudinal waves.

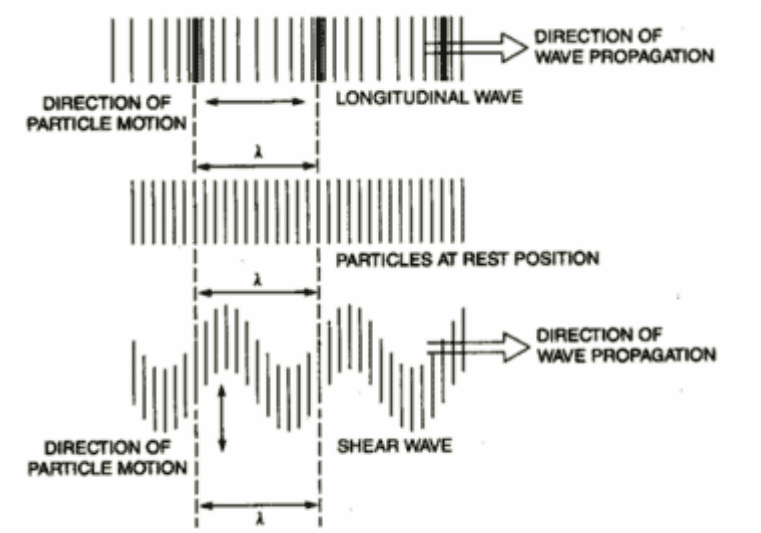

Figure1.4: Particle Movement Showing the Propagation of Longitudinal and Shear Waves.

- **Surface (or Rayleigh) waves:**

Surface (or Rayleigh) waves travel the surface of a relatively thick solid material penetrating to a depth of one wavelength. The particle movement has an elliptical orbit as shown in the image and animation below. Rayleigh waves are useful because they are very sensitive to surface defects and they follow the surface around curves. Because of this, Rayleigh waves can be used to inspect areas that other waves might have difficulty reaching.

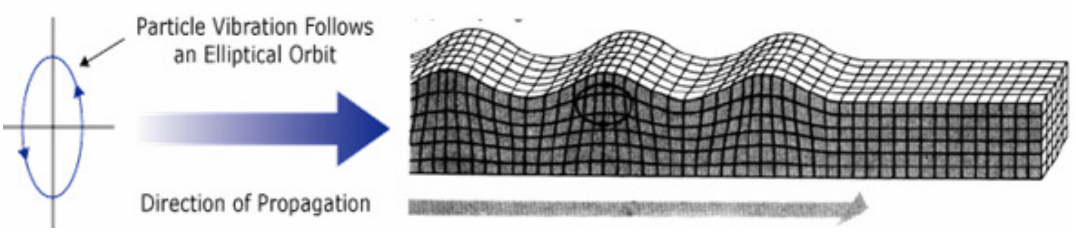

Figure 1.5: Propagation of Surface or Rayleigh Waves

- **Lamb waves or plate waves:**

Plate waves can be propagated only in very thin metals. Lamb waves are the most commonly used plate waves in NDT. Lamb waves are complex vibrational waves that travel through the entire thickness of a material. Propagation of lamb waves depends on the density and the elastic material properties of a component. They are also influenced a great deal by the test frequency and material thickness.

With lamb waves, a number of modes of particle vibration are possible, but the two most common are symmetrical and asymmetrical. The complex motion of the particles is similar to the elliptical orbits for surface waves. Symmetrical lamb waves move in a symmetrical fashion about the median plane of the plate. This is sometimes called the extensional mode because the wave is "stretching and compressing" the plate in the wave motion direction. Wave motion in the symmetrical mode is most efficiently produced when the exciting force is parallel to the plate. The asymmetrical lamb wave mode is often called the "flexural mode" because a large portion of the motion moves in a normal direction to the plate, and a little motion occurs in the direction parallel to the plate. In this mode, the body of the plate bends as the two surfaces move in the same direction.

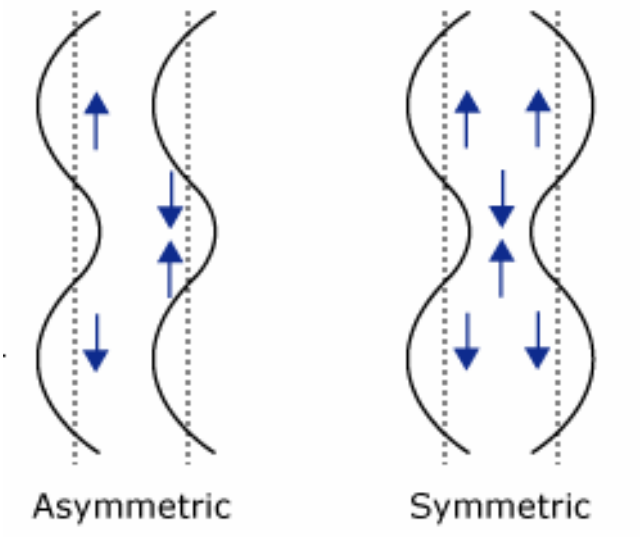

Figure 1.6: Lamb Waves Propagation (a) Symmetrical (Dilatational) and (b) Asymmetrical (Bending) waves

1.2.3 Mechanics of Wave propagation

Equilibrium Equations:

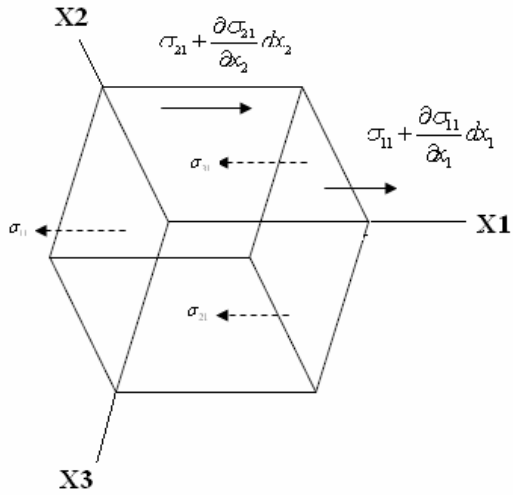

Figure1.7: Forces acting in the x_1 –direction on an elemental volume

If a body is in equilibrium, then the resultant force and moment on that body must be equal to zero. We have two equilibrium equations:

Force Equilibrium Equation: $$\frac{\partial \sigma_{ji}}{\partial x_j} + f_i = \sigma_{ji,j} + f_i = 0 \qquad (1.1)$$

Moment Equilibrium Equation: $$\sigma_{ij} = \sigma_{ji} \qquad (1.2)$$

The stress strain relation for isotropic material is given by **Green** as:

$$\sigma_{ij} = \lambda\, \delta_{ij}\, \varepsilon_{kk} + 2\,\mu\, \varepsilon_{ij} \qquad (1.3)$$

Where $\lambda = \frac{\nu}{(1-2\nu)(1+\mu)} E$, $\mu = \frac{E}{2(1+\nu)}$ are Lame's first and second constants

$$\varepsilon_{ij} = \sigma_{ii} \qquad (1.4)$$

Putting the above value of stress strain relationship 1.3 in equilibrium equation 1.1 we get: - $$(\lambda + \mu)\underline{\nabla}(\underline{\nabla}.u) + \mu\nabla^2 u + f = 0 \qquad (1.5)$$

This is the **Navier's Equation**. One dimensional problem can be easily solved by Navier's equation where only one component of the problem is nonzero, and this nonzero displacement component is a function of only one variable. But the displacement field in the half space material has two components of displacement, u_1 and u_2, and both of them will be functions of x_1 and x_2 in general. Thus it is very difficult to solve two and three dimensional problems directly from the Navier's equation. Thus ***Stokes- Helmholtz*** decomposition of the displacement field transforms the Navier's governing equation of motion into simple wave equation below.

Wave equations for a two dimensional case obtained by **Stokes-Helmholtz decomposition** are given by

$$\nabla^2\phi - \frac{\rho}{(\lambda+2\mu)}\ddot{\phi} = \nabla^2\phi - \frac{1}{c_P^2}\ddot{\phi} = 0 \qquad (1.6)$$

$$\nabla^2 A - \frac{\rho}{\mu}\ddot{A} = \nabla^2 A - \frac{1}{c_s^2}\ddot{A} = 0 \qquad (1.7)$$

These equations have solutions in the following form:

$$\phi(x,t) = \phi(n.x - c_p t) \qquad (1.8)$$

$$A(x,t) = A(n.x - c_s t) \qquad (1.9)$$

These equations represent two waves propagating in the n direction with the velocity of c_p and c_s, respectively. Note that n is the unit vector in any direction.

When A = 0 and φ = nonzero, then from the above solutions one gets

$$u = \underline{\nabla}\phi = n\phi'(n.x - c_p t) \qquad (1.10)$$

When A is not equal to 0 and ϕ is 0, then from the above solutions one gets

$$u = \underline{\nabla} \times A = \underline{\nabla} \times A(n.x - c_s t) \qquad (1.11)$$

Three components of displacement in the Cartesian coordinate system can be written from Equation 1.11:

$$\begin{aligned} u_1 &= n_2 A_3'(n.x - c_s t) - n_3 A_2'(n.x - c_s t) \\ u_2 &= n_3 A_1'(n.x - c_s t) - n_1 A_3'(n.x - c_s t) \\ u_3 &= n_1 A_2'(n.x - c_s t) - n_2 A_1'(n.x - c_s t) \end{aligned} \qquad (1.12)$$

Clearly the dot product between n and u (given in Equation 1.12) is zero; hence, the direction of the displacement vector us is perpendicular to the wave propagation direction n. Displacement fields given in Equation 1.10 and Equation 1.11 correspond to **P- and S-waves**, respectively.

- **P- and S-Waves**

Elastic waves in an infinite elastic solid can propagate in two different modes: P-wave mode and S-wave mode. When an elastic wave propagates as the P-wave, then only normal stresses (compressional or dilatational) are generated in the solid and the wave propagation speed is $c_p = \sqrt{\frac{\lambda + 2\mu}{\rho}}$. When the elastic wave propagates as the S-wave, then only shear stresses are generated in the solid and the propagation speed is $c_s = \sqrt{\frac{\mu}{\rho}}$.Wave potentials for these two types of waves, propagating in a three-dimensional space in direction n, are given by Equations 1.8 &1.9. If the problem is simplified to an in-plane problem where the waves propagate in one plane (say $x_1 x_2 - plane$), then the wave potentials, ϕ andψ, for these two types of waves can be written in the following form:

$$\begin{aligned} \phi(x,t) &= \phi(n.x - c_p t) = \phi(n_1 x_1 + n_2 x_2 - c_p t) = \phi(x_1 \cos\theta + x_2 \sin\theta - c_p t) \\ \psi(x,t) &= \psi(n.x - c_s t) = \psi(n_1 x_1 + n_2 x_2 - c_s t) = \psi(x_1 \cos\theta + x_2 \sin\theta - c_s t) \end{aligned} \qquad (1.13)$$

Equation 1.13 represents waves propagating in direction n in the $x_1 x_2$- plane. Note that in any plane normal to the wave propagation direction n the displacement and stress components are identical.

1.3 ULTRASONIC TESTING:

1.3.1 Basic Principle of Ultrasonic Testing:

Ultrasonic testing (UT) uses high frequency sound energy to conduct examinations and make measurements. A typical UT inspection system consists of several functional units, such as the pulser/receiver, transducer, and display devices. A pulser/receiver is an electronic device that can produce high voltage electrical pulses. Driven by the pulser, the transducer generates high frequency ultrasonic energy. The sound energy is introduced and propagates through the materials in the form of waves. When there is a discontinuity (such as a crack) in the wave path, part of the energy will be reflected back from the flaw surface. The reflected wave signal is transformed into an electrical signal by the transducer and is displayed on a screen.

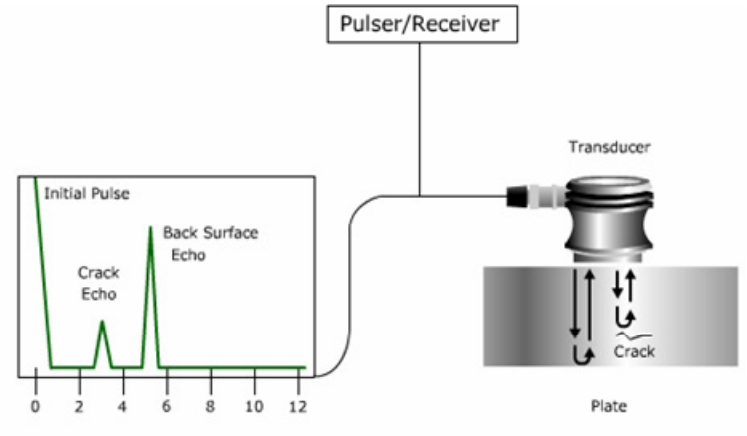

Figure 1.8: General ultrasonic Inspection Principle (pulse echo method)

1.3.2 Methods of Ultrasonic Testing:

1. Pulse echo method
2. Through transmission method
3. Two transducer method

Pulse Echo Method:

In the pulse-echo method, a piezoelectric transducer with its longitudinal axis located perpendicular to and mounted on or near the surface of the test material is used to transmit and receive ultrasonic energy. The ultrasonic waves are reflected by the opposite face of the material or by discontinuities, layers, voids, or inclusions in the material, and received by the same transducer where the reflected energy is converted into an electrical signal. The electrical signal is computer processed for display on a

video monitor or TV screen. The display can show the relative thickness of the material, depth into the material where flaws are located, and (with proper scanning hardware and software), where the flaws are located in the X-Y plane.

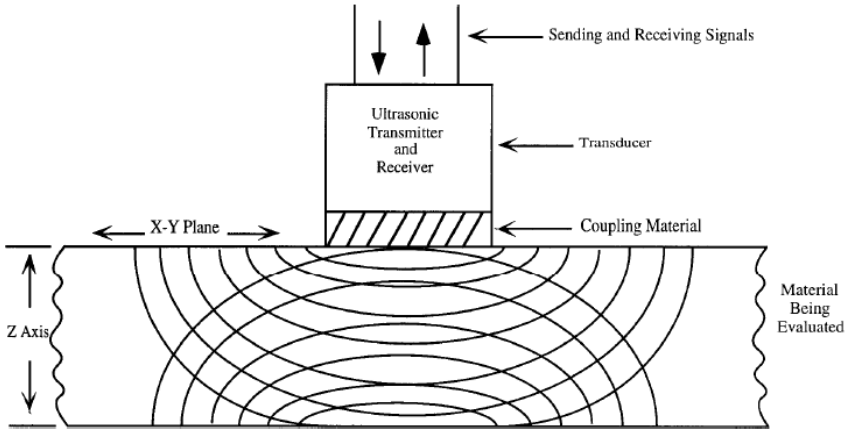

Figure 1.9: Principle of pulse echo method of inspection

Through Transmission Method:

In the through-transmission method, an ultrasonic transmitter is used on one side of the material while a detector is placed on the opposite side. One unit acts as transmitter and the other unit as receiver. The beam from the transmitter T travels through the material to its opposite surface where the receiving transducer R is placed. Scanning of the material using this method will result in the location of defects, flaws, and inclusions in the X-Y plane.

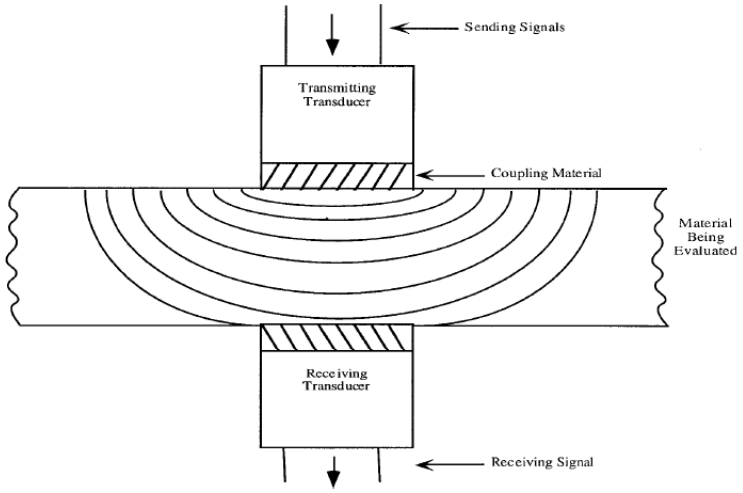

Figure 1.10: Principle of through transmission of ultrasonic testing

Two Transducer Method

The pulse echo method can be used with either single or double crystal unit in single transducer unit the probe acts as both transmitter and receiver .In two transducer arrangement ,one transmits and other receives the ultrasonic waves .These are placed on same side of specimen .pulse wave is send in to the specimen by the transducer T. And the echoes reflected from the back surface or any defect .Are received by the transducer R and displayed on the flaw detector screen. For specific applications like wall thickness measurement special type of transducers in which the transmitting and the receiving crystals are housed in a single unit are also used .These transducers are popularly known as 'twin' or T-R probes .

1.4 EXCITATION SIGNAL ANALYSIS

Fourier analysis:

Although the inputs and outputs (excitations and responses) are functions of time, they can also be represented as functions of frequency, through Fourier transformation. The resulting *Fourier spectrum* of a signal can be interpreted as the set of frequency components that the original signal contains. One immediate advantage of the Fourier transform is that, through its use, differential operations (differentiation and integration) in the time domain are converted into simpler algebraic operations (multiplication and division). Transform techniques are quite useful in mathematical applications.

Relation name	Fourier integral transform(FIT)	Discrete Fourier transform (DFT)
Forward transform	$X(\omega)=\int_{-\infty}^{\infty} x(t)e^{-i\omega t}dt$	$X_n=\Delta T\sum_{n=0}^{N-1} x_m e^{-j\frac{2\pi mn}{N}}$ $n=0,1,...,N-1$
Inverse transform	$x(t)=\frac{1}{2\pi}\int_{-\infty}^{\infty} X(\omega)e^{i\omega t}d\omega$	$x_m=\Delta F\sum_{k=0}^{N-1} X_n e^{j\frac{2\pi nm}{N}}$ $m=0,1,...,N-1$

Three versions of Fourier transform are important: the **Fourier integral transform** can be applied to any general signal, the **Fourier series expansion** is applicable only

to periodic signals, and the **discrete Fourier transform** is used for discrete signals. As shall be seen, all three versions of transform are interrelated. In particular, one must use the discrete Fourier transform in digital computation of both Fourier integral transform and Fourier series expansion

Frequency Spectrum:

An alternative graphical representation of the periodic signal shown in **Figure 1.11** is given in **Figure 1.12**. In this representation, the amplitude of each harmonic component of the signal is plotted against the corresponding frequency. This is known as the *amplitude or frequency spectrum* of the signal, and it forms the basis of the frequency domain representation. Note that this representation is often more compact and can be far more useful than the time domain representation

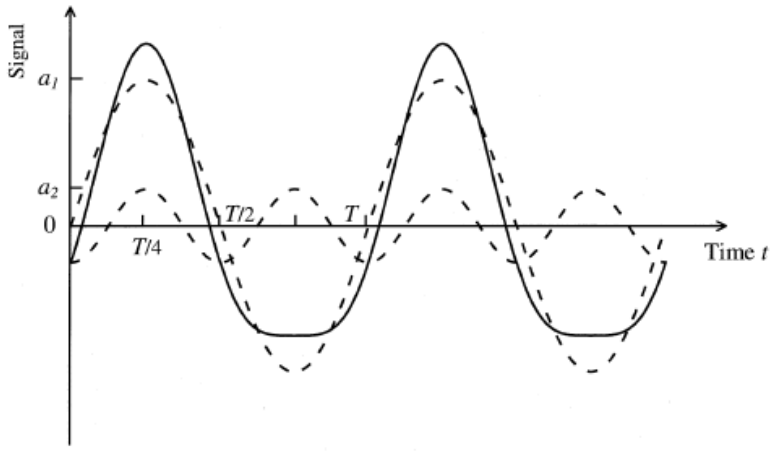

Figure 1.11: Time domain representation of a periodic signal.

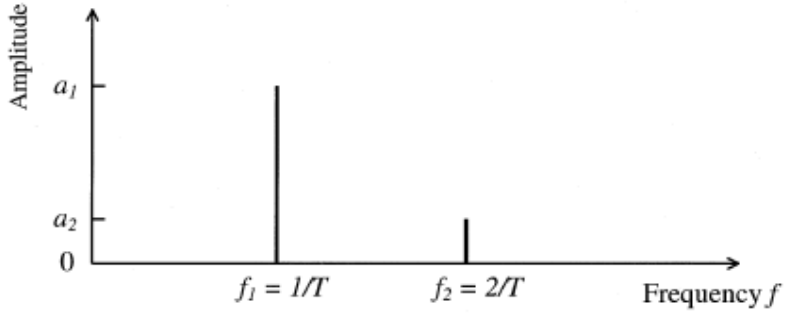

Figure 1.12: The amplitude spectrum of the periodic signal

Sampling: Taking measurements at regular time intervals ΔT is called sampling.

Sampling frequency: $f_s = \dfrac{1}{\Delta T}$

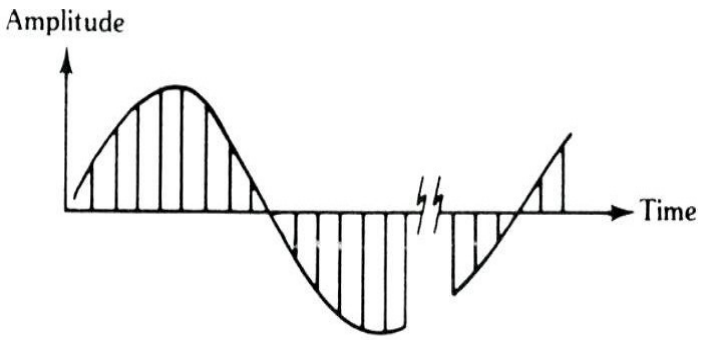

Figure1.13: Figure showing a time record of N equally spaced samples of the input

Fast Fourier Transform (FFT):

To perform a N point DFT,N^2 operations are required. To perform an N point FFT $N^2 * \log(N)$ operations required. FFT is just a smart and efficient algorithm for computing DFT. FFT Transforms these N equally spaced samples as shown in **figure (1.13)** to N/2 equally spaced lines in the Frequency Domain

Nyquist frequency:

Shannon's sampling theorem states that if a time signal x (t) is sampled at equal steps of ΔT, no information regarding its frequency spectrum X (f) is obtained for frequencies higher than $fc = 1/ (2\Delta T)$, and the limiting (cutoff) frequency (fc) is called the *Nyquist frequency*.

In this chapter it is concluded that among all NDT techniques our area of interest is ultrasonic testing .Principle and methods in the ultrasonic testing are also discussed in brief. In the last section it is also described how a signal is analyzed before it is fed to a DPSM model.

CHAPTER 2

LITERATURE REVIEW

The problem of wave propagation can be solved by several methods such as ray tracing method, spectral approach, finite element method etc. Ray tracing method is limited to one dimension wave propagation and cannot be applied to 2 or 3 dimensions. Spectral approach is a frequency based method and involves decomposition of the applied impulse into its many sinusoidal components (Fourier components). In this method, the governing partial differential wave equation is reduced to a set of ordinary differential equations. Their solution is easier than the original differential equation. However, often-approximate solutions are sought. The transformation is effected by Fast Fourier Transform (FFT) Algorithm. But the disadvantage of this method is exact solutions for complex differential equations are difficult to obtain and hence this method becomes inefficient in this case. Also non-linear problems are difficult to solve using this approach. The above two methods seem to be very useful to determine stress wave propagation in the 1-D models, however they prove to be futile when complex models are to be analyzed. In order to analyze linear and non-linear problems, conventional FEM proves to be more useful.

This chapter presents a review of literature on propagation of elastic waves through solids and fluids. This gives an idea of study carried out in this area up to this stage. This work can be classified based on the theoretical/analytical studies and experimental studies.

In analytical studies the prominent work done is listed here. Abrahams et al. (1992) have examined the scattering of Rayleigh waves by an inclined two-dimensional plane surface breaking crack in an isotropic elastic half-plane. Biwa et al. (2003) presented a computational procedure for multiple wave scattering in unidirectional fiber-reinforced composite materials. Bruck (2000) proposed a simple, one-dimensional model to develop insight into stress wave management issues. This model is initially applied to FGMs with discrete layering, and then extended to continuously graded architectures. The benefit of

the FGM over the sharp interface is to introduce a time delay to the reflected wave propagation when stresses approach peak levels which are highly dependent on the composition gradient and the differences in base material properties. Gilchrist, (1999) showed how horizontal symmetric crack-like defects can be detected rapidly in thin isotropic plates by using longitudinal ultrasonic waves. Joshi et al. (2003) discussed the characterization of functionally graded materials. Karagiozova (2004) obtained the speeds of the stress waves that can propagate in an elastic–plastic medium with isotropic linear strain hardening in a plane stress state, to analyze the influence of the transient deformation process on the initiation of buckling in square tubes under axial impact. It is shown that the plastic wave speeds depend on the stress state and on the direction of wave propagation. The material hardening properties have a stronger effect on the speed of the slow plastic wave, while the shear stress affects both the speeds of the fast and slow plastic waves. Krawczuk et al. (2004) presented the method of analysis of the wave propagation process in cracked plates. Elastic behavior of the plate at the crack location was considered as a line spring with a varying stiffness along the crack length. Lima and Hamilton (2003) investigated the propagation of finite-amplitude waves in a homogeneous, isotropic, stress-free elastic plate theoretically. Mal (2002) analyzed elastic waves generated by localized dynamic sources in structural composites. Sharma et al. (2004) studied the thermoelastic interaction in an infinite viscoelastic, thermally conducting plate whose upper and lower surfaces of the plate are subjected to stress-free, thermally insulated or isothermal conditions. Voyiadjis and Baluch (1981) developed a technical theory for the flexural motions of isotropic elastic plates, taking into account the influence of transverse normal strain and transverse normal stress, together with rotary inertia and transverse shear. Wang (2002) investigated shear horizontal (SH) wave propagation in a semi-infinite solid medium surface bonded by a layer of piezoelectric material abutting the vacuum. The dispersive characteristics and the mode shapes of the deflection, the electric potential, and the electric displacements in the thickness direction of the piezoelectric layer are obtained theoretically. Yang et al. (1966) deducted a two-dimensional linear theory of motions of heterogeneous plates. Transverse shear deformations and rotatory inertia were also included. Zak et al. (2006) present certain results of the analysis of wave propagation in an isotropic panel with damage in the form

of a fatigue crack. Mukherjee et al. (2006, 1) used ultrasonic piezoelectric transducers that are employed in various applications to produce a broadband frequency spectrum. However, interference from the sympathetic pulses generated by the transducer limits the duration of the waveform to a very short time. The paper discusses grading of the transducer as a means of alleviating the sympathetic pulses .A simple one dimensional model based on the spectral approach has been presented. The piezoelectric constant e_{33} is graded in various manners and their performances are evaluated .The signal qualities are evaluated by their Euclidean distances from the applied voltage pulse. Linearly graded transducers show the best results.

The second part of the literature review is about the experimentation carried out in this area. Francesco et al. (2004) dealt with the propagation of ultrasonic guided waves in adhesively bonded lap–shear joints. Phillips et al (1978) studied mechanical stress wave propagation in a long, thin, isotropic, elastic rod containing a single transverse edge crack theoretically and experimentally and found that one-dimensional wave theories, coupled with an effective "compliance" of the cracked region, predict reasonably well the observed dynamic strains induced by a longitudinal impact. Giurgiutiu (2005) explored the capability of embedded piezoelectric wafer active sensors (PWAS) to excite and detect tuned Lamb waves for structural health monitoring. Mukherjee et al propagation through solids to locate the position and extent of crack with single actuator and several surface mounted sensors. Mukherjee et al (2006, 2) did the characterization of discretely graded materials using acoustic wave propagation.

The third part of the literature review deals with the work done till date in the area of DPSM technique. This technique for ultrasonic field modelling was first developed by Placko and Kundu(2001).they successfully used this technique to model ultrasonic fields in a homogeneous fluid , and in a non –homogeneous field with one interface (Lee et al . 2002 ,Placko et al 2002)and multiple interfaces (Banerjee ,Kundu and Placko,2006).The interaction between two transducers ,for different transducer arrangements and source strengths ,placed in a homogenous fluid has been studied by Ahmed et. al. (2003).The scattered ultrasonic field generated by a solid scatter of finite dimension placed in a

homogeneous fluid has been modeled by the DPSM technique (Placko et al ,2003).The method has been extended to model the phased array transducers (Ahmad et. al. 2005) .All these works modeled the ultrasonic field in a fluid medium .This method is also applied to model the ultrasonic field in plates immersed in fluids (Banerjee and Kundu,2007).DPSM technique is applied for modeling ultrasonic field at fluid -solid interface also(Banerjee, Kundu and Alnuaimi,2007).semi-analytical modeling of ultrasonic fields in solids with internal anomalies immersed in a fluid(Banerjee and Kundu,2007). Recently distributed point source method is applied on Elastic wave scattering in a solid half space with a circular cylindrical Hole (Das, Banerjee and Kundu, 2008).

CHAPTER 3

NUMERICAL TECHNIQUES TO MODEL WAVE PROPAGATION

There are various methods for numerical modeling of wave propagation problems. These methods either use time based approach or frequency based techniques. Some of them are hybrid or extended from them using certain manipulations. The characteristics of wave propagation problems are that the frequency content of the exciting force is very high. As we know that, at very high frequencies the system becomes mass dominated where inertial effects need to be very accurately modeled. Some popular methods of modeling wave propagation are:

1. Ray tracing method
2. Spectral Approach
3. Finite Element Method
4. Distributed Point Source Method (DPSM)

3.1 RAY TRACING METHOD

A simple elegant, one-dimensional model based on ray tracing the path of wave movement was proposed by Bruck (2000) to develop insight into stress wave management issues. Ray Tracing is a unique method working independent of time or spectral approach.

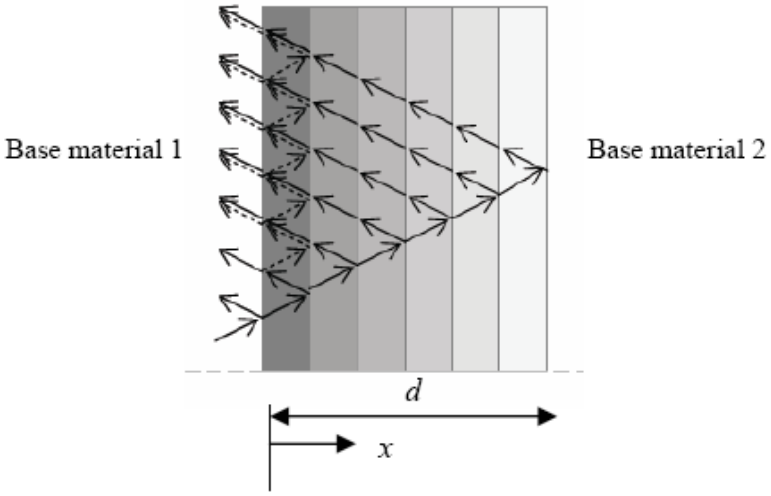

Figure 3.1.1: 1-D stress wave propagation through discretely layered FGM

3.1.1 Explanation of ray tracing method using FGMs:

Ray tracing method has wide applications in characterization of materials. So, it is used as a very promising means for characterization of functionally graded materials (FGMs).The method adopted by Bruck (2000), to characterize the discretely graded FGM, is a simple reflection-transmission method. When the stress waves come across an interface, some part of it is reflected and the remaining is transmitted in the next layer. The behavior of these waves, moving across the FGM is traced and hence it is called as the ray-tracing method. In this method, the path of waves emerging out of a point or a group of points is traced as rays through all interfaces. Ray tracing is useful when only a few trains of wave emerge and they traverse through simple interfaces **(Figure 3.1.1)**.

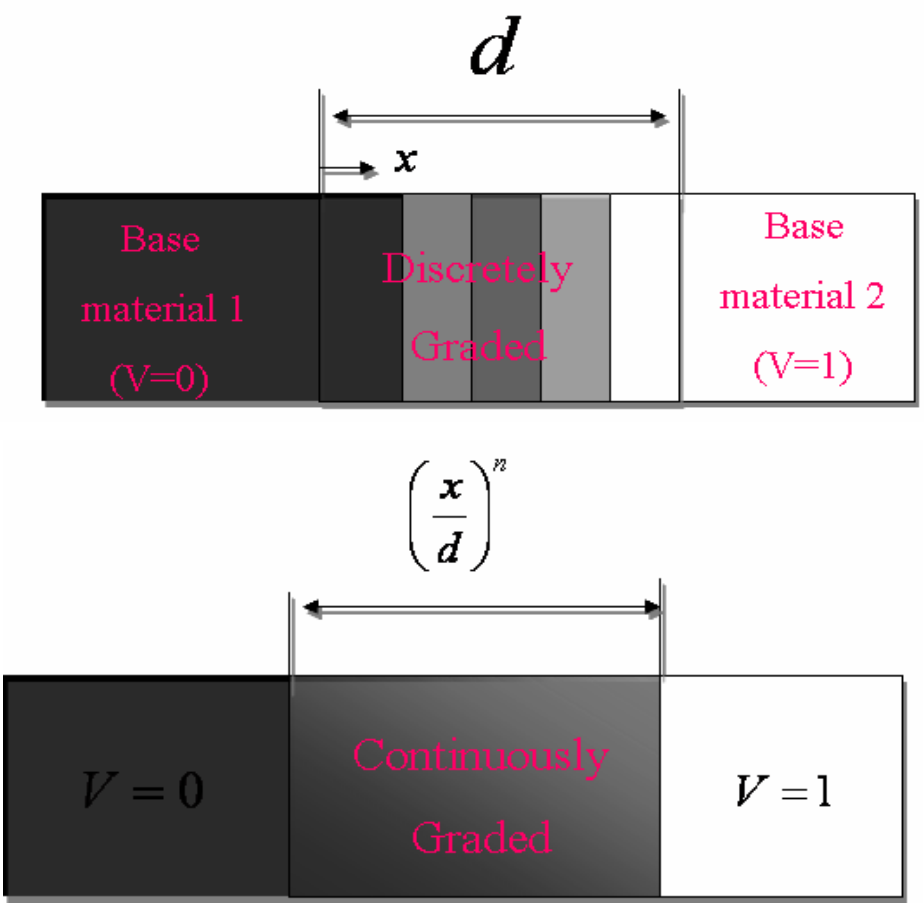

Figure 3.1.2: Gradient Architecture of FGMs

For designing the gradient architecture, a discrete graded layered structure is modeled as shown in ***Figure 3.1.2***. In addition, it can be infinitely refined to get the continuous graded structure. The layers follow power-law or complete polynomial variation in

composition $(x/d)^n$. Here d is the thickness of the graded part. Stress wave propagation in discretely layered FGMs can now be visualized as demonstrated in ***Figure 3.1.3***. If the graded interface consists of 'm' discretely graded layers between base materials 1 and 2, then the propagating stress wave will encounter (m+1) sharp interfaces. At each sharp interface, the stress wave will be partially reflected and transmitted. For one-dimension wave propagation, the amount of reflection and transmission from a sharp interface can be determined from

$$\sigma_t = \frac{2\sigma_i}{(1+\alpha)} \quad and \quad \sigma_r = \frac{\sigma_i(1-\alpha)}{(1+\alpha)} \qquad \text{..... (3.1)}$$

Where σ_i is the amount of stress in the incident wave, σ_t is the amount of stress in the transmitted wave; σ_r is the amount of stress in the reflected wave, and α is the ratio of the acoustic impedance of base material 1 to the acoustic impedance of base material 2.

Acoustic impedance as defined in chapter 1 can be defined as the ratio of pressure across the material to the flow through it. It is defined as $\rho c/A$. For unit area, it becomes the characteristic impedance, which is the material property. The thickness of each layer is d/m, and the total time, t, it takes for the incident wave to travel through a layer and then get reflected back is: $t = \frac{2d}{cm}$ where 'c' is the longitudinal wave speed of the layer

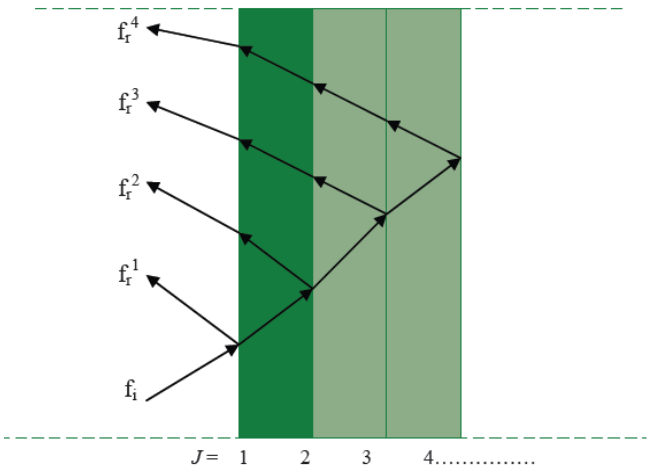

Figure 3.1.3: 1-D stress wave propagation through discretely layered FGM

For developing time-history profile of the stress wave reflected into base material 1 by the graded interface, we need summation of the stresses of waves reflected from each discrete layer and the time it takes for that wave to be generated and reach base

material 1. Assuming that the period of the stress wavelength, λ, is much longer than the thickness of the graded interface (i.e., λ>> d), the normalized magnitude of the reflected wave as shown in base material 1 will be,

$$\frac{\sigma_r^{\,1}}{\sigma_i}=\frac{(1-\alpha_0)}{(1+\alpha_0)}+\frac{2}{(1+\alpha_0)}\left[\frac{(1-\alpha_1)}{(1+\alpha_1)}\frac{(2\alpha_0)}{(1+\alpha_0)}+\frac{(2\alpha_0)}{(1+\alpha_1)}\frac{(1-\alpha_2)}{(1+\alpha_2)}\frac{(2\alpha_1)}{(1+\alpha_1)}\frac{(2\alpha_0)}{(1+\alpha_0)}\right]$$

This can be written in summation form for *m* layers as

$$\frac{\sigma_r^{\,1}}{\sigma_i}=\frac{(1-\alpha_0)}{(1+\alpha_0)}+\sum_{j=1}^{m}\left[\frac{(1-\alpha_j)}{(1+\alpha_j)}\prod_{k=1}^{j}\frac{4\alpha_{k-1}}{(1+\alpha_{k-1})^2}\right]+HOTs \quad \text{..... (3.2)}$$

where $\sigma_r^{\,1}$ is the amount of stress in the wave reflected into base material 1, α_j is the ratio of acoustic impedance of layer *j+1* to *j*, and HOTs are higher order terms comprised of three or more reflections and one or more transmissions. Also, layer 0 and layer m+1 are base materials 1 and 2 respectively, and each intermediate layer is a composite of the two base materials. The normalized time it takes for the wave reflected from the j^{th} layer to reach base material 1, *t* is given by,

$$\bar{t}=\frac{t}{(d/c_0)}=\frac{2}{m}\sum_{k=1}^{f}\frac{c_0}{c_k} \quad \text{..... (3.3)}$$

Where *t* is the time it takes to reach base material 1, c_0 is the wave speed in base material 1, and c_k is the wave speed in layer k.

For analyzing the effects of gradient architecture on stress wave propagation in continuous FGMs, assume that the normalized physical properties of each layer can be described using a linear rule-of-mixtures (ROM) formula as follows:

$$\frac{p_j}{p_0}=1+(\bar{p}-1)\,p_j \quad \text{..... (3.4)}$$

Where p_0 is the property of base material 1, *p* is the ratio of the property for base material 2 to the property for base material 1, and p_j is the property of the j^{th} layer. Thus

$$\alpha_j=\frac{k_{j+1}}{k_j}=\frac{1+(\bar{k}-1)v_{j+1}}{1+(\bar{k}-1)v_j} \quad \text{..... (3.5)}$$

Arranging the above equation in the form

$$\frac{1-\alpha_j}{1+\alpha_j}=\frac{(\bar{k}-1)(v_j-v_{j+1})}{2+(\bar{k}-1)(v_j+v_{j+1})} \quad \text{..... (3.6)}$$

Now in equation as $m\to\infty$, $\alpha_k\to 1$

Hence,

$$\lim_{m\to\infty} \frac{4\alpha_{k-1}}{\left(1+\alpha_{k-1}\right)^2} = 1$$

Also we can write that $V_j - V_{j+1} \cong dV$ and $V_j + V_{j+1} \cong 2dV$

Hence, from Equation (3.2) and above conditions we can write that as **m**$\to\infty$ **i**.e. for continuous grading,

$$\frac{f_r}{f_i} = \frac{1}{2}\int_0^v \frac{1}{(\bar{k}-1)(1+(\bar{k}-1)V_x)}\,dV \quad \ldots\ldots\ldots\ldots\ldots\ldots\ldots \textit{(3.7)}$$

Proceeding in the same manner as above we can write the normalized time as,

$$\frac{tc_0}{d} = 2\int_0^V (1+(\bar{c}-1)V_x)^{-1}\,dV \qquad \ldots\ldots\ldots\ldots\ldots\ldots\ldots\ldots \textit{(3.8)}$$

When there is a sharp interface, the peak magnitude predicted by Equation (3.7) should be identical to the magnitude of a wave reflected from sharp interface. However, it is not so and peak magnitude exceeds by a factor

$$\frac{\left(1+\bar{k}\right)}{2\left(1-\bar{k}\right)}\ln(\bar{k})$$

This discrepancy is a direct result of neglecting higher order terms. Simulation of stress waves in discretely and continuously graded FGMs was done to validate the same. But from this ray tracing model, it is determined that the peak stress of waves reflected from the FGM interface is slightly greater than for materials with sharp interfaces. The benefit of the FGM over the sharp interface is to introduce a time delay to the reflected wave propagation when stresses approach peak levels. This time delay is highly dependent on the composition gradient and the differences in base material properties, consequently the optimal choice of FGM architecture will depend significantly on the critical design conditions for specific applications.

Disadvantages in this method

- This method is limited only up to 1-dimension wave propagation and cannot be extended to 2 or 3 dimensions.
- It cannot be used under arbitrary forcing functions.

3.2 SPECTRAL APPROACH

One of the shortcomings of Ray Tracing Method is its difficulty in extending it to two-dimensional wave propagation. Also another problem faced in modeling of wave propagation was that the frequency content of the exciting force is very high. Therefore, a very fine mesh of finite elements is necessary to adequately model the problem. This problem can be alleviated if we use frequency-based methods, such as the spectral method instead of the time-based techniques. It has many advantages over time-based approaches like it takes very less time for running simulation models. In addition, the inertial effects are exactly represented in it and hence often-exact solutions are obtained for the transformed partial differential equation. In this method, the governing partial differential wave equation is reduced to a set of ordinary differential equations. Their solution is easier than the original differential equation. However, often-approximate solutions are sought. The transformation occurs as a result of Fast Fourier transformation (FFT). These solutions to the governing equations are used as shape functions for spectral element formulation. In addition, often the resulting element is super convergent and very few elements are required to model the system.

Spectral analysis method (Doyle, 1989) is a means of solving wave propagation problems in structures. While it is possible to solve structural dynamics problems by starting with partial differential equations of motion and integrating, the task is horrendously large even for the biggest computer available. It has been known long back that an arbitrary time signal can be thought of as the superposition of many sinusoidal components. This is the basis of Fourier (or spectral) analysis. In wave analysis, the time domain for the disturbance is from minus infinity to plus infinity and thus the components have a continuous distribution (known as Continuous Fourier transform). However, the numerical evaluation of the transform requires discretizing the distribution in some manner, and the one chosen here is by the way of discrete Fourier transform (DFT). This has two advantages. First, many of the ideas and methods of time series analysis can be borrowed and used for present purposes. Second, it allows the use of the very efficient Fast Fourier Transform (FFT) computer algorithm.

Spectral analysis of differential equations

The key to the spectral description of waves is to be able to express the phase changes incurred as the wave propagates from location to location. This is done conveniently through the use of the governing differential equations for particular structural models (although other schemes are possible).The idea of representing the time variation of a function by a summation of harmonic functions is to represent arbitrary functions of time and positions resulting from solution to wave equation. The approach is to remove the time variation by using the spectral representation of the solution. This leaves a new differential equation for the coefficients, which in many cases can be integrated directly.

General functions of space and time

The solutions in wave propagation are general functions of space and time. If the time variation of the solution is focused on at a particular point in space, then it has the spectral representation

$$u(x_1, y_1, t) = f_1(t) = \sum C_{1n} e^{i\omega t} \qquad \text{..... (3.9)}$$

At another point, it behaves as a time function $f_2(t)$ and is represented by the Fourier coefficients. That is, the coefficients are different at each spatial point. Thus, the solution at any arbitrary position has the following spectral representation

$$u(x, y, t) = \sum \hat{u}_n(x, y, \omega_n) e^{i\omega_n t} \qquad \text{..... (3.10)}$$

where u are the spatially dependent Fourier coefficients.

Derivatives

The differential equations have terms of both space and time derivatives. Now apply the spectral representation to each differential term appearing in the differential equation. Thus the spectral representation for the time derivatives is

$$\frac{\partial u}{\partial t} = \frac{\partial}{\partial t} \sum \hat{u}_n e^{i\omega_n t} = \sum i\omega_n \hat{u}_n e^{i\omega_n t} \qquad \text{..... (3.11)}$$

In fact, time derivatives of general order have the representation

$$\frac{\partial^m u}{\partial t^m} \Rightarrow i^m \omega_n{}^m \hat{u}_n \quad or \quad i^m \omega^m{}_n \hat{u}_n \qquad \text{..... (3.12)}$$

Herein lays the advantages of the spectral approach to solving differential equations. The algebraic expressions in the Fourier coefficients replace the time derivatives. That is, there is a reduction in the number of derivatives occurring.

Similarly, the spatial derivatives are represented by,

$$\frac{\partial u}{\partial x} = \frac{\partial}{\partial x}\sum \hat{u}_n e^{i\omega t} = \sum \frac{\partial \hat{u}_n}{\partial x} e^{i\omega t} \qquad \text{..... (3.13)}$$

And in shorthand notation, it becomes

$$\frac{\partial u}{\partial x} \Rightarrow \frac{\partial \hat{u}_n}{\partial x} \quad or \quad \frac{\partial \hat{u}_n}{\partial x}$$

Differential Equations

Consider the following general, linear, one-dimensional, homogenous differential equation in the dependent variable u(x,t).

$$u + a\frac{\partial u}{\partial x} + b\frac{\partial u}{\partial t} + c\frac{\partial^2 u}{\partial x^2} + d\frac{\partial^2 u}{\partial t^2} + e\frac{\partial^2 u}{\partial x \partial t} + ... = 0 \text{ ..... (3.14)}$$

The coefficients *a*, *b*, *c* are assumed not to depend on time, but could be functions of positions, if now, the solution is given the spectral representation

$$u(x,t) = \sum_n \hat{u}_n(x,\omega_n)e^{i\omega t} \qquad \text{..... (3.15)}$$

then on substitution into the differential equation we get

$$\sum_n \left\{ u_n + a\frac{\partial \hat{u}_n}{\partial x} + (i\omega)b\hat{u}_n + c\frac{\partial^2 \hat{u}}{\partial x^2} + (i\omega)^2 d\hat{u}_n + (i\omega)e\frac{\partial \hat{u}}{\partial x} + ... \right\} e^{i\omega t} = 0 \quad \text{..... (3.16)}$$

Since each term is independent, then this equation must be satisfied for each *n*. That is, there are *n* simultaneous equations of the form.

$$(1 + (i\omega_n)b + (i\omega_n)^2 d + ..)\hat{u}_n + (a + (i\omega_n)e + ...)\frac{d\hat{u}}{dx} + (c + ...)\frac{d^2\hat{u}}{dx^2} + ... = 0 \qquad \text{..... (3.17)}$$

These equations become,

$$A_1(x,\omega)\hat{u} + A_2(x,\omega)\frac{d\hat{u}}{dx} + A_3(x,\omega)\frac{d^2\hat{u}}{dx^2} + ... = 0 \qquad \text{..... (3.18)}$$

on grouping terms, where, A_1 , A_2… depend on frequency and position and are complex. It is seen that the original partial differential equations becomes a set of ordinary linear differential equations in the Fourier coefficients.

Spectral relation

Linear differential equations with constant coefficients have solutions of the form, where λ is obtained by solving algebraic characteristics equation

$$A_1 + A_2\lambda + A_3\lambda^2 + ... = 0 \qquad \text{…….. } (3.19)$$

It is usual in wave analysis, however to assume that λ is complex to begin with, that is, that the solutions are of the form.

$$\hat{u}(x) = Ce^{ikx}$$

For example, consider the differential equation

$$au + \frac{d\hat{u}}{dx} = 0 \Rightarrow \left[a - k^2\right]C = 0$$

This gives *k* and the solution as

$$k = -a \quad and \quad \hat{u}(x) = Ce^{-ax}$$

where C is a constant of integration. Similarly, following second-order differential equation

$$au + \frac{d^2\hat{u}}{dx^2} = 0 \Rightarrow \left[a - k^2\right]C = 0$$

gives k and the solution as,

$$k = \pm\sqrt{a} \quad and \quad \hat{u}(x) = C_1e^{i\sqrt{ax}} + C_2e^{-i\sqrt{ax}}$$

There are two solutions (and constant of integration) because occurred to the power of two. Note that, even if the coefficients in the differential equation are real, it is possible for to be complex.

In general, then, the characteristics equation becomes

$$A_1 + (ik)A_2 + (ik)^2A_3 + ... = 0$$

and this has many values of k that satisfies it. That is, *k*

$$k_{mn} = f_m(A_1, A_2, A_3, ..., \omega_n)$$

This relation between the exponent *k* (called the wave number) and frequency ω is called the spectral relation and is fundamental to the spectral analysis of waves. The different values of *m* correspond to the different modes. The solution is given as the superposition of modes in the form,

$$u(x) = C_1e^{ik_1x} + C_2e^{ik_2x} + ... + C_{mn}e^{ik_mx}$$

There are as many modes (or solutions) are there are roots of the characteristics equation and these should be confused with the number of solutions at each frequency. To reinforce this, the solution in total form is written as,

$$u(x) = \sum_n \left\{ C_1 e^{ik_1 x} + C_2 e^{ik_2 x} + ... + C_{mn} e^{ik_m x} \right\} e^{i\omega t} \qquad \text{..... (3.20)}$$

The exponential form for each term is due to the coefficients of the differential equation being constant; however, the solution for any problem can be always be expressed as

$$u(x,t) = \sum F_n G(K_{mn} x) e^{i\omega t} \qquad \text{..... (3.21)}$$

where F_n is the amplitude spectrum and G (which may be combination of modes) is the system transfer function. Analysis of the partial differential equation combined with the boundary conditions determines the particular forms for *G* and in fact, G determines the phase shifts with respect to space. Further, it is noted that the wave number *k* acts as a scale factor on the position variable in the same way that the frequency acts on the time. The analysis of the scaling done by *k* provides a good deal of insight into the solution before the actual solution is obtained.

Propagating and Reconstructing waves

The significance of the spectral approach to waves coupled with the use of the differential equations is that once the signal is characterized at one space position then it is known at all positions, therefore propagating it becomes a fairly simple matter. This section illustrates the basic algorithm for doing this.

- **Basic Algorithm**

In its simplest terms, the solutions to a waves problems is represented as,

$$u(x) = \sum_n \left\{ C_1 e^{ik_1 x} + C_2 e^{ik_2 x} + ... + C_{mn} e^{ik_m x} \right\} e^{i\omega t} = \sum \hat{F}_n G(K_{mn} x) e^{i\omega t} \quad \text{.... (3.22)}$$

where G is the analytically known transfer function of the problems. It is a function of position x and has different numerical values at each frequency. $\hat{F}$ is the amplitude spectrum; this is known from the input conditions or from some measurement. This $\hat{F}_n G$ is recognized as the Fourier transform of the solution. Of course it is different at each position but once it is evaluated at a particular position then its inverse immediately gives the time history of the solution at that point**. Figure.3.2.1** is a flow diagram for its

evaluation. Briefly, the time input $F(t)$ is converted to its spectrum $\hat{F}_n$ through a use of the forward FFT. The transform solution is the obtained by evaluating the product, at each frequency.

$$\hat{u}_n = \hat{F}_n G(k_{mn}) \qquad \text{…….. (3.23)}$$

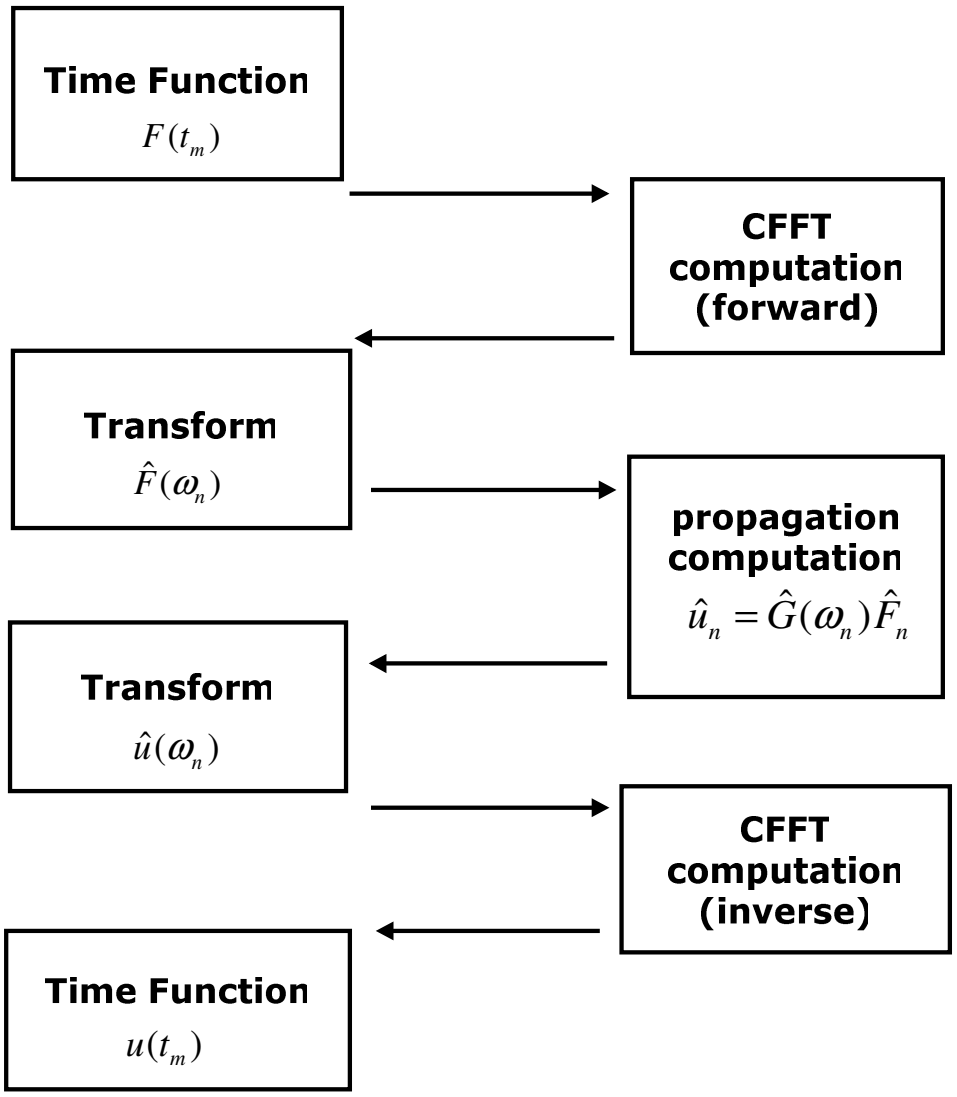

Figure 3.2.1: Flow diagram for wave reconstruction program

This is finally reconstructed in the time domain by the use of the inverse FFT. In the process, it is necessary to realize (when using the FFT to perform the inversion) that $\hat{F}_n G$ is evaluated only up to the Nyquist frequency and the remainder is obtained by imposing

that it must be complex conjugate of the initial part, This ensures that reconstructed time history is real only.

Disadvantages of Spectral element method

- Exact solutions for complex differential equations are difficult to obtain, hence this method becomes inefficient in this case
- Non-linear problems are difficult to solve using this approach.

3.3 FINITE ELEMENT APPROACH

As already discussed, Ray tracing method is limited to 1-D wave propagation and cannot be applied to 2 or 3 dimensions. Spectral approach is a frequency based method and involves decomposition of the applied impulse into its many sinusoidal components (Fourier components). In this method, the governing partial differential wave equation is reduced to a set of ordinary differential equations whose solution is easier than the original differential equation. The transformation is effected by Fast Fourier Transform (FFT) Algorithm. But the disadvantage of this method is exact solutions for complex differential equations are difficult to obtain and hence this method becomes inefficient in this case. Also non-linear problems are difficult to solve using this approach. The above two methods seem to be very useful to determine stress wave propagation in the 1-D models, however they prove to be futile when complex models are to be analyzed. In order to analyze linear and non-linear problems, conventional FEM proves to be more useful.

A coordinated theoretical and experimental program was carried out by Deepti et al. (2006) in an effort to develop the knowledge base required for the design of a damage monitoring system in structures consisting of distributed surface mounted sensors. The behavior of isotropic was studied numerically and experimentally for undamaged and damaged conditions. Study aimed at detection of the damage in beam/plate using wave propagation technique. The experimental and numerical investigations were being made to locate the position and extent of crack approximately with single actuator and several surface mounted sensors. Numerical modeling of wave propagation was done using

ABAQUS/EXPLICIT through isotropic and isotropic medium with damages. Now a days so many solvers for solving FEM problems are coming among them ABAQUS/EXPLICIT is superior in solving wave propagation problems so a brief introduction is given in this chapter about it.

3.3.1 Finite element method for explicit dynamics

This section contains a conceptual and an algorithmic description of the ABAQUS/Explicit analysis product as well as a discussion on the advantages of the method.

3.3.1.1 Stress wave propagation illustrated

This section attempts to provide some conceptual understanding of how forces propagate through a model when using the explicit dynamics method. In this illustrative example we consider the propagation of a stress wave along a rod modeled with three elements, as shown in **figure.3.3.1.** We study the state of the rod as we increment through time.

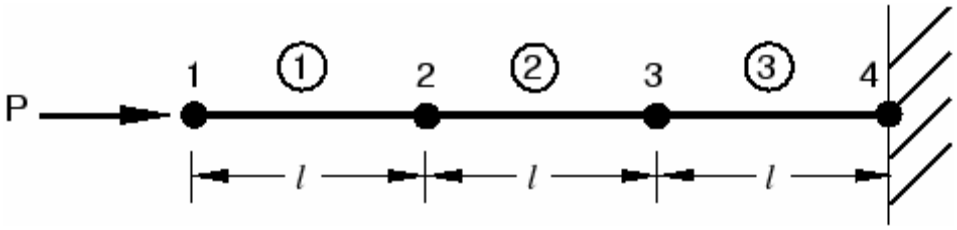

Figure 3.3.1: Initial configuration of a rod with a concentrated load, P, at the free end.

In the first time increment node 1 has acceleration, $\ddot{u}_1$ as a result of the concentrated force, *P*, applied to it. The acceleration causes node 1 to have a velocity, $\dot{u}_1$ which, in turn, causes a strain rate, $\dot{\varepsilon}_{el1}$ in element 1. The increment of strain, d_{el1} in element 1 is obtained by integrating the strain rate through the time of increment 1. The total strain, ε_{el1} , is the sum of the initial strain, ε_0 , and the increment in strain. In this case the initial strain is zero. Once the element strain has been calculated, the element stress σ_{el1} is obtained by applying the material constitutive model. For a linear elastic material the

stress is simply the elastic modulus times the total strain. This process is shown in **figure 3.3.2.** Nodes 2 and 3 do not move in the first increment since no force is applied to them.

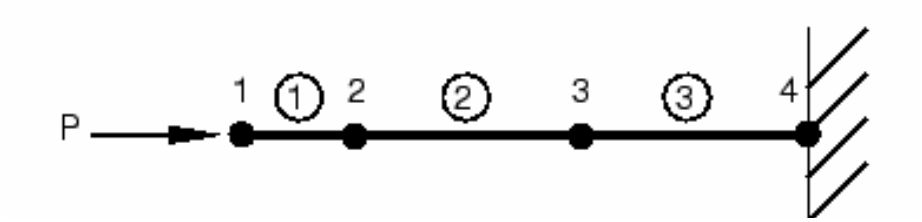

Figure 3.3.2: Configuration at the end of increment 1 of a rod with a concentrated load, P, at the free end.

$$\ddot{u}_1 = \frac{P}{M_1} \Rightarrow \dot{u}_1 = \int \ddot{u}_1 dt \Rightarrow \dot{\varepsilon}_{el1} = \frac{\ddot{u}_1}{l} \Rightarrow d\varepsilon_{el1} = \int \dot{\varepsilon}_{el1} dt \Rightarrow \varepsilon_{el1} = \varepsilon_0 + d\varepsilon_{el1} \Rightarrow \sigma_{el1} = E\varepsilon_{el1} \quad (3.30)$$

In the second increment the stresses in element 1 apply internal, element forces to the nodes associated with element 1, as shown in **figure 3.3.3.** These element stresses are then used to calculate dynamic equilibrium at nodes 1 and 2.

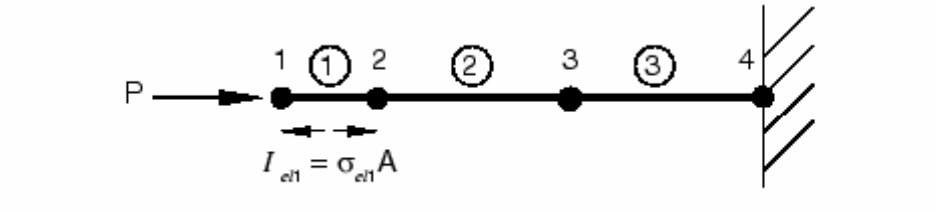

Figure 3.3.3: Configuration of the rod at the beginning of increment 2.

$$\ddot{u}_1 = \frac{P - I_{el1}}{M_1} \Rightarrow \dot{u}_1 = \dot{u}_1^{old} + \int \ddot{u}_1 dt \qquad \ldots\ldots (3.31)$$

$$\ddot{u}_2 = \frac{I_{el1}}{M_2} \Rightarrow \dot{u}_2 = \int u_2 dt \qquad \ldots\ldots. (3.32)$$

$$\dot{\varepsilon}_{el1} = \frac{\dot{u}_2 - \dot{u}_1}{l} \Rightarrow d\varepsilon_{el1} = \int \dot{\varepsilon}_{el1} dt \Rightarrow \varepsilon_1 + d\varepsilon_{el1} \Rightarrow \sigma_{el1} = E\varepsilon_{el1} \qquad \ldots.. (3.33)$$

The process continues so that at the start of the third increment there are stresses in both elements 1 and 2, and there are forces at nodes 1, 2, and 3, as shown in **figure 3.3.4**. The process continues until the analysis reaches the desired total time.

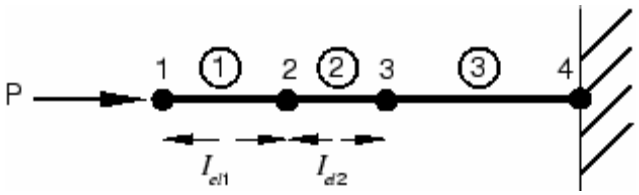

Figure 3.3.4: Configuration of the rod at the beginning of increment 3

3.3.1.2 Time integration

ABAQUS/Explicit uses a central difference rule to integrate the equations of motion explicitly through time, using the kinematic conditions at one increment to calculate the kinematic conditions at the next increment. At the beginning of the increment the program solves for dynamic equilibrium, which states that the nodal mass matrix, *M*, times the nodal accelerations, $\ddot{u}$, equals the total nodal forces (the difference between the external applied forces, P, and internal element forces, I):

$$M\ddot{u} = P - I \qquad \text{..... (3.34)}$$

The accelerations at the beginning of the current increment (time) are calculated as

$$\ddot{u}\,|_{(t)} = (M)^{-1}.(P-I)\,|_{(t)} \qquad \text{.... (3.35)}$$

Since the explicit procedure always uses a diagonal, or lumped, mass matrix, solving for the accelerations is trivial; there are no simultaneous equations to solve. The acceleration of any node is determined completely by its mass and the net force acting on it, making the nodal calculations very inexpensive.

The accelerations are integrated through time using the central difference rule, which calculates the change in velocity assuming that the acceleration is constant. This change in velocity is added to the velocity from the middle of the previous increment to determine the velocities at the middle of the current increment:

$$\dot{u}\,|_{\left(t+\frac{\Delta t}{2}\right)} = \dot{u}\,|_{\left(t-\frac{\Delta t}{2}\right)} + \frac{\left(\Delta t\,|_{(t+\Delta t)} + \Delta t\,|_{(t)}\right)}{2}\ddot{u}\,|_{(t)} \qquad \text{.... (3.36)}$$

The velocities are integrated through time and added to the displacements at the beginning of the increment to determine the displacements at the end of the increment:

$$u|_{(t+\Delta t)} = u|_{(t)} + \Delta t|_{(t+\Delta t)}\ \dot{u}|_{\left(t+\frac{\Delta t}{2}\right)} \qquad \text{…. (3.37)}$$

Here is a summary of the explicit dynamics algorithm:

1. Nodal calculations.

   a. Dynamic equilibrium.

$$\ddot{u}_{(t)} = \left(M\right)^{-1}.(P_{(t)} - I_{(t)}) \qquad \text{…… (3.38)}$$

   b. Integrate explicitly through time.

$$\dot{u}|_{\left(t+\frac{\Delta t}{2}\right)} = \dot{u}|_{\left(t-\frac{\Delta t}{2}\right)} + \frac{\left(\Delta t|_{(t+\Delta t)} + \Delta t|_{(t)}\right)}{2}\ddot{u}|_{(t)} \qquad \text{….. (3.39)}$$

$$u|_{(t+\Delta t)} = u|_{(t)} + \Delta t|_{(t+\Delta t)}\ \dot{u}|_{\left(t+\frac{\Delta t}{2}\right)} \qquad \text{….. (3.40)}$$

2. Element calculations.

   a. Compute element strain increments, $d\varepsilon$, from the strain rate, $\dot{\varepsilon}$.

   b. Compute stresses, σ, from constitutive equations.

$$\sigma_{(t+\Delta t)} = (\sigma_{(t)}, d\varepsilon) \qquad \text{…… (3.41)}$$

   c. Assemble nodal internal forces, $I_{(t+\Delta t)}$

3. Set $t + \Delta t$ to t and return to Step 1.

3.4 DISTRIBUTED POINT SOURCE METHOD

3.4.1 Introduction:

This method is used specifically for modeling of ultrasonic field .The main originality of DPSM method is that it is not necessary to mesh the totality of the computation volume, but only the surface of interest, in the contrary to a classical finite elements method. The implementation of the model simply requires discretization of the active surface of the transducer or the interfaces to obtain an array of point sources, so that the initial complexity is changed into a superposition of elementary problems. The active surfaces like transducers, emitters, or interfaces reflecting a part of an incident field are discretized into a finite number of elementary surfaces, a point source being placed at the centroid of every elemental surface. DPSM technique for ultrasonic field modeling was first developed by Placko and Kundu (2001). They successfully used this technique to model ultrasonic fields in a homogeneous fluid, and in a non-homogeneous fluid with one interface (Lee et al. 2002, Placko et al. 2002) and multiple interfaces (Banerjee, Kundu and Placko, 2005). The interaction between two transducers, for different transducer arrangements and source strengths, placed in a homogeneous fluid has been studied by Ahmad et al.(2003).

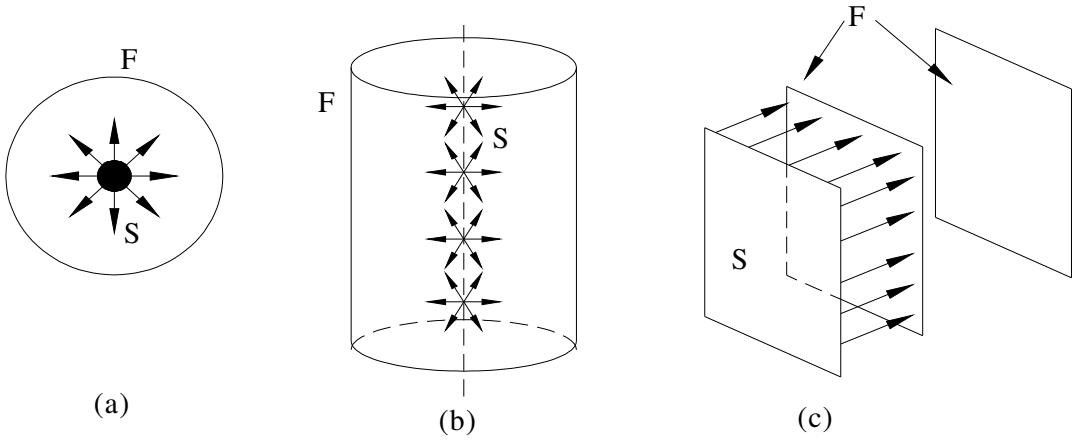

Figure 3.4.1: (a) Point source generating spherical wavefront
(b) Line source generating cylindrical wavefront
(c) Infinite plane source generating plane wavefront

The scattered ultrasonic field generated by a solid scatterer of finite dimension placed in a homogeneous fluid has also been modeled by the DPSM technique (Placko et al. 2003). Recently the method has been extended to model the phased array transducers (Ahmad et. al. 2005). All these works modeled the ultrasonic field in a fluid medium. The ultrasonic field generated inside the solid half-space or the leaky waves in the fluid produced by guided waves propagating along the fluid-solid interface have not been modeled yet. ***Figure (3.4.1)) shows*** spherical waves generated by a point source in an infinite medium, cylindrical waves generated by a line source and plane waves generated by an infinite plane. The pressure field due to a finite plane source can be assumed to be the summation of pressure fields generated by a number of point sources distributed over the finite source as shown in ***Figure 3.4.2***. The finite source can be the front face of the transducer. A harmonic point source, which expands and contracts alternately, can be represented by a point and a sphere as shown in ***Figure 3.4.3(a)***. The point represents the contracted position and the sphere represents the expanded position. When a large number of point sources are placed side by side on a plane surface, then the contacted and expanded positions are shown in ***Figure 3.4.3(b)***. The combined effect of a large number of point sources placed side by side is shown in ***Figure 3.4.3(c)***. From this figure it is clear that the combined effect of a large number of point sources distributed on a plane surface is the vibration of particles in the direction normal to the plane surface. Non-normal components of motion at a point on the surface generated by neighboring source points cancel each other as shown in ***Figure 3.4.3(d).*** However, non normal components do not vanish along the edge of surface. The particles not only vibrate normal to the surface but also expand to a hemisphere and contract to a point on the edge as shown.

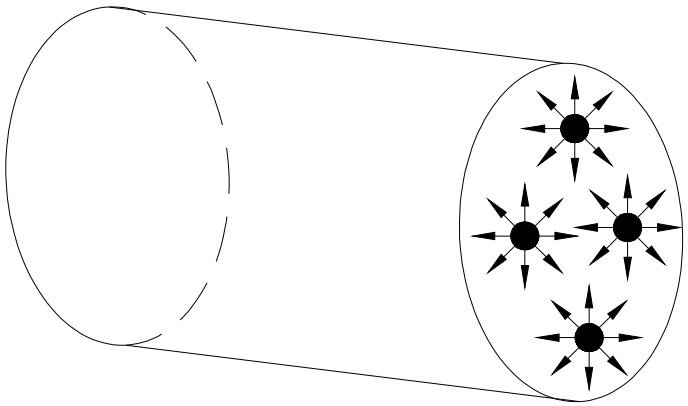

Figure 3.4.2: Four point sources distributed over a finite surface

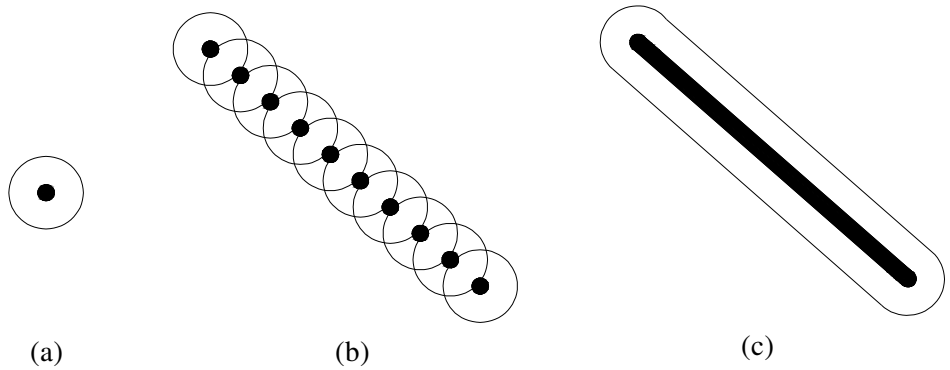

(a) (b) (c)

Source expanded - Thin line Source contracted - Dark point

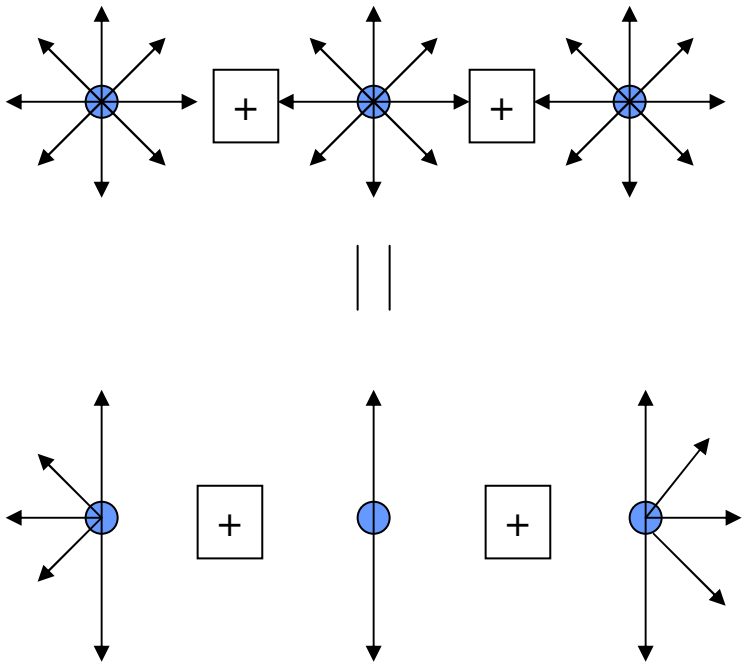

(d)

Figure 3.4.3: Position of particles for (a) Point source (b) Distributed finite number of points (c) Large number of point sources (d) components of motion of multiple point sources

3.4.2 THEORY

DPSM is briefly described in Section 3.4.2.1 then detail mathematical derivations are presented in the following sections.

3.4.2.1 Distributed Point Source Method

If the front face of a transducer is considered as the main source of an ultrasonic field, then the ultrasonic field generated by that source can be assumed to be the summation of the ultrasonic fields generated by a number of point sources distributed near that finite source. Any interface is responsible for generating reflected and transmitted ultrasonic fields. Therefore, the interface can be replaced by two layers of sources - one layer generating the reflected field and the second layer generating the transmitted field. Two layers of interface sources are distributed on two sides of the interface. Strengths of the point sources distributed near the transducer face and the interface are obtained by satisfying the boundary conditions and interface continuity conditions. For solving this problem we need to calculate the stress and displacement Green's functions in the solid, and pressure and displacement Green's functions in the fluid.

3.4.2.2 Mathematical derivations:

Calculation of Displacement Green's functions in the solid

A point source acting in a solid, can be modeled as a concentrated body force,

$$F(x,t) = \mathrm{P}f(t)\delta(x) \; or \; F_i = P_i f(t)\delta(x_j) \ldots\ldots\ldots\ldots\ldots\ldots\ldots\ldots \; (3.42)$$

where P is the force vector. For harmonic time dependence [$f(t) = e^{-i\omega t}$], when the point source is at y then the displacement field at x can be expressed in terms of the Green's functions $G_{ij}(x; y)$,

$$u_i = U_i e^{-i\omega t} = G_{ij}(x; y) P_j e^{-i\omega t} \ldots\ldots\ldots\ldots\ldots\ldots\ldots\ldots\ldots\ldots \; (3.43)$$

The displacement Green's function for isotropic solids can be written as (Mal and Singh, 1991),

$$G_{ij}(x;y)=\frac{1}{4\pi\rho\omega^2}\left[\begin{array}{l}\dfrac{e^{ik_p r}}{r}\left(k_p{}^2R_iR_j+(3R_iR_j-\delta_{ij})\left(\dfrac{ik_p}{r}-\dfrac{1}{r^2}\right)\right)+\\ \dfrac{e^{ik_s r}}{r}\left(k_s{}^2(\delta_{ij}-R_iR_j)-(3R_iR_j-\delta_{ij})\left(\dfrac{ik_s}{r}-\dfrac{1}{r}\right)\right)\end{array}\right]$$

$$\text{where } R_i=\frac{x_i-y_i}{r} \qquad (3.44)$$

where, x_i are the coordinates at the observation point, y_i are the coordinates at the source point, r is the distance between the observation point and the source point, k_p is the P-wave number and k_s is the S-wave number of the solid. In matrix form,

$$G(x;y)=\left[G_1(x;y)\quad G_2(x;y)\quad G_3(x;y)\right]^{\mathrm{T}} \text{ and } u=G(x;y)P \ldots\ldots\ldots\ldots\ldots\ldots (3.45)$$

If the unit excitation force at y acts in the x_j direction, then the displacement at x in x_i direction is given by $G_{ij}(x;y)$.

Calculation of Stress Green's function in the solid

For isotropic homogeneous solids the expression for stresses can be written as

$$\sigma_{ij}=2\mu\varepsilon_{ij}+\lambda\delta_{ij}\varepsilon_{kk} \ldots\ldots\ldots\ldots\ldots\ldots\ldots\ldots\ldots\ldots\ldots (3.46)$$

Where, λ,μ are the two Lamé constants and δ_{ij} is the Kronecker Delta.

We know that strain can be expressed as a function of displacement,

$$\varepsilon_{ij}=\frac{1}{2}(u_{i,j}+u_{j,i})\,.$$

Substituting the expression for displacement in the expression for strains,

$$\varepsilon_{ij}=\frac{1}{2}\left(G_{ik,j}+G_{jk,i}\right)P_k \qquad \ldots\ldots\ldots\ldots\ldots\ldots\ldots\ldots (3.47)$$

For isotropic homogeneous linearly elastic material, we can write the expression for the stress Green's function at **x** due to a concentrated harmonic force at **y** by substituting the expression for strains in Eq.(3.46)as

$$\sigma_{ij}(\mathbf{x};\mathbf{y})=\mu\left(G_{ik,j}+G_{jk,i}\right)P_k+\lambda\delta_{ij}G_{kq,k}P_q \ldots\ldots\ldots\ldots\ldots\ldots (3.48)$$

$$\text{Or } \sigma_{ij}(\mathbf{x};\mathbf{y})=\left(\mu\left(G_{ik,j}+G_{jk,i}\right)\delta_{kq}+\lambda\delta_{ij}G_{kq,k}\right)P_q \ldots\ldots\ldots (3.49)$$

Calculation of pressure and displacement Green's functions in the fluid

A perfect fluid can be considered as a homogeneous isotropic medium, it cannot have shear stress and the pressure at a point in all directions in the fluid must be the same. Therefore, the stress or pressure at any point can be written as

$$\sigma_{ij} = \lambda \delta_{ij} \varepsilon_{kk} = -p \qquad \text{.....(3.50)}$$

Following the usual notation $\varepsilon_{ij} = \frac{1}{2}(u_{i,j} + u_{j,i})$, the constitutive relation can be expressed in terms of the displacement components as

$$\lambda\left(u_{1,1} + u_{2,2} + u_{3,3}\right) = \lambda \nabla.\mathbf{u} = -p \qquad \text{..... (3.51)}$$

The governing equation or the equation of motion in the fluid can be written as

$$-p_{,i} + F_i = \rho \ddot{u}_i \qquad \text{..... (3.52)}$$

$$-\nabla p + \mathbf{F} = \rho \ddot{\mathbf{u}} \qquad \text{..... (3.53)}$$

Applying divergence on both sides and using equation (3.53) we get

$$-\nabla.\nabla p + \nabla.\mathbf{F} = \rho \frac{\partial^2 (\nabla.\mathbf{u})}{\partial t^2} = -\frac{\rho}{\lambda} \ddot{p} \qquad \text{..... (3.54)}$$

Assuming $f = \nabla.\mathbf{F}$ and the wave velocity in fluid $c_f = \sqrt{\frac{\lambda}{\rho}}$, we can rewrite the above equation,

$$\nabla^2 p - \frac{1}{c_f^2} \ddot{p} = f \qquad \text{.....(3.55)}$$

I. Bulk wave in the fluid

Spherical Bulk wave in a fluid can be generated by a point source in an infinite fluid medium as shown in **Figure 3.4.1(a).** If the point source is a harmonic source, then it will generate harmonic spherical waves. If a point source is generating the bulk wave in a fluid, then the harmonic dirac-delta impulsive force will contribute to the body force.

For an infinite fluid medium with point source acting on it, Equation (3.55) can be expressed as

$$\nabla^2 G_f - \frac{1}{c_f^2}\ddot{G}_f = \delta(\mathbf{x}-\mathbf{y})e^{-i\omega t} \qquad \ldots (3.56)$$

Where, G_f is the pressure Green's function in fluid at **x** due to the point source acting at **y.**

If $G_f(r,t) = G_f(r,\omega)e^{-i\omega t}$ then the above equation takes the following form,

$$\nabla^2 G_f(r,\omega) + \frac{\omega^2}{c_f^2} G_f(r,\omega) = \delta(\mathbf{x}-\mathbf{y}) \qquad \ldots\ldots.. (3.57)$$

Where, G_f is now a function of r and ω. The Laplacian operator in spherical coordinates can be written as

$$\nabla^2 v \equiv \frac{1}{r^2}\left[\frac{\partial}{\partial r}\left(r^2 \frac{\partial v}{\partial r}\right)\right] \qquad \ldots\ldots (3.58)$$

Where, v is any scalar function of r and

$r = |\mathbf{x}-\mathbf{y}| = \sqrt{(x_1-y_1)^2 + (x_2-y_2)^2 + (x_3-y_3)^2}$.

Hence, the particular solution of Equation (3.57) is

$$G_f(r,\omega) = \frac{e^{ik_f r}}{4\pi r} \qquad \ldots\ldots\ldots (3.59)$$

$$\text{where } k_f = \frac{\omega}{c_f}.$$

The pressure in the fluid can also be represented by a potential function (Placko and Kundu 2003). The pressure-potential and the displacement-potential relations can be written as

$$p = -\rho\omega^2\phi_f \qquad \ldots\ldots\ldots (3.60)$$

$$u_i = \frac{\partial \phi_f}{\partial x_i} \qquad \ldots\ldots\ldots \quad (3.61)$$

where ϕ_f is the scalar potential. Therefore, for the pressure Green's function, the potential function can be expressed as

$$\phi_f(r,\omega) = -\frac{e^{ik_f r}}{4\pi\rho\omega^2 r} \qquad \ldots\ldots\ldots \quad (3.62)$$

Taking derivatives of ϕ_f with respect to x_i, the displacement components in the three directions can be obtained,

$$u_1 = \frac{1}{4\pi\rho\omega^2}\left[\frac{1}{r} ik_f R_1 e^{ik_f r} - \frac{e^{ik_f r}}{r^2} R_1\right] \qquad \ldots\ldots\ldots\ldots \quad (3.63)$$

$$u_2 = \frac{1}{4\pi\rho\omega^2}\left[\frac{1}{r} ik_f R_2 e^{ik_f r} - \frac{e^{ik_f r}}{r^2} R_2\right] \qquad \ldots\ldots\ldots\ldots \quad (3.64)$$

$$u_3 = \frac{1}{4\pi\rho\omega^2}\left[\frac{1}{r} ik_f R_3 e^{ik_f r} - \frac{e^{ik_f r}}{r^2} R_3\right] \qquad \ldots\ldots\ldots\ldots \quad (3.65)$$

where $R_i = \dfrac{x_i - y_i}{r}$

CHAPTER 4

Ultrasonic Field Modeling in Homogenous Fluid Using - DPSM Technique

4.1 Computation of Velocity, Pressure and Displacement Fields in a fluid generated by a group of point sources:

Homogenous fluid is fluid which is having same properties and they does not change from point to point .For a flat surface transducer, where all point sources are excited at the same time, the pressure field generated at a point **x** (see **Figure. 4.1(a)**) by the transducer can be obtained by integrating the spherical waves, as done in the conventional surface integral technique. The combined effect of a large number of point sources distributed over a plane surface such as the transducer face is the vibration of particles in a direction normal to the plane surface

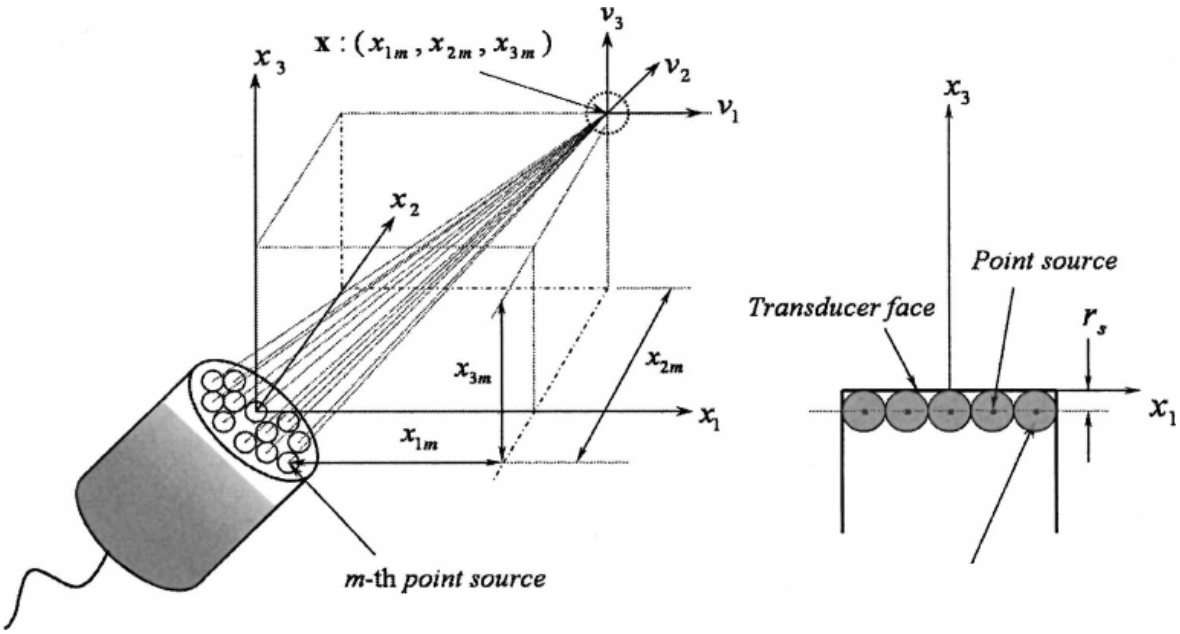

(a) (b)

Figure 4.1 (a) Position of an observation point (target point) and its distance from the nth point source on the transducer surface, (b) Side view of a transducer and actual positions of the point sources.

From the surface integral technique, the pressure field at point **x** in front of a group of point sources at **y** can be written as (Schmerr 1998),

$$p(\mathbf{x}) = \int_S B.G_f \, dS(\mathbf{y}) = \int_S B \frac{e^{ik_f r}}{r} dS(\mathbf{y}) \qquad \text{……. (4.1)}$$

where B represents the source strength of the point sources. This integral can also be written in the summation form

$$p(\mathbf{x}) = \sum_{m=1}^{N} \left(\frac{B}{4\pi} \Delta S_m \right) \frac{\exp(ik_f r_m)}{r_m} = \sum_{m=1}^{N} A_m \frac{\exp(ik_f r_m)}{r_m} \qquad \text{…….. (4.2)}$$

In the DPSM technique it has been assumed that each point source distributed over the surface has different source strengths as specified by A_m, where m designates the m^{th} point source and r_m is the distance of the target point **x** from the m^{th} point source. Hence, pressure at any point at a distance r_m from the m^{th} point source with source strength A_m can be written as

$$p_m(r) = A_m \frac{\mathrm{e}^{ik_f r_m}}{r_m} \qquad \text{…… (4.3)}$$

For 'N' number of point sources distributed on a surface, the pressure at the target point is given by

$$p(\mathbf{x}) = \sum_{m=1}^{N} p_m(r_m) = \sum_{m=1}^{N} A_m \frac{\mathrm{e}^{ik_f r_m}}{r_m} \qquad \text{……. (4.4)}$$

From the pressure velocity relation, it is also possible to obtain the velocity in all three directions at **x** due to M number of point sources placed at **y.**

$$-\frac{\partial p}{\partial n} = \rho \frac{\partial v_n}{\partial t} = \pm i\omega\rho v_n \qquad \text{……. (4.5)}$$

Where, $\frac{\partial p}{\partial n}$ is the derivative of pressure along the direction *n*.

The velocity can be written as $v_n = \frac{1}{i\omega\rho} \frac{\partial p}{\partial n}$ ……. (4.6)

Therefore, the velocity in the radial direction, at a distance r from the m-th point source, is given by

$$v_m(r) = \frac{A_m}{i\omega\rho}\frac{\partial}{\partial r}\left(\frac{\exp(ik_f r)}{r}\right) = \frac{A_m}{i\omega\rho}\left(\frac{ik_f \exp(ik_f r)}{r} - \frac{\exp(ik_f r)}{r^2}\right) = \frac{A_m}{i\omega\rho}\frac{\exp(ik_f r)}{r}\left(ik_f - \frac{1}{r}\right) \quad \text{..... (4.7)}$$

and the three components of velocity are

$$v_{1m}(r) = \frac{A_m}{i\omega\rho}\frac{\partial}{\partial x_1}\left(\frac{\exp(ik_f r)}{r}\right) = \frac{A_m}{i\omega\rho}\frac{x_1 \exp(ik_f r)}{r^2}\left(ik_f - \frac{1}{r}\right) \quad \text{..... (4.8)}$$

$$v_{2m}(r) = \frac{A_m}{i\omega\rho}\frac{\partial}{\partial x_2}\left(\frac{\exp(ik_f r)}{r}\right) = \frac{A_m}{i\omega\rho}\frac{x_2 \exp(ik_f r)}{r^2}\left(ik_f - \frac{1}{r}\right) \quad \text{..... (4.9)}$$

$$v_{3m}(r) = \frac{A_m}{i\omega\rho}\frac{\partial}{\partial x_3}\left(\frac{\exp(ik_f r)}{r}\right) = \frac{A_m}{i\omega\rho}\frac{x_3 \exp(ik_f r)}{r^2}\left(ik_f - \frac{1}{r}\right) \quad \text{..... (4.10)}$$

When the contributions of all M sources are added, the total velocity in x_1, x_2 and x_3 directions at point **x** can be written as

$$v_1(\mathbf{x}) = \sum_{m=1}^{N} v_{1m}(r_m) = \sum_{m=1}^{N}\frac{A_m}{i\omega\rho}\frac{x_{1m}\exp(ik_f r_m)}{r_m^2}\left(ik_f - \frac{1}{r_m}\right) \quad \text{..... (4.11)}$$

$$v_2(\mathbf{x}) = \sum_{m=1}^{N} v_{2m}(r_m) = \sum_{m=1}^{N}\frac{A_m}{i\omega\rho}\frac{x_{2m}\exp(ik_f r_m)}{r_m^2}\left(ik_f - \frac{1}{r_m}\right) \quad \text{..... (4.12)}$$

$$v_3(\mathbf{x}) = \sum_{m=1}^{N} v_{3m}(r_m) = \sum_{m=1}^{N}\frac{A_m}{i\omega\rho}\frac{x_{3m}\exp(ik_f r_m)}{r_m^2}\left(ik_f - \frac{1}{r_m}\right) \quad \text{..... (4.13)}$$

Where, x_{im} is the shortest distance along x_i direction between the m^{th} point source and the target point, as shown in Figure 4.1(a). If the transducer surface is parallel to the x_1x_2-plane and its velocity in the x_3 direction is given by v_0 then for all **x** values on the transducer surface the velocity should be equal to v_0. Therefore,

$$v_3(\mathbf{x}) = \sum_{m=1}^{N} \frac{A_m}{i\omega\rho} \frac{x_{3m} \exp(ik_f r_m)}{r_m^2} \left(ik_f - \frac{1}{r_m} \right) = v_0 \qquad \text{..... (4.14)}$$

Special Case: Transducer Face is Inclined at an Angle of θ:

If the transducer face is inclined at an angle of θ, measured from x_3-axis when rotated about the x_2 axis **(Figure 4.2),** the velocity of the transducer face can be expressed as

$$\begin{aligned} v_3(x) &= v_1(\mathbf{x}) Sin\theta + v_3(\mathbf{x}) Cos\theta \\ &= \sum_{m=1}^{N} \frac{A_m}{i\omega\rho} \left(ik_f - \frac{1}{r_m} \right) \left(\frac{x_{1m} \exp(ik_f r_m)}{r_m^2} Sin\theta + \frac{x_{3m} \exp(ik_f r_m)}{r_m^2} Cos\theta \right) = v_0 \end{aligned} \qquad \text{..... (4.15)}$$

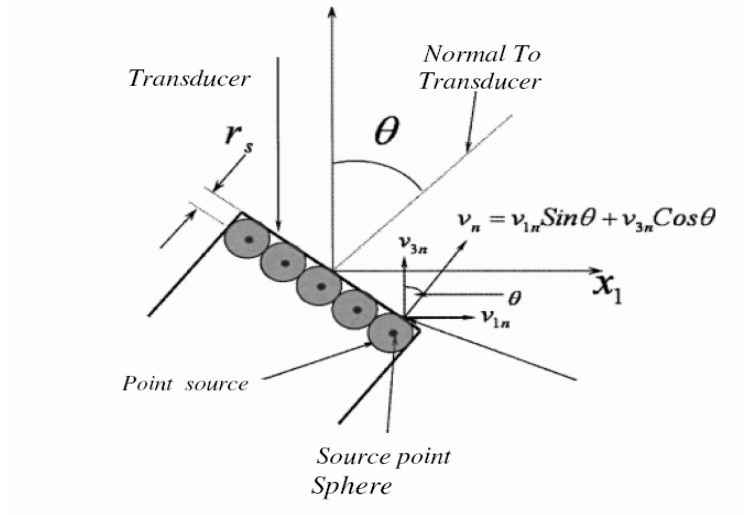

Figure.4.2 Rotation of the transducer with respect to x_3-axis and velocity of the n^{th} observation point adjacent to the transducer face

4.2 Matrix representation:

Velocity of the N target points placed on the transducer face due to point sources distributed just below the transducer surface at a distance r_s, can be written in matrix form as

$$\mathbf{V}_S = \mathbf{M}_{SS} \mathbf{A}_S \qquad \text{..... (4.16)}$$

where, $\mathbf{V}_S$ is the (Nx1) vector of the velocity components, perpendicular to the transducer surface. If the velocity of the transducer face is given by $v_{0,}$ then $\mathbf{V}_S$ can be written as:

$$\{\mathbf{V}_S\}^T = \begin{bmatrix} v_0^{\,1} & v_0^{\,2} & v_0^{\,3} & \dots & \dots & \dots & \dots & \dots & v_0^{\,N-1} & v_0^{\,N} \end{bmatrix}^T_{N\times 1} \qquad \dots\dots\dots (4.17)$$

where, v_0^n is the velocity of the *n*-th target point. If $\mathbf{A}_S$ is the (Nx1) vector of the source strengths, then

$$\{\mathbf{A}_S\}^T = \begin{bmatrix} A_1 & A_2 & A_3 & A_4 & A_5 & A_6 & \dots\dots\dots & A_{N-2} & A_{N-1} & A_N \end{bmatrix}^T \qquad \dots\dots\dots (4.18)$$

From the earlier discussion, we know that each point source is placed inside a sphere and hence, the number of apex points of the spheres touching the transducer surface will be the same as the number of point sources. When the target points are placed at the apex of the spheres of the point sources, then M is equal to N. Therefore, for the target points at the apex of the spheres of the point sources, the square matrix $\mathbf{M}_{SS}$ can be written as:

$$\mathbf{M}_{SS} = \begin{bmatrix} f\left(x_{t1}^1, r_1^1\right) & f\left(x_{t2}^1, r_2^1\right) & f\left(x_{t3}^1, r_3^1\right) & f\left(x_{t4}^1, r_4^1\right) & \dots & \dots & f\left(x_{tN-1}^1, r_{N-1}^1\right) & f\left(x_{tN}^1, r_N^1\right) \\ f\left(x_{t1}^2, r_1^2\right) & f\left(x_{t2}^2, r_2^2\right) & f\left(x_{t3}^2, r_3^2\right) & f\left(x_{t4}^2, r_4^2\right) & \dots & \dots & f\left(x_{tN-1}^2, r_{N-1}^2\right) & f\left(x_{tN}^2, r_N^2\right) \\ f\left(x_{t1}^3, r_1^3\right) & f\left(x_{t2}^3, r_2^3\right) & f\left(x_{t3}^3, r_3^3\right) & f\left(x_{t4}^3, r_4^3\right) & \dots & \dots & f\left(x_{tN-1}^3, r_{N-1}^3\right) & f\left(x_{tN}^3, r_N^3\right) \\ f\left(x_{t1}^4, r_1^4\right) & f\left(x_{t2}^4, r_2^4\right) & f\left(x_{t3}^4, r_3^4\right) & f\left(x_{t4}^4, r_4^4\right) & \dots & \dots & f\left(x_{tN-1}^4, r_{N-1}^4\right) & f\left(x_{tN}^4, r_N^4\right) \\ \dots & \dots & \dots & \dots & \dots & \dots & \dots & \dots \\ \dots & \dots & \dots & \dots & \dots & \dots & \dots & \dots \\ \dots & \dots & \dots & \dots & \dots & \dots & \dots & \dots \\ f\left(x_{t1}^N, r_1^N\right) & f\left(x_{t2}^N, r_2^N\right) & f\left(x_{t3}^N, r_3^N\right) & f\left(x_{t4}^N, r_4^N\right) & \dots & \dots & f\left(x_{tN-1}^N, r_{N-1}^N\right) & f\left(x_{tN}^N, r_N^N\right) \end{bmatrix}_{N\times N} \qquad (4.19)$$

where,

$$f\left(x_{tm}^n, r_m^n\right) = \frac{x_{tm}^n \exp(ik_f r_m^n)}{i\omega\rho\left(r_m^n\right)^2}\left(ik_f - \frac{1}{r_m^n}\right) = \frac{\exp(ik_f r_m^n)}{i\omega\rho\left(r_m^n\right)^2}\left(ik_f - \frac{1}{r_m^n}\right)\left(x_{3m}^n Cos\theta + x_{1m}^n Sin\theta\right) \quad (4.20)$$

and r_m^n is the distance between the *m*-th point source and the *n*-th target point.

Special Case: For large number of point sources

In Eq.(4.20) r_m^n appears in the denominator .Therefore for small values of r_m^n Eq.(4.20) can be simplified in the following manner.

$$f(x_{tm}^n, r_m^n) = \frac{x_{tm}^n \exp(ik_f r_m^n)}{i\omega\rho\left(r_m^n\right)^2}\left(ik_f - \frac{1}{r_m^n}\right) = \frac{x_{tm}^n \exp(ik_f r_m^n)}{i\omega\rho\left(r_m^n\right)^2}\left(-\frac{1}{r_m^n}\right) = -\frac{x_{tm}^n \exp(ik_f r_m^n)}{i\omega\rho\left(r_m^n\right)^3} \quad (4.21)$$

Note that all spheres have the same radius $r_m = r_s = r$, and therefore $x_{tm}^n = r$ .substituting in the above expression and expanding the exponential term in the series expansion we get

$$f(x_{tm}^n, r_m^n) = -\frac{x_{tm}^n \exp(ik_f r_m^n)}{i\omega\rho\left(r_m^n\right)^3} = -\frac{r}{i\omega\rho\left(r_m^n\right)^3}\left(1 + ik_f r_m^n + ...\right) = -\frac{r}{i\omega\rho\left(r_m^n\right)^3} \quad (4.22)$$

For $m = n, \quad r_m^n = r_m^m = r$, substituting it in above equation, we get

$$f(x_{tm}^n, r_m^n) \approx -\frac{r}{i\omega\rho\left(r_m^n\right)^3} \approx -\frac{r}{i\omega\rho r^3} \approx -\frac{1}{i\omega\rho r^2} \quad \text{..... (4.23)}$$

Substitution of above two equations yields

$$M_{SS} = -\frac{1}{i\omega\rho r^2}\begin{bmatrix} 1 & \left(\frac{r}{r_2^1}\right)^3 & \left(\frac{r}{r_3^1}\right)^3 & \dots & \left(\frac{r}{r_N^1}\right)^3 \\ \left(\frac{r}{r_1^2}\right)^3 & 1 & \left(\frac{r}{r_3^2}\right)^3 & \dots & \left(\frac{r}{r_N^2}\right)^3 \\ \left(\frac{r}{r_1^3}\right)^3 & \left(\frac{r}{r_2^3}\right)^3 & 1 & \dots & \left(\frac{r}{r_N^3}\right)^3 \\ \dots & \dots & \dots & \dots & \dots \\ \left(\frac{r}{r_1^N}\right)^3 & \left(\frac{r}{r_2^N}\right)^3 & \left(\frac{r}{r_3^N}\right)^3 & \dots & 1 \end{bmatrix}_{N\times N} \quad \text{..... (4.24)}$$

For a general set of target points located on any surface, the velocity due to the transducer sources can be written as:

$$\mathbf{V}_T = \mathbf{M}_{TS}\mathbf{A}_S \quad \text{..... (4.25)}$$

where $\mathbf{V}_T$, the velocity vector (Nx1) contains the normal velocity components of the target points distributed on the surface. The matrix $\mathbf{M}_{TS}$ has elements that are similar to those of $\mathbf{M}_{SS}$, with different x_{tm}^n values and the size of the matrix is (MxN), where N is the number of target points and M is the number of source points. Following the same

concept, the pressure at any N number of target points due to M number of source points can be written as:

$$\underline{\mathbf{PR}}_T = \mathbf{Q}_{TS}\mathbf{A}_S \qquad \text{……. (4.26)}$$

Where, $\underline{\mathbf{PR}}_T$ is the (Nx1) vector of pressure values at N target points, and $\mathbf{Q}_{TS}$ is a (NxM) matrix given below

$$\mathbf{Q}_{TS} = \begin{bmatrix} \frac{\exp\left(ik_f r_1^1\right)}{r_1^1} & \frac{\exp\left(ik_f r_2^1\right)}{r_2^1} & \frac{\exp\left(ik_f r_3^1\right)}{r_3^1} & \cdots & \cdots & \frac{\exp\left(ik_f r_M^1\right)}{r_M^1} \\ \frac{\exp\left(ik_f r_1^2\right)}{r_1^2} & \frac{\exp\left(ik_f r_2^2\right)}{r_2^2} & \frac{\exp\left(ik_f r_3^2\right)}{r_3^2} & \cdots & \cdots & \frac{\exp\left(ik_f r_M^2\right)}{r_M^2} \\ \frac{\exp\left(ik_f r_1^3\right)}{r_1^3} & \frac{\exp\left(ik_f r_3^2\right)}{r_2^3} & \frac{\exp\left(ik_f r_3^3\right)}{r_3^3} & \cdots & \cdots & \frac{\exp\left(ik_f r_M^3\right)}{r_M^3} \\ \cdots & \cdots & \cdots & \cdots & \cdots & \cdots \\ \cdots & \cdots & \cdots & \cdots & \cdots & \cdots \\ \frac{\exp\left(ik_f r_1^N\right)}{r_1^N} & \frac{\exp\left(ik_f r_2^N\right)}{r_2^N} & \frac{\exp\left(ik_f r_3^N\right)}{r_3^N} & \cdots & \cdots & \frac{\exp\left(ik_f r_M^N\right)}{r_M^N} \end{bmatrix}_{M\times N} \qquad (4.27)$$

When the target points are located at the apex of the spheres of the point sources, Equation (4.26) takes the form,

$$\underline{\mathbf{PR}}_S = \mathbf{Q}_{SS}\mathbf{A}_S \qquad \text{……. (4.28)}$$

where, $\mathbf{Q}_{SS}$ is a (NxN) matrix.

The definition of r_m^n is identical to that given in Equation (4.20). It is the distance between the *m*-th point source and the *n*-th target point.

In the same manner, the matrix expression for displacements at general target points in the fluid can be written as:

$$\mathbf{U1}_T = \mathbf{DF1}_{TS}\mathbf{A}_S \qquad \text{……. (4.29)}$$

$$\mathbf{U2}_T = \mathbf{DF2}_{TS}\mathbf{A}_S \qquad \text{……. (4.30)}$$

$$\mathbf{U3}_T = \mathbf{DF3}_{TS}\mathbf{A}_S \qquad \text{……. (4.31)}$$

where

$$\mathbf{DF}i_{TS} = \begin{bmatrix} g(R_{i1}^1, r_1^1) & g(R_{i2}^1, r_2^1) & g(R_{i3}^1, r_3^1) & \dots & g(R_{iM-1}^1, r_{M-1}^1) & g(R_{iM}^1, r_M^1) \\ g(R_{i1}^2, r_1^2) & g(R_{i2}^2, r_2^2) & g(R_{i3}^2, r_3^2) & \dots & g(R_{iM-1}^2, r_{M-1}^2) & g(R_{iM}^2, r_M^2) \\ g(R_{i1}^3, r_1^3) & g(R_{i2}^3, r_2^3) & g(R_{i3}^3, r_3^3) & \dots & g(R_{iM-1}^3, r_{M-1}^3) & g(R_{iM}^3, r_M^3) \\ g(R_{i1}^4, r_1^4) & g(R_{i2}^4, r_2^4) & g(R_{i3}^4, r_3^4) & \dots & g(R_{iM-1}^4, r_{M-1}^4) & g(R_{iM}^4, r_M^4) \\ \dots & \dots & \dots & \dots & \dots & \dots \\ g(R_{i1}^N, r_1^N) & g(R_{i2}^N, r_2^N) & g(R_{i3}^N, r_3^N) & \dots & g(R_{iM-1}^N, r_{M-1}^N) & g(R_{iM}^N, r_M^N) \end{bmatrix}_{(NxM)} \quad (4.32)$$

where $g(R_{im}^n, r_m^n) = \dfrac{1}{\rho\omega^2}\left[\dfrac{1}{r_m^n} ik_f R_{im}^n e^{ik_f r_m^n} - \dfrac{e^{ik_f r_m^n}}{\left(r_m^n\right)^2} R_{im}^n\right]$ ..... (4.33)

$$R_{im}^n = \frac{x_{im}^n - y_{im}^n}{r_m^n} \quad \text{and } i = 1,2,3$$

In this chapter through mathematical expressions it is shown how the ultrasonic fields such a pressure, displacement fields and velocity fields are generated in Homogenous fluids using DPSM method.

CHAPTER 5

Ultrasonic Field Modeling in Layered Fluids (or) Non-Homogeneous Media using –DPSM Technique

5.1 Introduction:

We are interested in computing the ultrasonic field in multilayered fluid systems. In the multilayered problem geometry several interfaces may be present. When fluids with different densities and acoustic properties form a multilayered system, the fluid density should monotonically vary from top to bottom. If we have 'n' number of fluids in the system, we should have (n-1) number of interfaces. Each interface acts as a transmitter as well as a reflector of elastic wave energy generated by the ultrasonic transducers. When the entire system is considered, several continuity conditions across the interfaces and boundary conditions at the transducer surface are to be satisfied.

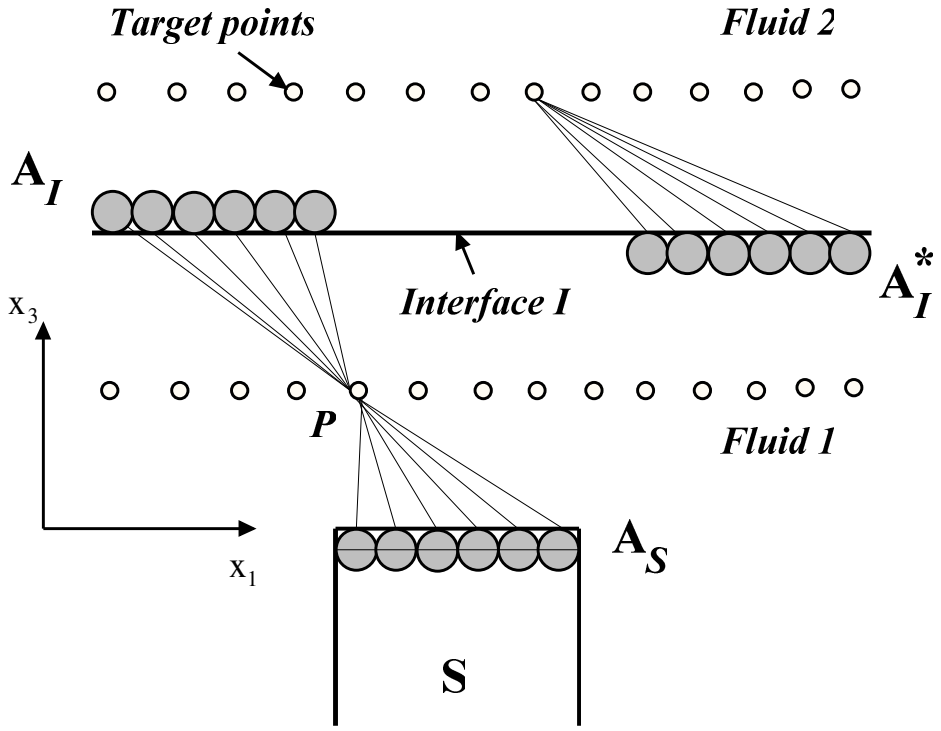

Figure.5.1 Distribution of point sources in the layered fluid system

Let the transducer be immersed in a fluid medium consisting of two fluids, with a plane interface between two fluids located in front of the transducer, as shown in

Figure.5.1. We can introduce three layers of point sources A_S , A_I and A_I^*, as shown in the **Figure.5.1** to model the incident field, reflected field and transmitted field, respectively. The sources with source strength A_I generate the ultrasonic field in the fluid below it and the sources with source strength A_I * generate the ultrasonic field in the fluid above it. Observation points or target points are shown by open small circles in the **Figure.5.1.**The total ultrasonic field in each medium is obtained by superimposing the fields generated by two sets of sources as listed below:

Fluid 1: Summation of fields generated by A_S and A_I .

$$P_T = Q_{TS} A_S + Q_{TI} A_I \quad \text{..... (5.1)}$$

$$V_T = M_{TS} A_S + M_{TI} A_I \quad \text{..... (5.2)}$$

Fluid 2: Fields generated by A_I *

$$P_T = Q_{TI}^* A_I^* \quad \text{..... (5.3)}$$

$$V_T = M_{TI}^* A_I^* \quad \text{..... (5.4)}$$

5.2 Methods for Finding Source Strength vectors:

5.2.1 Computation of the source strength vectors when multiple reflections between the transducer and the interface are ignored:

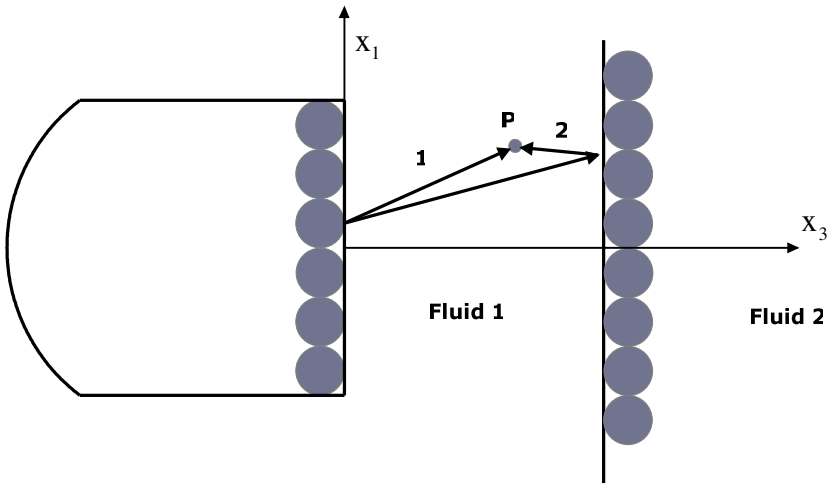

Figure 5.2: Point P can receive two rays, 1 (direct ray) and 2 (reflected from interface) from a single point source.

As shown in **Figure 5.2**, two rays can reach the point **P** that is located close to the interface, first one is the direct ray denoted by ray 1 and the second one is ray 2, which first propagates from the transducer to the interface, is reflected by the interface and then reaches point **P.** The pressure fields due to rays 1 and 2 are modeled by $Q_{TS}A_S$ and $Q_{TI}A_I$ expressions, respectively. Note that pressure field generated by ray 2 can be alternately obtained by the first multiplying the elements of Q_{TS} terms by appropriate reflection coefficient, thus forming Q_{TS}^R matrix given in Eq. (5.5) and then multiplying this matrix with A_S vector.

$$\mathbf{Q}_{TS}^R = \begin{bmatrix} R(\theta_1^1)\frac{\exp(ik_f r_1^1)}{r_1^1} & R(\theta_2^1)\frac{\exp(ik_f r_2^1)}{r_2^1} & R(\theta_3^1)\frac{\exp(ik_f r_3^1)}{r_3^1} & \dots & \dots & R(\theta_M^1)\frac{\exp(ik_f r_M^1)}{r_M^1} \\ R(\theta_1^2)\frac{\exp(ik_f r_1^2)}{r_1^2} & R(\theta_2^2)\frac{\exp(ik_f r_2^2)}{r_2^2} & R(\theta_3^2)\frac{\exp(ik_f r_3^2)}{r_3^2} & \dots & \dots & R(\theta_M^2)\frac{\exp(ik_f r_M^2)}{r_M^2} \\ R(\theta_1^3)\frac{\exp(ik_f r_1^3)}{r_1^3} & R(\theta_2^3)\frac{\exp(ik_f r_2^3)}{r_2^3} & R(\theta_3^3)\frac{\exp(ik_f r_3^3)}{r_3^3} & \dots & \dots & R(\theta_M^3)\frac{\exp(ik_f r_M^3)}{r_M^3} \\ \dots & \dots & \dots & \dots & \dots & \dots \\ \dots & \dots & \dots & \dots & \dots & \dots \\ R(\theta_1^N)\frac{\exp(ik_f r_1^N)}{r_1^N} & R(\theta_2^M)\frac{\exp(ik_f r_2^N)}{r_2^N} & R(\theta_3^N)\frac{\exp(ik_f r_3^N)}{r_3^N} & \dots & \dots & R(\theta_M^N)\frac{\exp(ik_f r_M^N)}{r_M^N} \end{bmatrix}_{M\times N} \quad (5.5)$$

where θ_m^n denotes the angle of incidence at the interface of the ray traveling from the m^{th} point source on the transducer surface to the n^{th} target point close to the interface .The reflection coefficient $R(\theta_m^n)$ for the angle of incidence θ_m^n is obtained from the following equation.

$$R(\theta) = \frac{\rho_2 c_{f2}\cos(\theta) - \rho_1 c_{f1}\left\{1 - \frac{c_{f2}^2}{c_{f1}^2} + \frac{c_{f2}^2}{c_{f1}^2}\cos^2(\theta)\right\}^{\frac{1}{2}}}{\rho_2 c_{f2}\cos(\theta) + \rho_1 c_{f1}\left\{1 - \frac{c_{f2}^2}{c_{f1}^2} + \frac{c_{f2}^2}{c_{f1}^2}\cos^2(\theta)\right\}^{\frac{1}{2}}} \quad \dots\dots (5.6)$$

Because the pressure field generated by $Q_{TI}A_I$ and $Q_{TS}^R A_S$ should be same

$$Q_{TI}A_I = Q_{TS}^R A_S \quad \dots\dots (5.7)$$

$$\Rightarrow A_I = [Q_{TI}]^{-1} Q_{TS} A_S \quad \dots\dots (5.8)$$

From the above equation A_I can be obtained after knowing A_S .

In the same manner A_I^* can be computed by equating the pressure fields generated to rays traveling from A_I^* sources directly to the target points in fluid 2 and from A_S sources after being transmitted at the interface.

$$Q_{TI}^* A_I^* = Q_{TS}^T A_S \qquad \ldots\ldots\ldots (5.9)$$

$$\Rightarrow A_I^* = [Q_{TS}^*]^{-1} Q_{TS}^T A_S \qquad \ldots\ldots\ldots (5.10)$$

$$\mathbf{Q}_{TS}^T = \begin{bmatrix} T(\theta_1^1)\frac{\exp(ik_f r_1^1)}{r_1^1} & T(\theta_2^1)\frac{\exp(ik_f r_2^1)}{r_2^1} & T(\theta_3^1)\frac{\exp(ik_f r_3^1)}{r_3^1} & \ldots & \ldots & T(\theta_M^1)\frac{\exp(ik_f r_M^1)}{r_M^1} \\ T(\theta_1^2)\frac{\exp(ik_f r_1^2)}{r_1^2} & T(\theta_2^2)\frac{\exp(ik_f r_2^2)}{r_2^2} & T(\theta_3^2)\frac{\exp(ik_f r_3^2)}{r_3^2} & \ldots & \ldots & T(\theta_M^2)\frac{\exp(ik_f r_M^2)}{r_M^2} \\ T(\theta_1^3)\frac{\exp(ik_f r_1^3)}{r_1^3} & T(\theta_2^3)\frac{\exp(ik_f r_2^3)}{r_2^3} & T(\theta_3^3)\frac{\exp(ik_f r_3^3)}{r_3^3} & \ldots & \ldots & T(\theta_M^3)\frac{\exp(ik_f r_M^3)}{r_M^3} \\ \ldots & \ldots & \ldots & \ldots & \ldots & \ldots \\ \ldots & \ldots & \ldots & \ldots & \ldots & \ldots \\ T(\theta_1^N)\frac{\exp(ik_f r_1^N)}{r_1^N} & T(\theta_2^M)\frac{\exp(ik_f r_2^N)}{r_2^N} & T(\theta_3^N)\frac{\exp(ik_f r_3^N)}{r_3^N} & \ldots & \ldots & T(\theta_M^N)\frac{\exp(ik_f r_M^N)}{r_M^N} \end{bmatrix}_{M\times N} \qquad (5.11)$$

The transmission coefficient $T(\theta_m^n)$ for the angle of incidence θ_m^n is obtained from the following equation.

$$T(\theta) = \frac{2\rho_2 c_{f2}\cos\theta}{\rho_2 c_{f2}\cos\theta + \rho_1 c_{f1}\left\{1 - \frac{c_{f2}^2}{c_{f1}^2} + \frac{c_{f2}^2}{c_{f1}^2}\cos^2(\theta)\right\}^{\frac{1}{2}}} \qquad \ldots\ldots\ldots (5.12)$$

5.2.2 Computation of the source strength vectors considering the interaction effects between the transducer and the interface: In this case A_S, A_I *and* A_I^* are to be computed simultaneously by satisfying the given boundary conditions on the transducer surface and continuity conditions across the interface. If the transducer surface velocity is defined as V_{SO}, then the velocity at the transducer surface computed from sources A_S *and* A_I should be equal to V_{SO}; therefore,

On the transducer surface

$$\mathbf{M}_{SS}\mathbf{A}_S + \mathbf{M}_{SI}\mathbf{A}_I = \mathbf{V}_{S0} \qquad \ldots\ldots\ldots (5.13)$$

On the interface, from the continuity of the normal stress,

$$\mathbf{Q}_{IS}\mathbf{A}_S + \mathbf{Q}_{II}\mathbf{A}_I = Q^*_{II}\mathbf{A}^*_I \quad \ldots\ldots\ldots (5.14)$$

$$M_{IS}A_S + M_{II}A_I = M^*_{II}A^*_I \quad \ldots\ldots\ldots (5.15)$$

Equations (5.13) to (5.15) can be written in matrix form

$$\begin{bmatrix} M_{SS} & M_{SI} & 0 \\ Q_{IS} & Q_{II} & -Q^*_{II} \\ M_{IS} & M_{II} & -M^*_{II} \end{bmatrix}_{3M\times 3M} \begin{bmatrix} \mathbf{A}_S \\ \mathbf{A}_I \\ \mathbf{A}_I{}^* \end{bmatrix}_{3M\times 1} = \begin{bmatrix} \mathbf{V}_{S0} \\ \mathbf{0} \\ \mathbf{0} \end{bmatrix}_{3M\times 1} \quad \ldots\ldots\ldots (5.16)$$

$$\text{or,} \qquad [\mathbf{MAT}]\{\mathbf{\Lambda}\} = \{\mathbf{V}\} \quad \ldots\ldots\ldots (5.17)$$

The vector of source strengths of the total system can be calculated by taking inverse of $[\mathbf{MAT}]$ and multiplying it with the vector $\{\mathbf{V}\}$,

$$\{\mathbf{\Lambda}\} = [\mathbf{MAT}]^{-1}\{\mathbf{V}\} \quad \ldots\ldots\ldots (5.18)$$

Among these two methods ray tracing method is easy to use and most promising results are coming from this method compared to the matrix inversion method. So entire non-homogenous fields are modeled using ray tracing method.

5.3 Obtaining the Ultrasonic fields after knowing the source strength vectors:

After calculating the source strengths, the pressure, velocity, displacement values at any point in fluid 1 can be obtained by the following equations:

Pressure Field: $$PR_{(F)} = Q_{(F)S}A_S + Q_{(F)I}A_I \quad \ldots\ldots\ldots (5.19)$$

Velocity Field: $$V_{(F)} = M_{(F)S}A_S + M_{(F)S}A_I \quad \ldots\ldots\ldots (5.20)$$

Displacement Field: $$U3_{(F)} = DF3_{(F)S}A_S + DF3_{(F)I}A_I \quad \ldots\ldots\ldots (5.21)$$

For example, the pressure field at the target point 'P' in the fluid 1 as shown in the **figure 5.2** can be written as:

$$PR_P = Q_{PS}A_S + Q_{PI}A_I \quad \ldots\ldots\ldots (5.22)$$

In this chapter it shown how DPSM method is used to develop ultrasonic fields generated in Non-Homogenous fluids.

CHAPTER 6

Numerical Results and Discussions

MATHCAD programs have been developed to model the ultrasonic field based on the DPSM formulation presented above. In the simplest case, the transducer is immersed in homogenous fluid. More complex problem geometries involve two fluids with a plane interface. The numerical results clearly show how the ultrasonic field decays as the distance from the transducer increases and the field becomes more collimated as the size of the transducer increase. Following two separate cases have been studied

Case 1: *Wave Propagation in Homogenous Fluid:* In this case single fluid is used to study generated Ultrasonic field .Here both steady and Transient Wave propagation is studied.

Name of Fluid	Density (gm/cc)	P-Wave Speed (C_p) (Km/sec)
Water ($20°C$)	1	1.49

Case 2: *Wave Propagation in Non-Homogenous Fluid:* In this case two layers of fluids are arranged such that their density monotonically increases from bottom to top and Transient wave propagation is studied in this.

Name of Fluid	Density (gm/cc)	P-Wave Speed (C_p) (Km/sec)
Fluid 1	1	1.49
Fluid 2	1.5	2.00

For convenience from now onwards the X_1 axis is called the 'X' axis and X_3 axis is called the 'Z' axis.

6.1 Method used for Finding Source point Coordinates:

Before writing the MathCAD programs Center Point Coordinates of the Points sources must be obtained. For getting them AutoCAD drawings are made according to the given dimensions of the Transducer and number of point sources .The center point coordinates of all the point sources are then exported from AutoCAD in to an excel file and this data is fed to MathCAD programs. For example **figure (6.1)** shows a Transducer having 133 points sources and shows plot of **figure (6.2)** extracted data of point sources distributed on flat circular Transducer. Similarly **figure (6.3)** and **figure (6.4)** shows the same for 348 point sources for the transducer of same diameter.

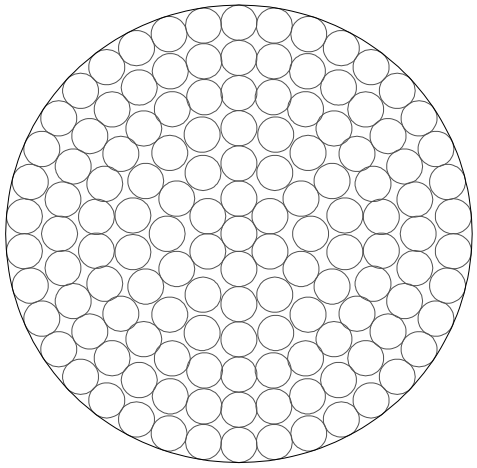

Dia.of Transducer =0.1inch
No. of point sources=133
Dia of source point sphere=0.016cm

Figure .6.1: AUTOCAD drawing showing polar array of 133 point sources

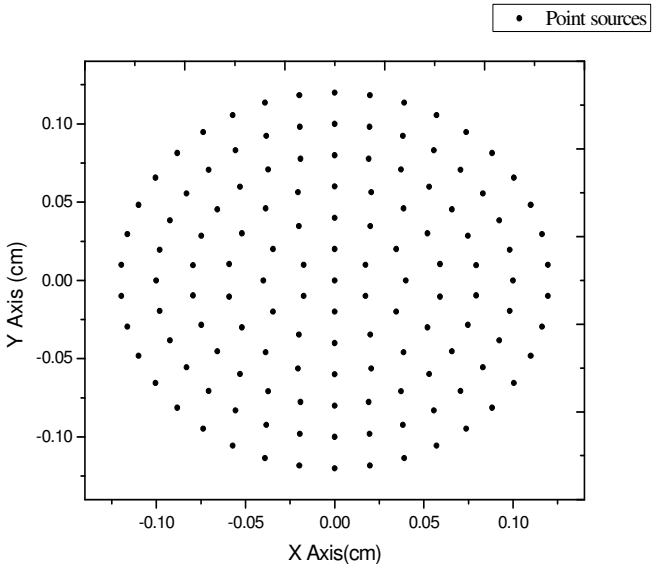

Figure.6.2: Distribution of 133 Point sources on the face of flat circular Transducer

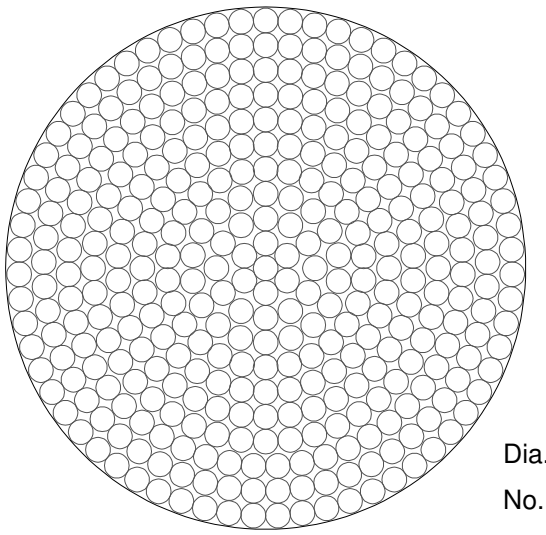

Figure.6.3: AUTOCAD drawing showing polar array of 348 point sources

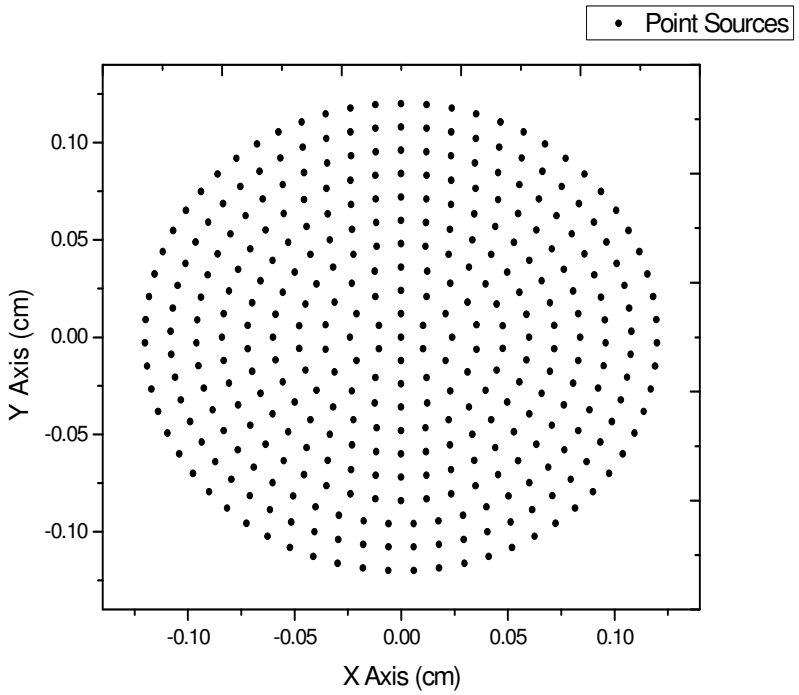

Figure.6.4: Distribution of 348 Point sources on the face of flat circular Transducer

6.2 Ultrasonic Field in a Homogenous Fluid-DPSM technique:

6.2.1 Steady wave propagation in Homogenous fluid:

Following the DPSM technique described in previous chapters, the ultrasonic field generated in a homogeneous fluid (water) by a flat circular transducer is computed. For such simple problem geometry the expression of the near field zone length and the divergence angle of the emitted beam can be calculated in closed form (Kundu, 2000). Numerically computed values of these two parameters are compared with the closed form analytical values to check the accuracy of the numerical results. From Kundu (2000),

$$N_F = \frac{D^2}{4\lambda} \quad for\ \lambda \square\ D \tag{6.1}$$

where N_F is near field length. The analytical expression of the pressure in a homogeneous fluid along the central axis of a circular transducer is (Placko and Kundu, 2003)

$$p(Z) = \rho.c_f v_0 \left[\exp(ik_f Z) - \exp(ik_f \sqrt{Z^2 + a^2}\,) \right] \tag{6.2}$$

Figure 6.5 and **Figure 6.6** shows acoustic pressure variations for the DPSM modeling of 133 point sources (1 MHz and 5 MHz signal frequencies) and 348 point sources (1 MHz and 5 MHz signal frequencies) along the central axis (Z axis) of a circular transducer computed by the DPSM technique described above (dashed curve) and the analytical expression [Eq. (6.2), solid curve]. Coordinate Z is measured from the transducer face. The transducer area is 5.02mm^2, its diameter (D) = 2.528 mm. For example DPSM modeling for 348 sources is made by locating all of them at Z= - r_s, while the transducer face is at Z = 0. For this problem geometry

$$r_s = \sqrt{\frac{\pi D^2}{4 \times 2\pi N}}. = \frac{D}{\sqrt{8N}} = \frac{2.528}{8 \times 348} = 0.04791mm \tag{6.3}$$

Figure 6.5 shows that for 133 point sources DPSM curve is closely moving above the EXACT curve but there is no well match with it. **Figure 6.6** shows that with 348 point sources DPSM result match well with exact solution. Hence it can be concluded that as the number of point sources increases accuracy of DPSM increases. As the waves speed in the surrounding fluid is 1.49 km/sec, wave length λ is equal to 0.298 mm for 5 MHz signal. From Eq.(6.1) N_F is found to be 5.3mm that matches with last peak obtained numerically as shown in **figure (6.6).**

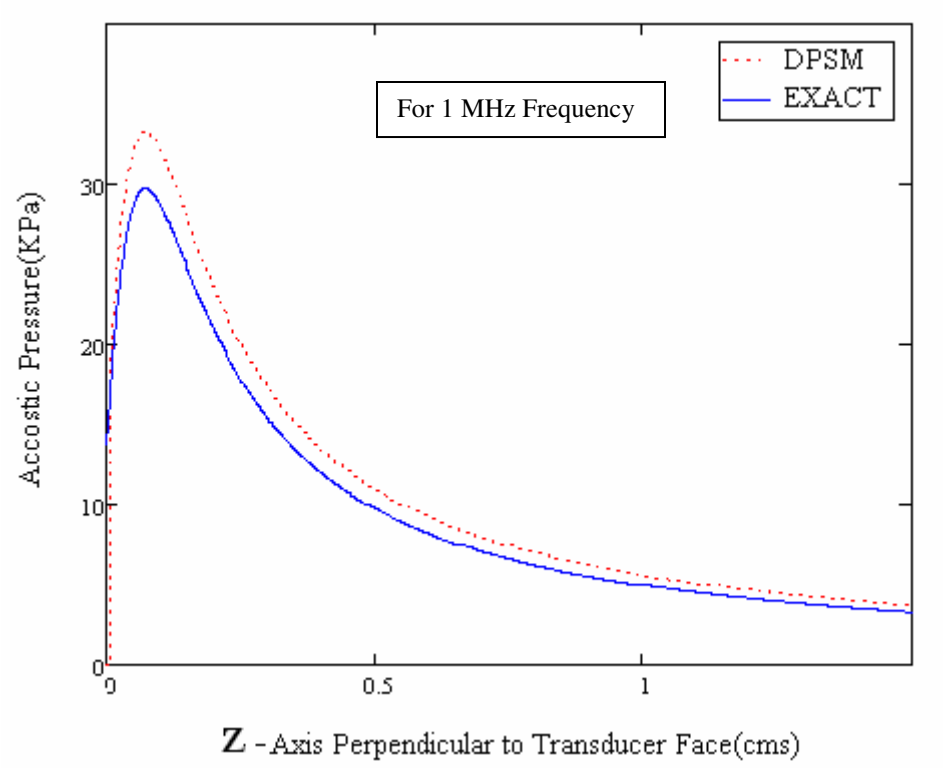

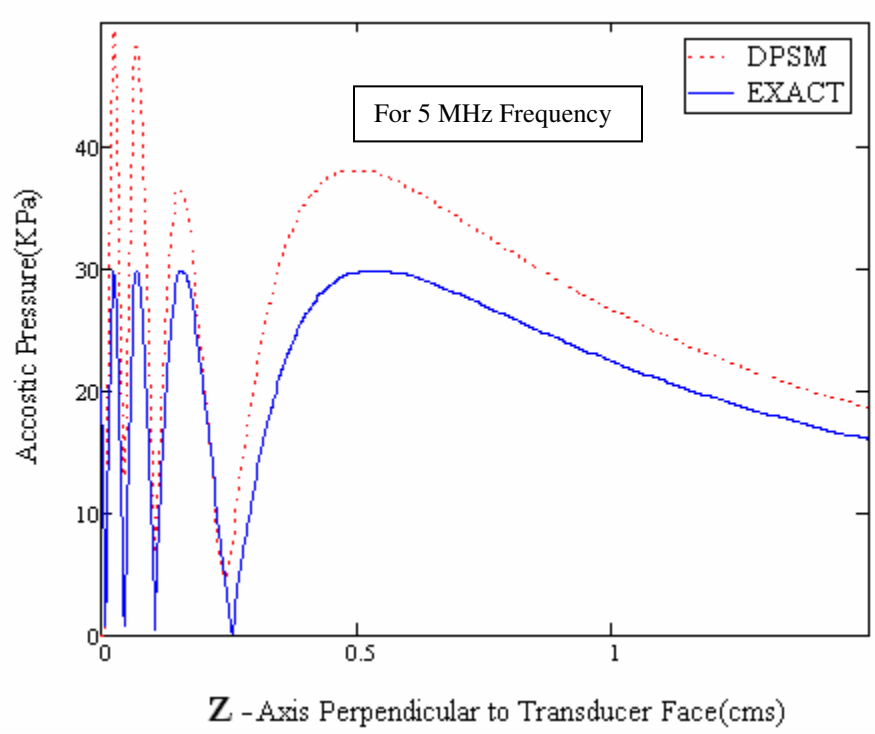

Figure.6.5: Acoustic Pressure Variation for 133 point sources along Z axis Perpendicular to Transducer Face.

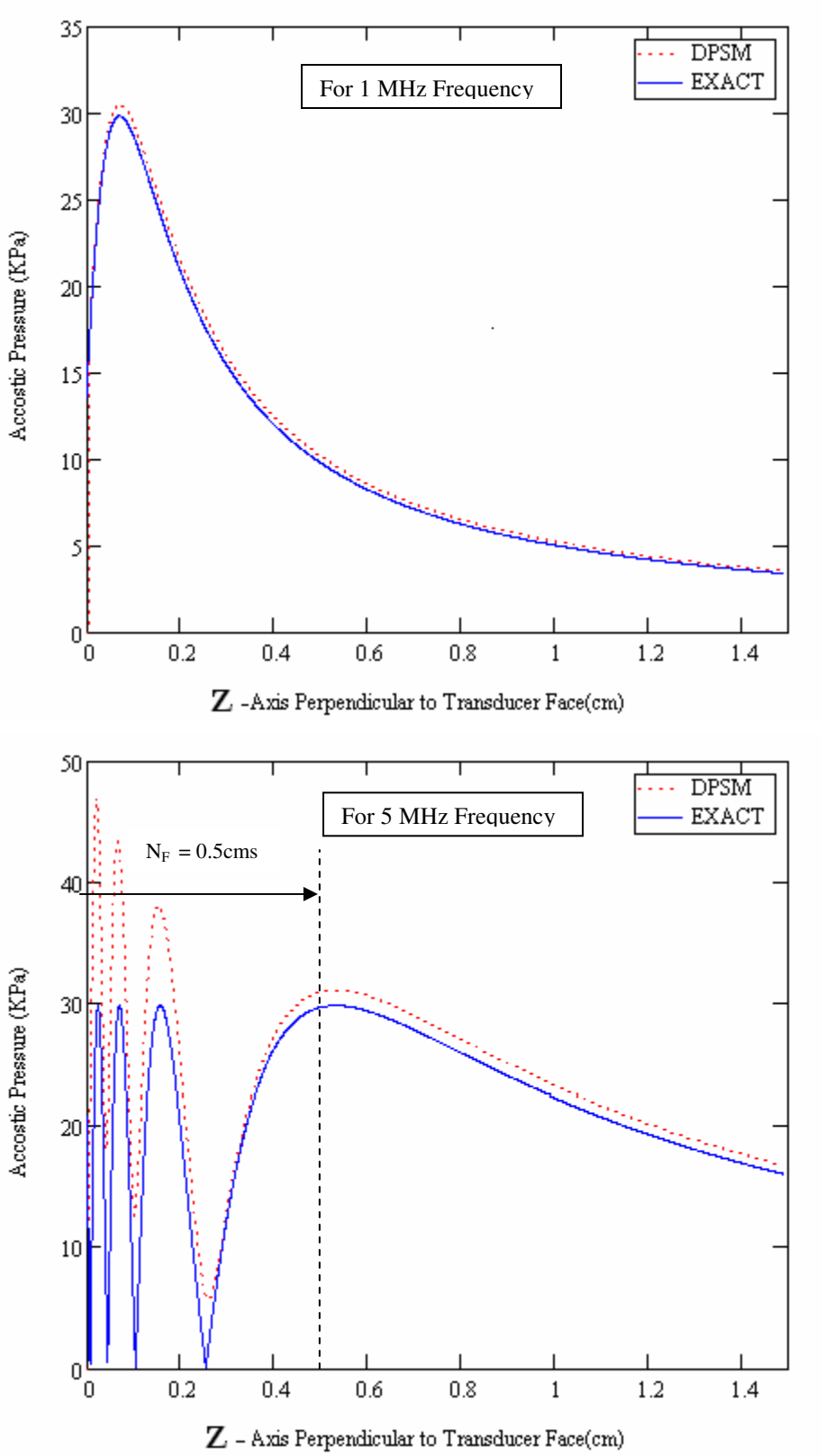

Figure 6.6*:* Acoustic Pressure Variation for 348 point sources along Z axis Perpendicular to Transducer Face.

6.2.2 Transient Wave Propagation in homogenous Fluid:

Same steady state model is used to predict transient wave propagation in homogeneous fluid. Fast Fourier transform (FFT) is used to convert time domain impulse into frequency domain pulse. Then for each frequency, DPSM method is applied and obtained response is again transformed to time domain using inverse Fourier transforms (IFFT). Frequencies up to Nyquist frequencies are used for analysis and effect of remaining frequencies are taken care by superimposing antisymmetry behavior of imaginary part about Nyquist frequency. **Figure 6.8** shows the flowchart for reconstruction of transient wave program in homogenous fluid using DPSM techniques.

For non-homogeneous fluid case same flowchart is applicable only changes to be made are matrix '***Mss*** 'is replaced by '***MAT***" as per equation (5.18) and appropriate velocity vector '***V'*** depending upon the location of transducer with respect to interfaces.

Figure 6.7 shows variation of acoustic pressure at transducer face verses input signal frequency. In this graph variation of acoustic pressure at three different locations (i.e. center, half radius and periphery of circular transducer) is plotted and it is clear that variation of Acoustic pressure at center of transducer seems to be sensitive with change in input signal frequency compared to that of acoustic pressure near the periphery of transducer surface. Due to this reason rest of the analysis is done about center of transducer.

Same model is used to study the response of various input impulses and results are presented from **Figure. 6.9** To **Figure 6.18.** They are

- Half sine wave pulse as shown in **Figure.6.9** is applied as velocity input at transducer face and ultrasonic field response in terms of acoustic pressure, displacement and velocity at transducer centre are presented in **Figure 6.10**.Displacement response does not attenuate completely in given time window and hence the plot show typical leakage problem. This problem can be eliminated by proper selection of window instead of rectangular window.
- **Figure 6.11** shows the input full sine wave velocity pulse and **Figure.6.12** shows its acoustic field response. As the wave completes full cycle, all responses (velocity, pressure and displacement) get attenuated within given time window.
- **Figure.6.13** and **Figure.6.14** shows the input positive spike pulse and ultrasonic wave response for half triangular input pulse (positive spike).

- **Figure.6.15** and **Figure.6.16** shows input triangular pulse and ultrasonic wave response for triangular input pulse.
- **Figure.6.18** shows ultrasonic wave response for tone burst signal.

It can be seen from **Figures 6.10, 6.12, 6.14, 6.16, 6.18** that for various input impulses, tone burst input pulse seems to be better than others as response peaks can be distinctly identified in this case. The reason may be that the energy entered and get removed from system smoothly. The same input pulse is used for further study of transient wave propagation in homogeneous and non-homogeneous fluids. **Figure 6.17** show the tone burst signal in time domain and it's FFT.

Figure 6.19((a), (b), (c)) shows the acoustic pressure at three different target points lying along Z-axis of transducer face. Transducer is immersed in homogeneous fluid having density (ρ) =1 gm/cc and wave speed is (C_f) = 1.49 km/sec.

- For point close to transducer face (Z= 0) acoustic wave pressure peak lies around 95 μ-sec as shown in **figure 6.19(a)** with markers, same as the input velocity pulse peak time as shown in **figure 6.17 (a).**
- Acoustic pressure pulse response at target point 2 at a distance of 50 mm from Transducer face shows that a peak arrives at 128 μ-sec as shown in the **figure 6.19(b)**(having time lag R1 = 33 μ-sec) .
- Similarly for third point at a distance 150 mm from transducer face, pressure peak reaches at time 195 μ-sec as shown in the **figure 6.19(c)** (having time lag R2 = 100 μ-sec).

These time lags are matching with the actual time required for wave to travel above two distances (50mm and 150 mm) as shown in the table of time validation given below.

Also the pressure amplitudes are matching with the close form solution as shown in the table of amplitude validation shown below. These two checks validate the transient wave propagation model result.

Time Validation:

$$Distance\ Travelled\ by\ the\ wave = Velocity\ of\ \ wave(C_f) \times Time\ taken\ to\ travel$$

Method	Z=50mm	Z=150mm
Analytical(formula)	33.55 μ-secs	100.67 μ-secs
DPSM (graph)	33 μ-secs	100 μ-secs

Pressure amplitude validation:

Closed form (Exact) solution: $p(x_3) = \rho.c_f v_0 \left[\exp(ik_f x_3) - \exp(ik_f \sqrt{x_3^2 + a^2}\right]$

Method	Z=50mm	Z=150mm
Exact solution	0.1013 KPa	0.0334 KPa
DPSM (graph)	0.0906 KPa	0.0303 KPa

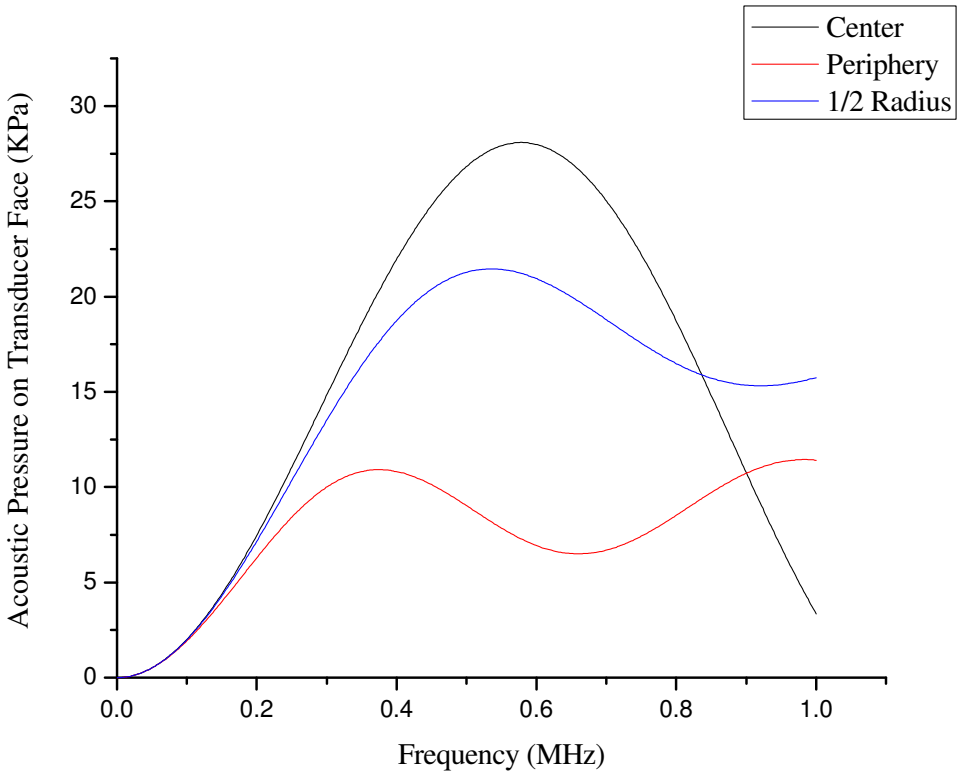

Figure 6.7: Plot showing Acoustic pressure variation Vs frequency

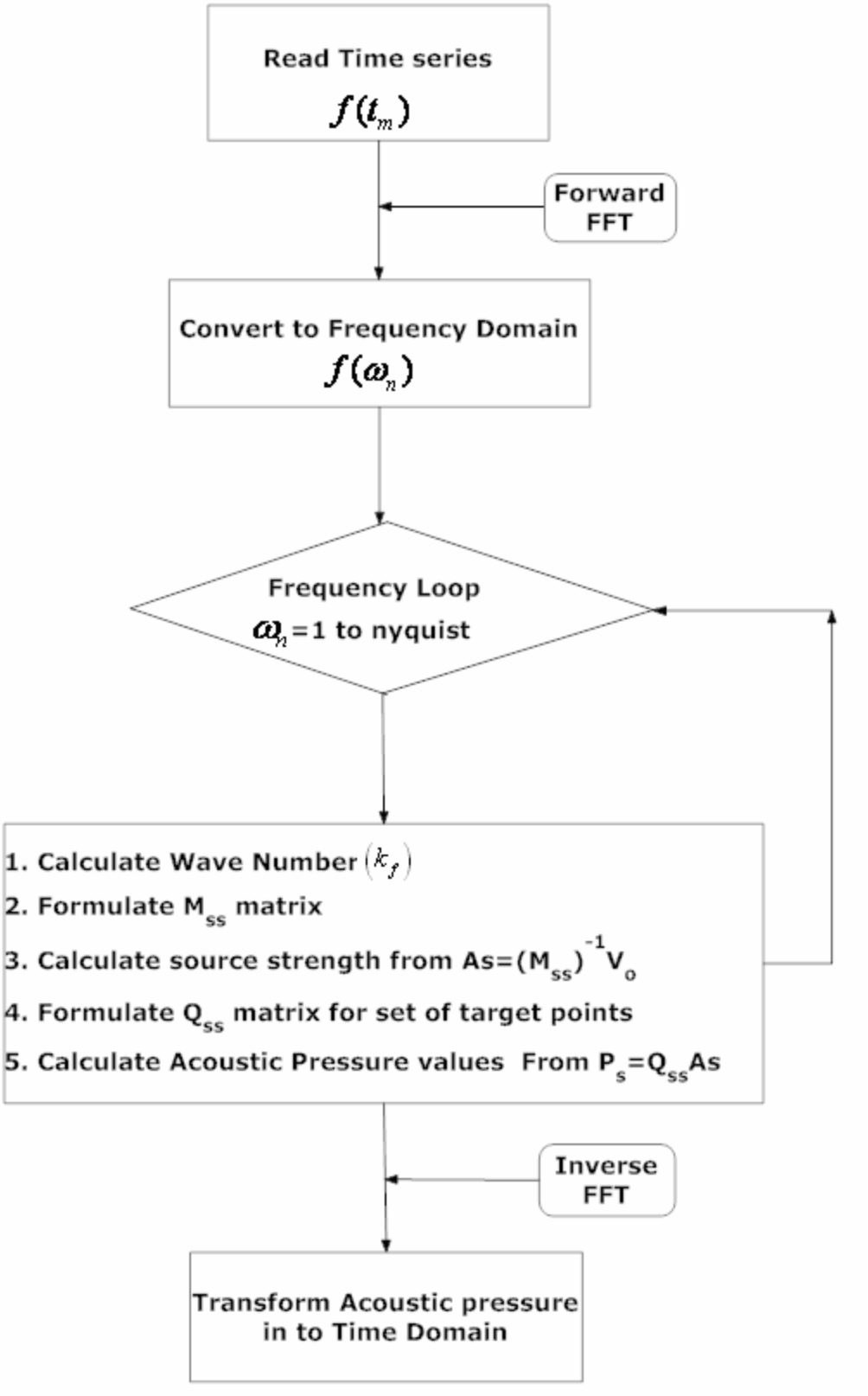

Figure 6.8: Flow chart for Wave Reconstruction program

Half sine wave velocity Impulse:

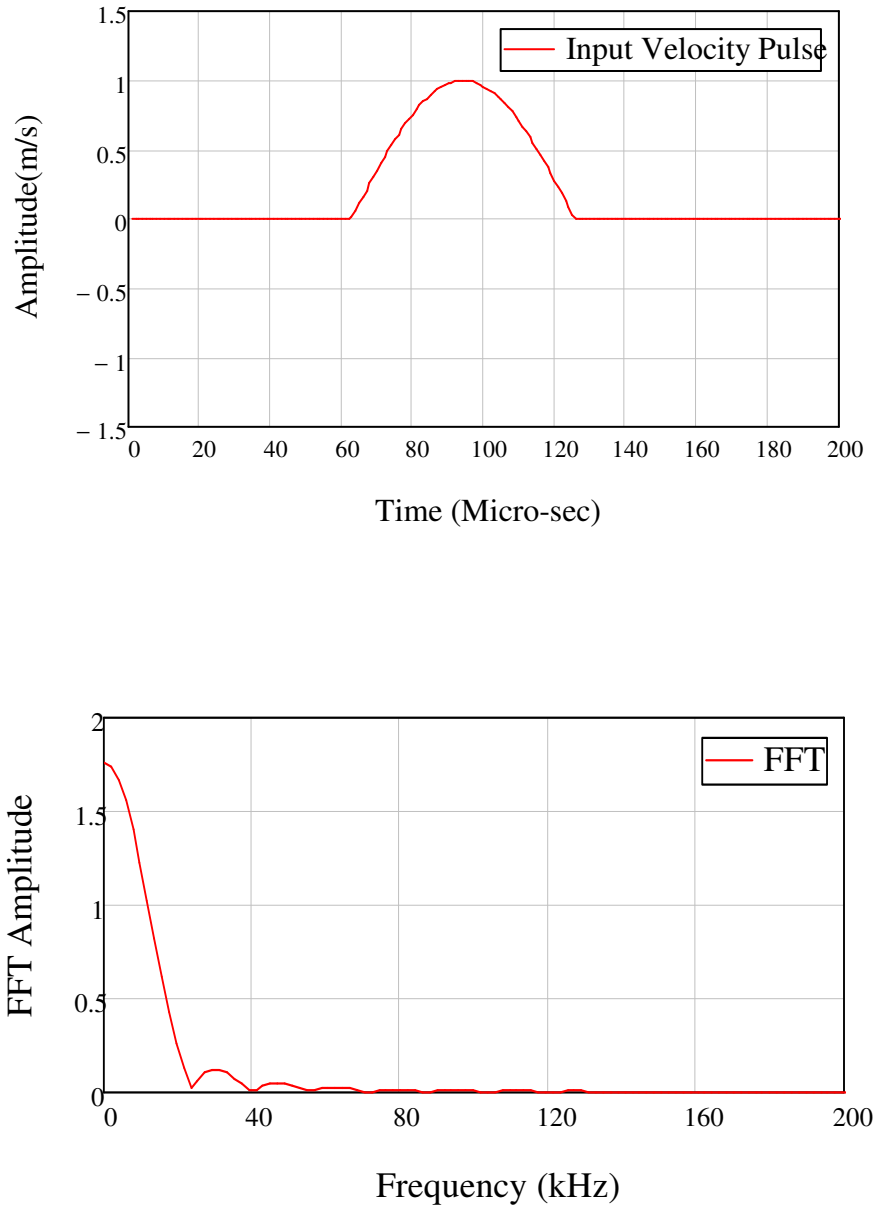

Figure 6.9: Half sine wave as input pulse and its FFT

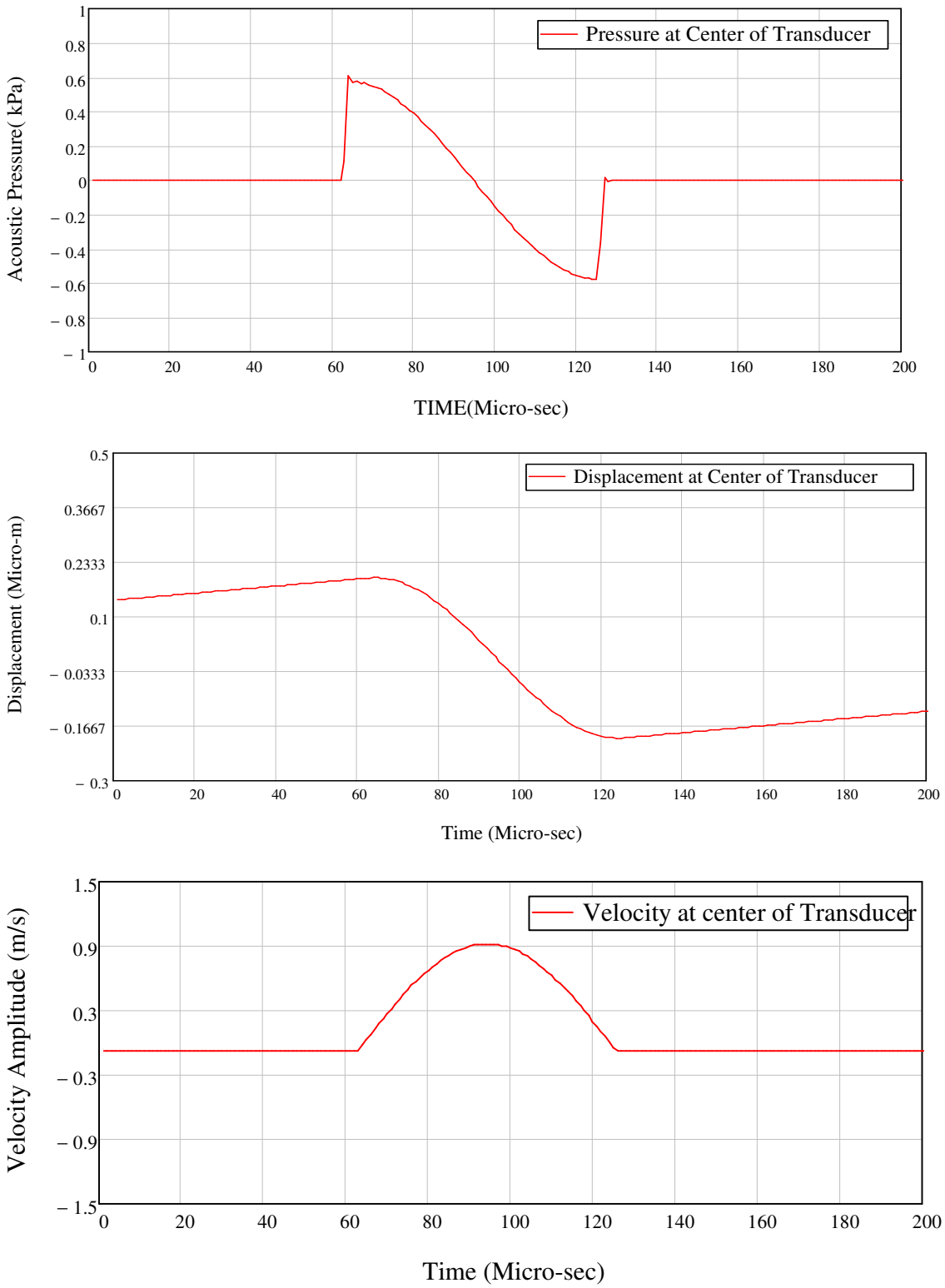

Figure 6.10: Ultrasonic field response at transducer face for Half Sine Wave Velocity Impulse

Full Sine Wave Velocity Impulse:

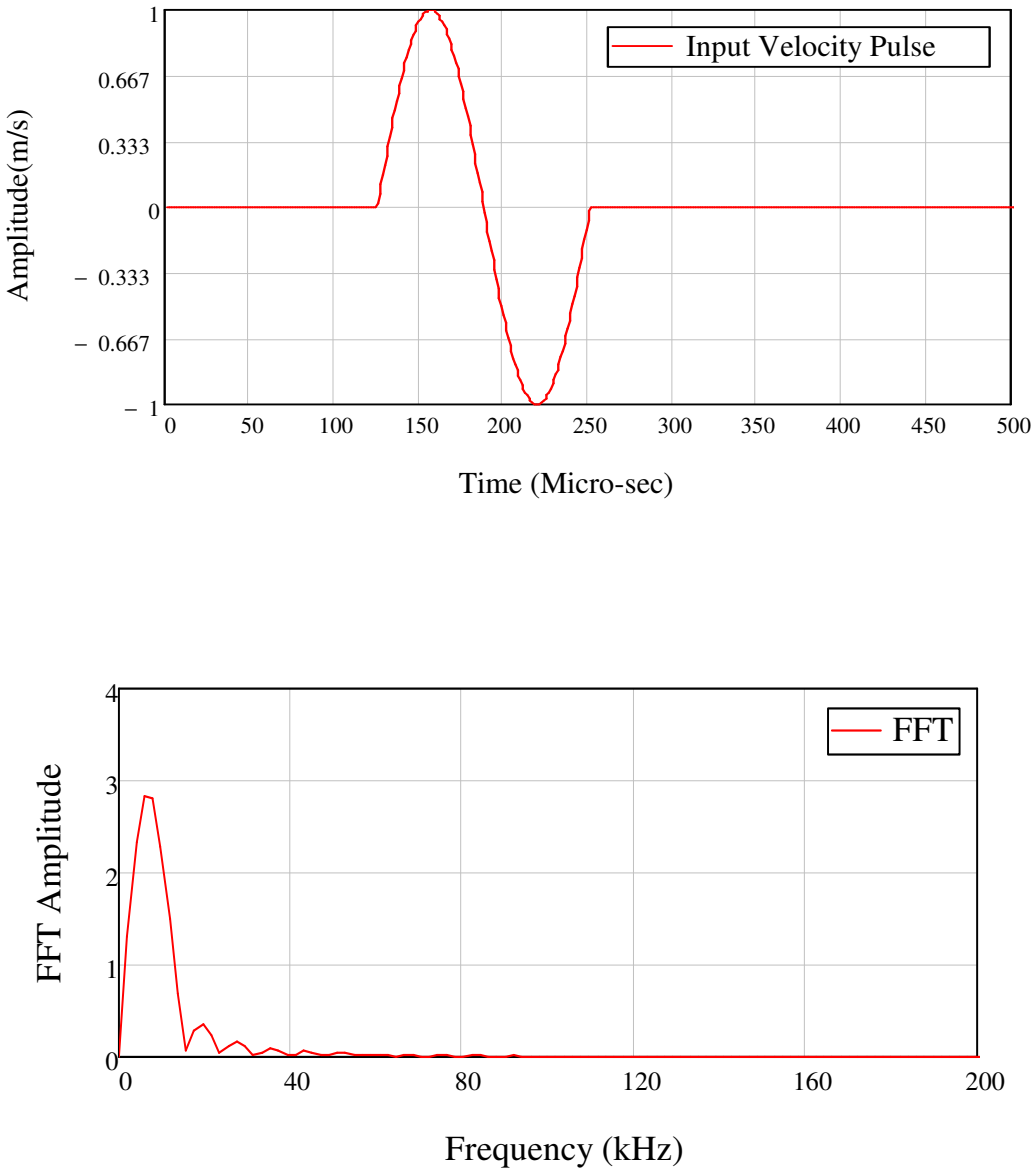

Figure 6.11: Full Sine wave as input pulse and its FFT

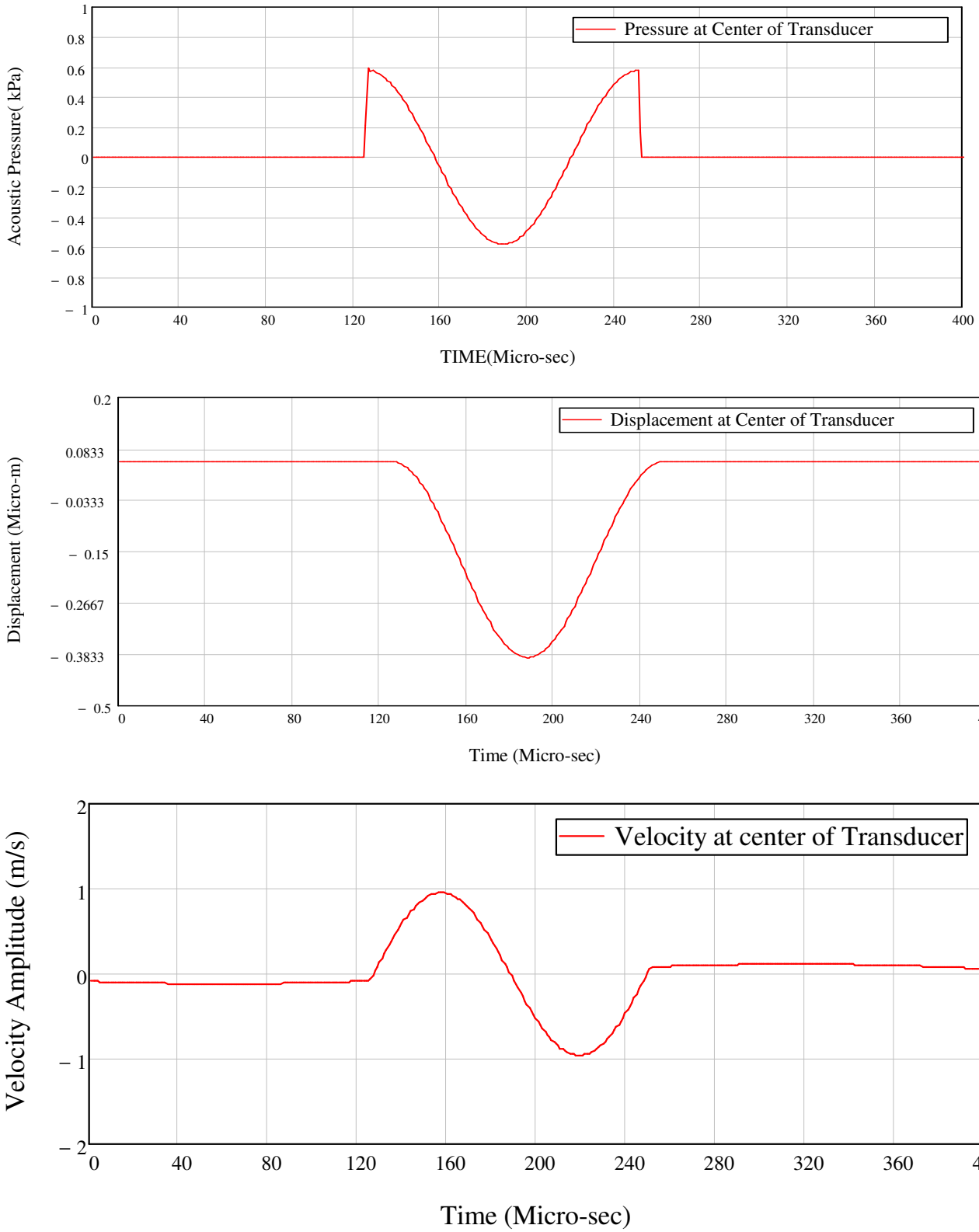

Figure 6.12: Ultrasonic field response at transducer face for Full Sine Wave Velocity Impulse

Half Triangular Wave Velocity Impulse:

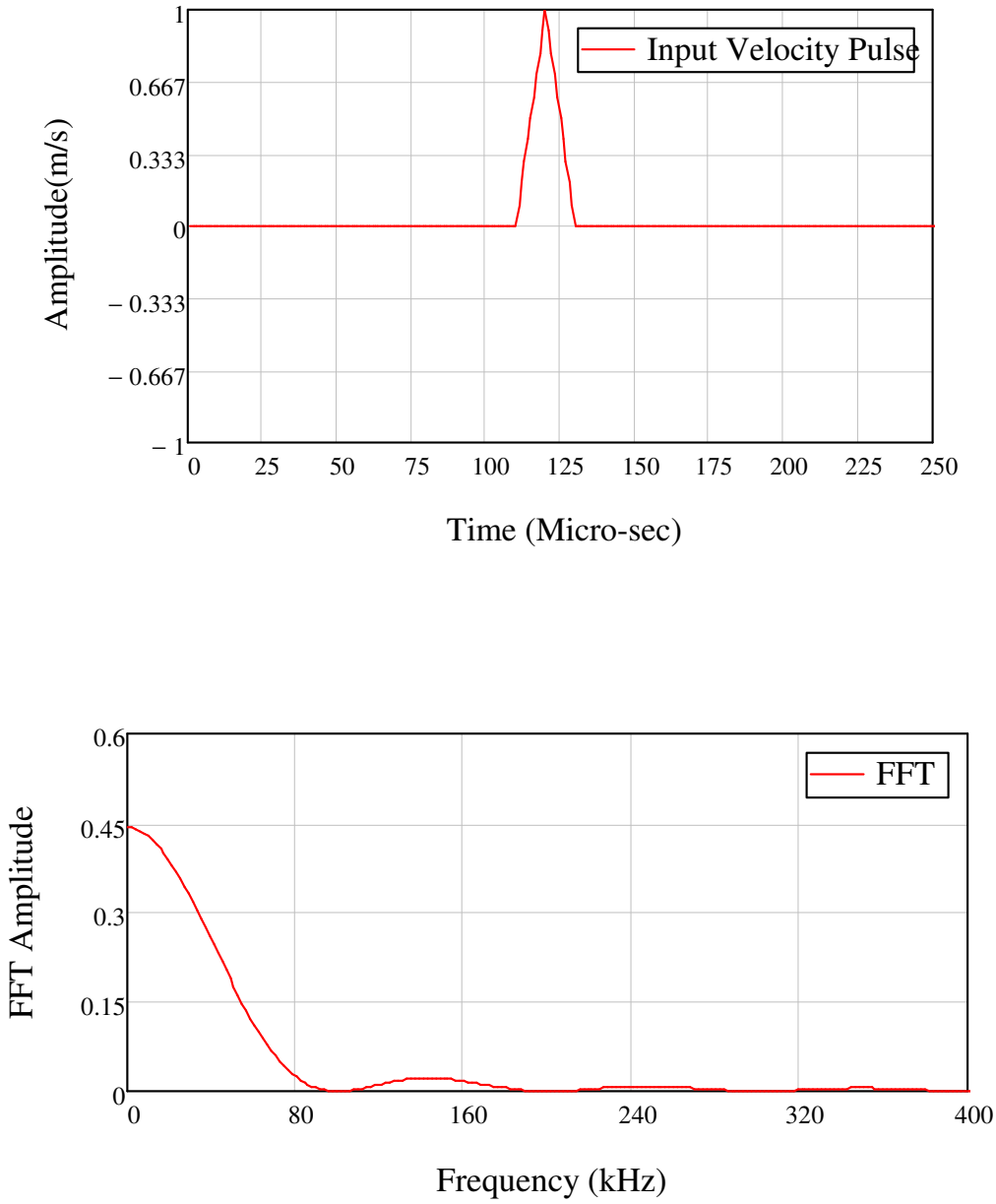

Figure 6.13: Half Triangular wave as input pulse and its FFT

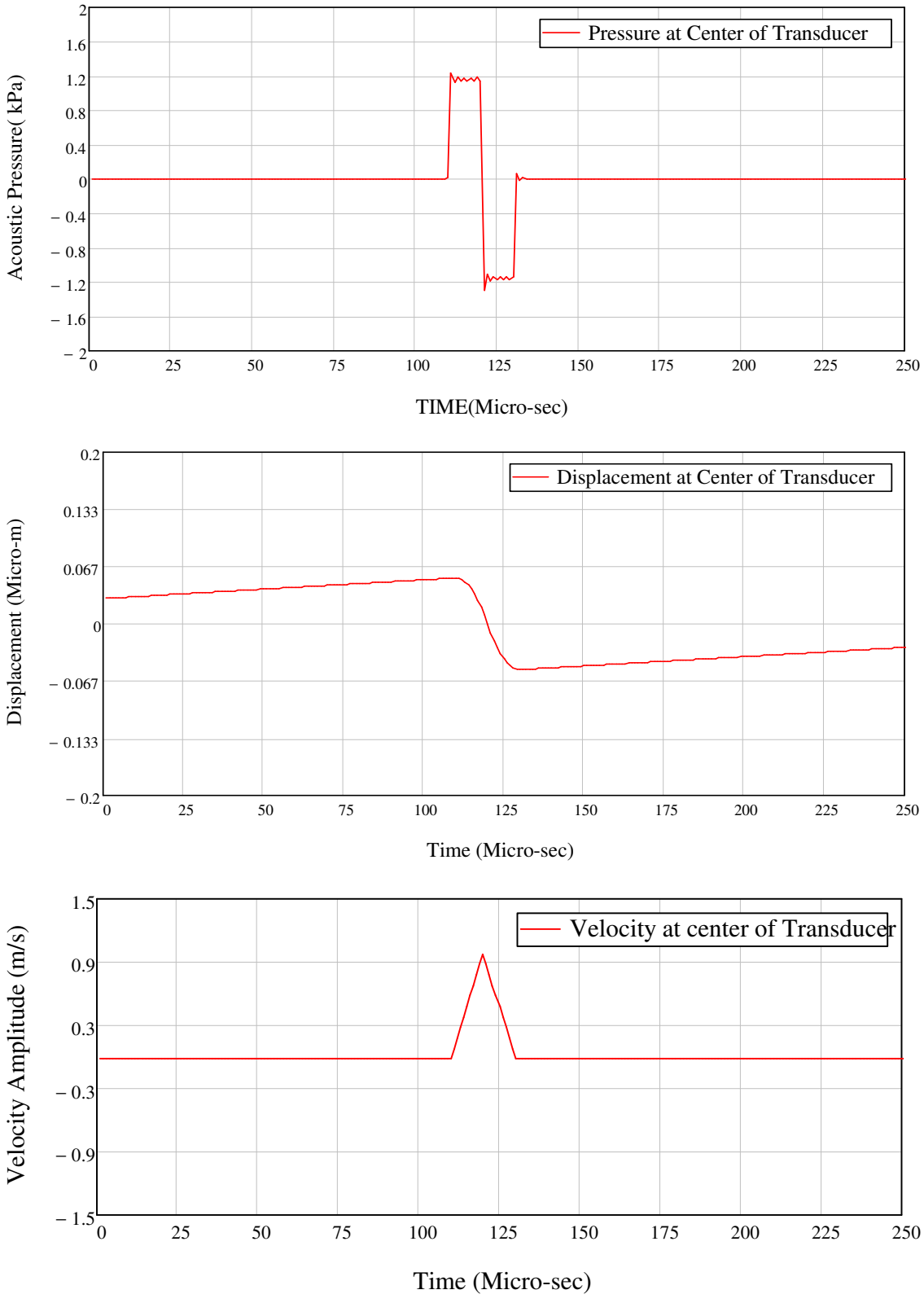

Figure 6.14: Ultrasonic field response at transducer face for Half Triangular Wave Velocity Impulse

Triangular Wave Velocity Impulse:

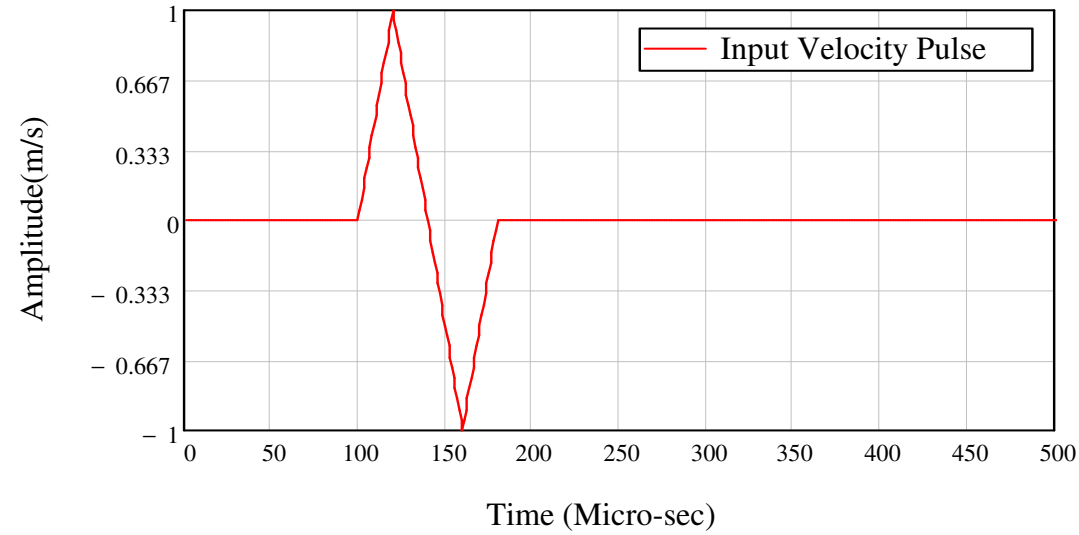

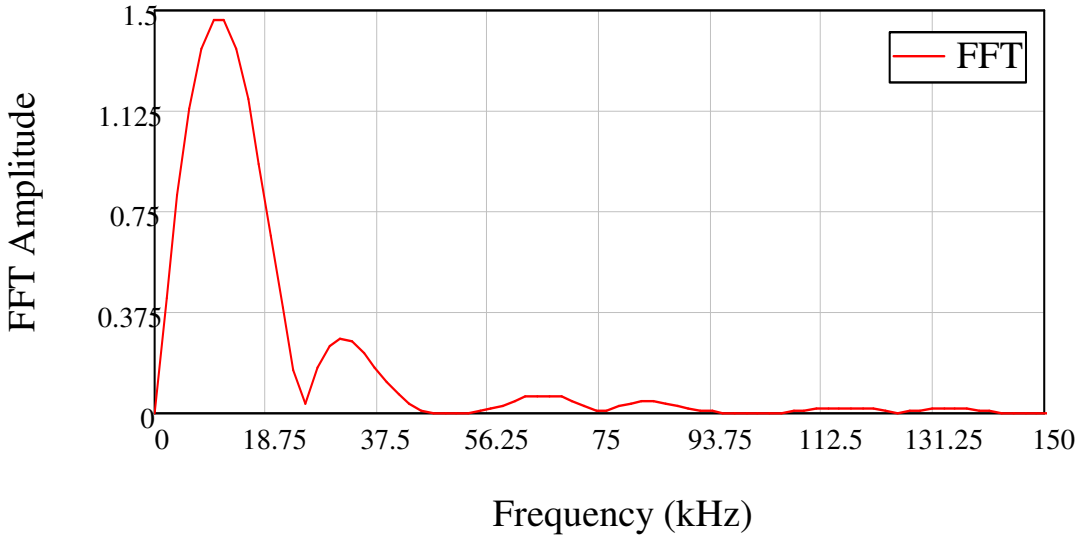

Figure 6.15: Triangular wave as input pulse and its FFT

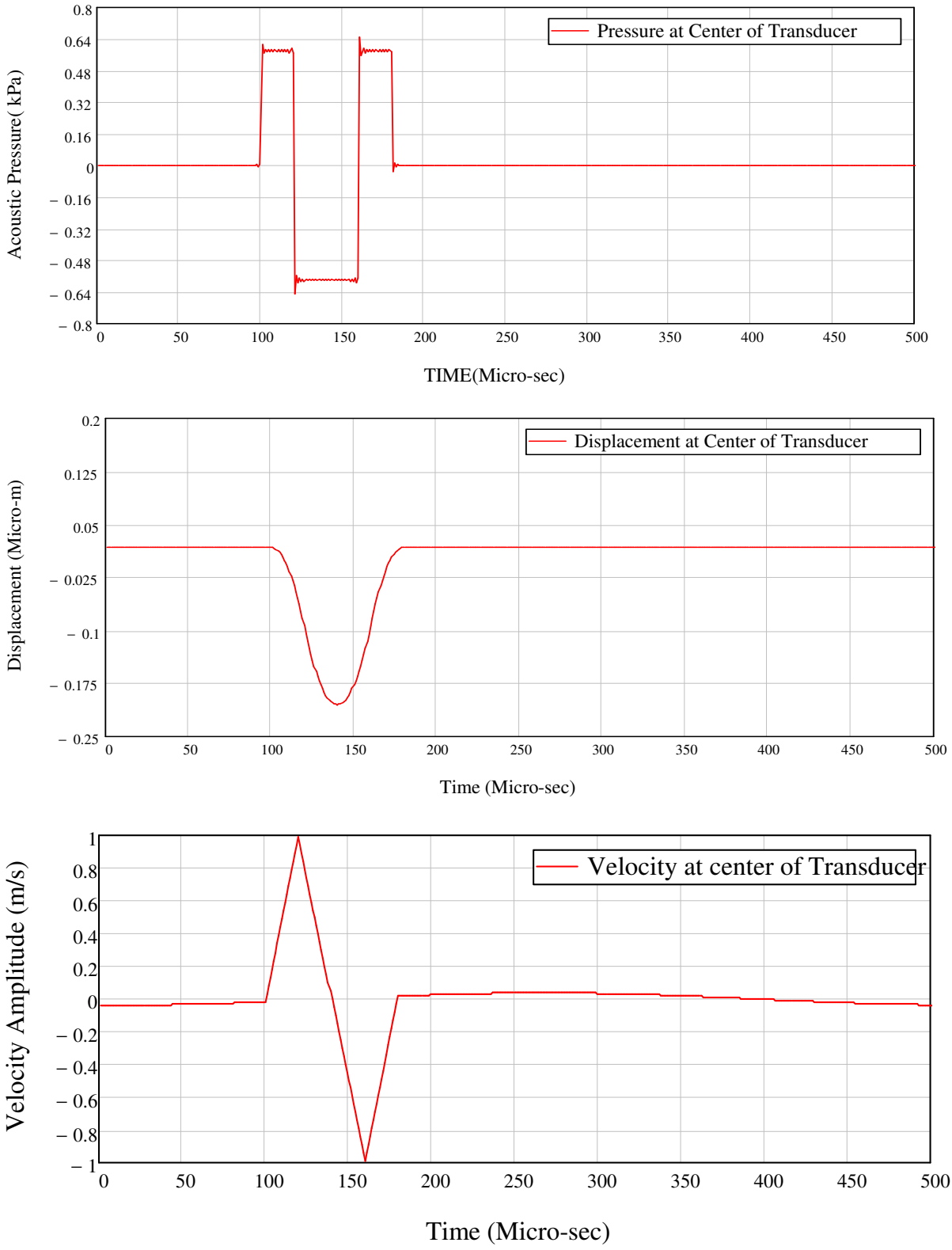

Figure 6.16: Ultrasonic field response at transducer face for Triangular Wave Velocity Impulse

Tone Burst Velocity Impulse:

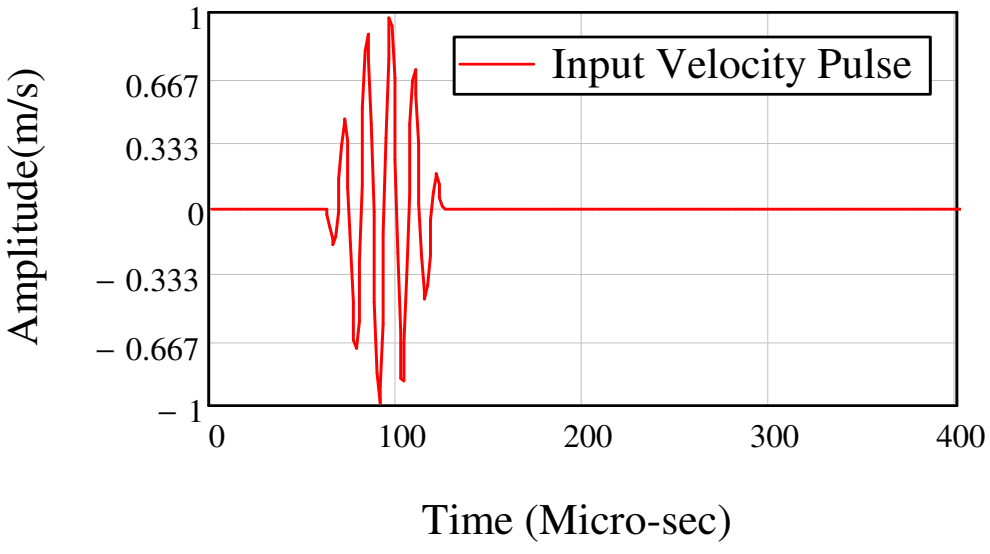

(a)

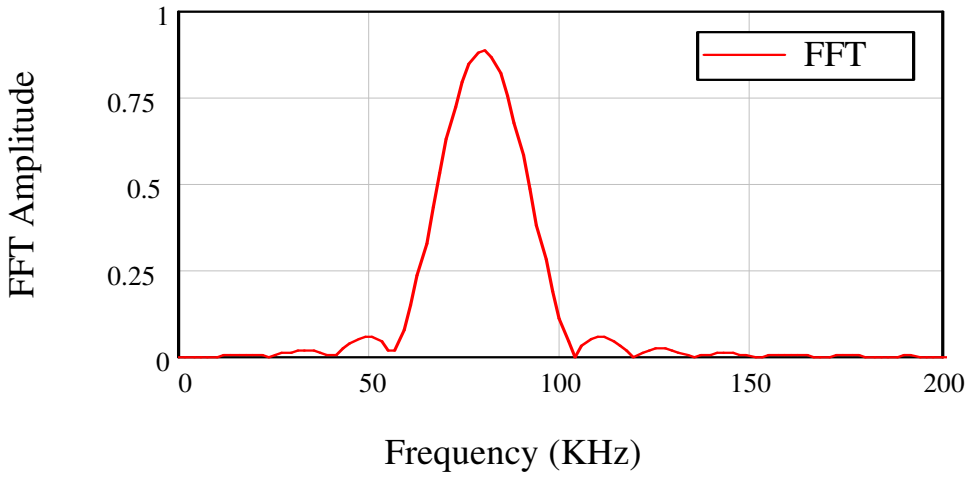

(b)

Figure 6.17: Tone Burst wave as input pulse and its FFT

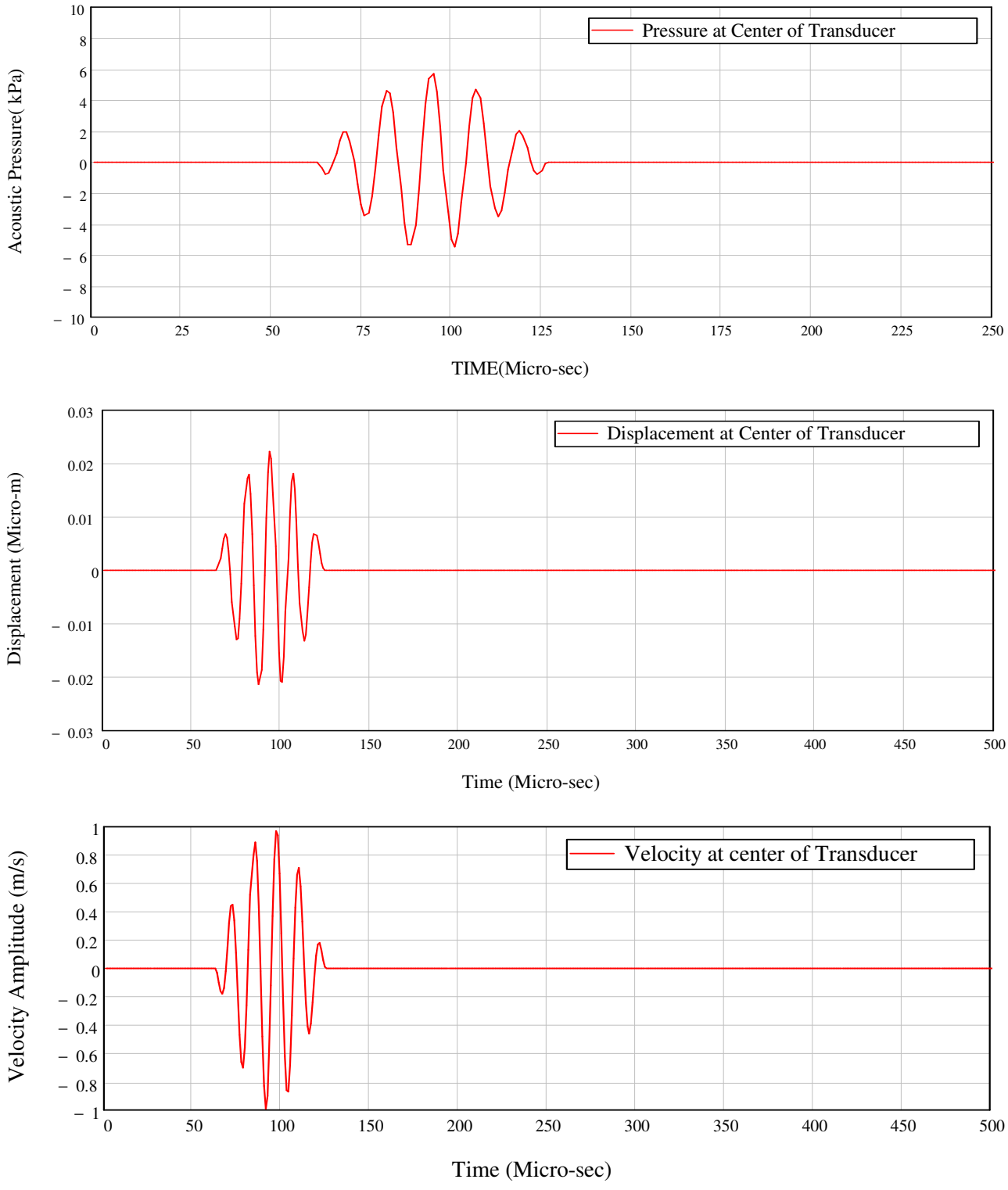

Figure 6.18: Ultrasonic field response at transducer face for Tone Burst Wave Velocity Impulse

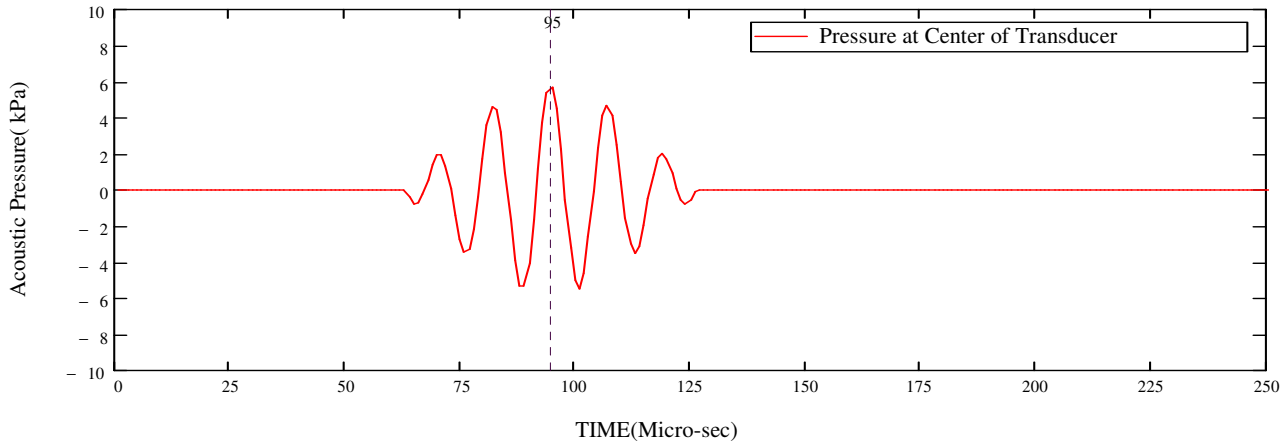

(a) Acoustic Pressure at distance Z=0 From Transducer Face

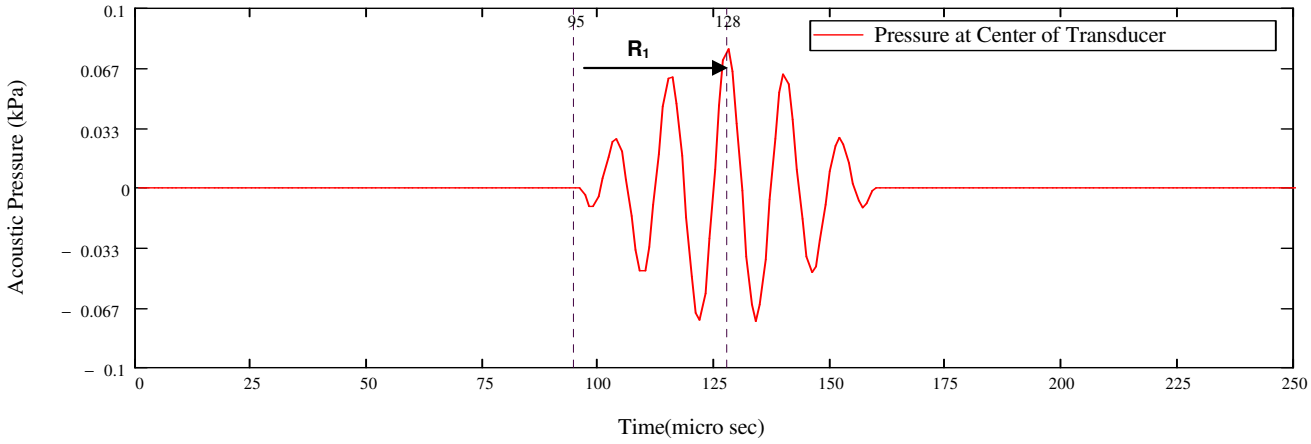

(b) Acoustic Pressure at distance Z=50mm from transducer Face

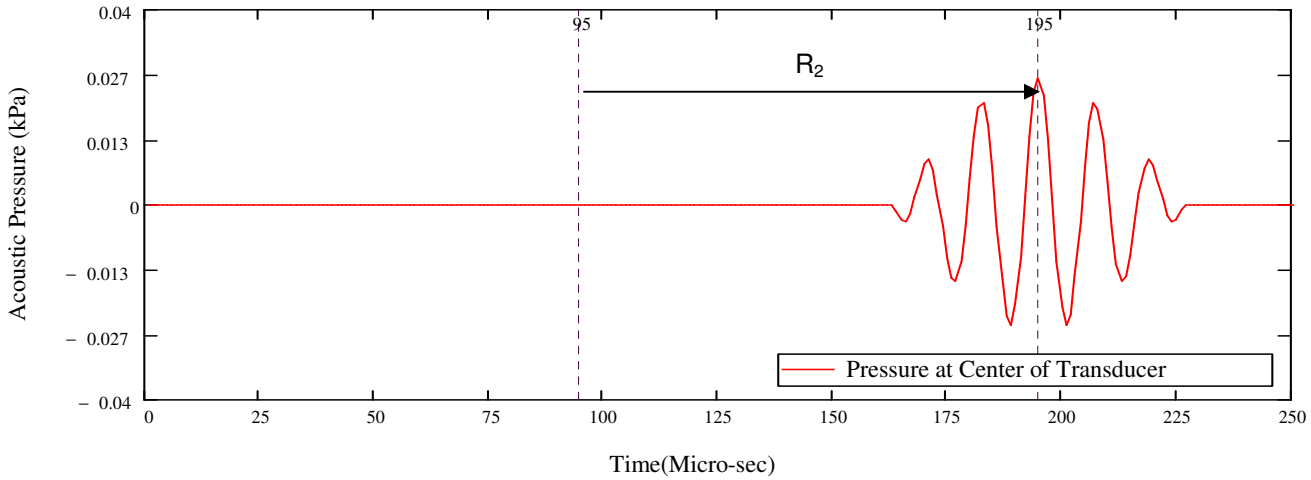

(c) Acoustic Pressure at distance Z=150mm from transducer Face

Figure 6.19*:* Acoustic pressure Response at various points along transducer axis (Z-direction)

6.3 Ultrasonic Field in a Non-Homogenous Fluid-DPSM technique:

6.3.1 Steady Wave Propagation in a Non-homogenous fluid:

DPSM technique for homogenous fluid can be extended to Non-homogeneous fluid having interface using concepts mentioned in chapter 5, and MathCAD code is developed using the method mentioned in section 5.2.1. Developed code is first validated for steady wave propagation in non homogeneous fluid.

Figure 6.20 and **Figure 6.21** shows pressure field developed at transducer face and at interface. The distance between the transducer face and the interface of two fluids is kept as 10 mm. The transducer is kept in fluid 1 (having P-wave speed 1.49 km/sec and density = 1 gm/cc) and the P-wave speed and density of fluid 2 is 2 km/sec and 1.5 gm/cc respectively. Transducer diameter is 0.1 inch and transducer frequency is 1 MHz. The results are matching with kundu [15].

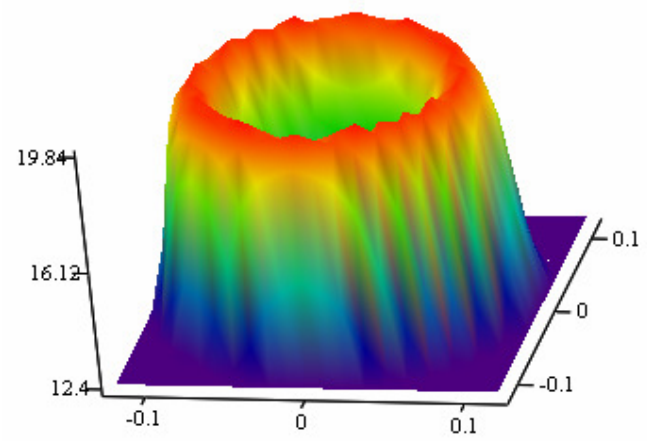

Figure 6.20: Acoustic Pressure in XY Plane close to the transducer Face

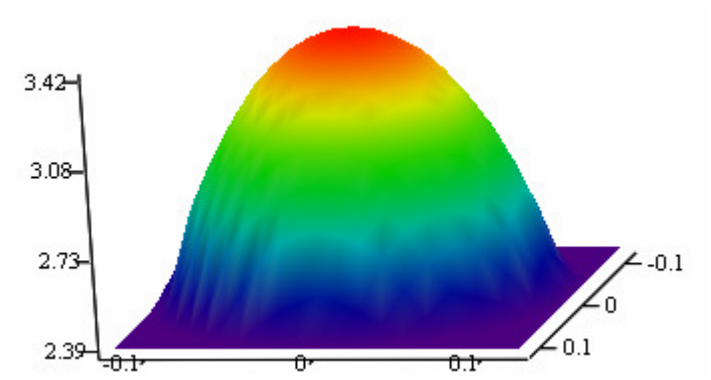

Figure 6.21: Acoustic Pressure in XY Plane at Interface (Z=10mm) of two fluids

6.3.2. Transient wave fields in a Non-homogeneous fluid

Same steady state model is used to study the transient wave using FFT engine. Tone burst signal is used as input signal and the acoustic pressure & velocity are recorded at two points lying along transducer axis at Z=0 as shown in **figure 6.22** as target point 1 and at Z=100 as shown in **figure 6.23** as target point 2. To get clear distinct pulse peak, interface is kept at 250 mm from the transducer face and also the FFT sampling points are taken as 512.

- **Figure 6.24** shows the acoustic pressure response at Target point ***1*** close to transducer face. First pulse is input pulse where as second pulse is reflected pulse from interface. The time lag between the peaks is 335 μ-secs, which is the matching with the theoretical time that the wave shall take to reach interface and rebound back to transducer face.

- **Figure.6.25** shows the acoustic pressure response at Target point ***2***. This plot show the time lag between input pulse peak and reflected pulse peak is less as compared to earlier case. This is obvious as input pulse will take more time to reach the target point 2 and also the reflected pulse will reach early at point 2 as it is nearer to interface.

It is important to note that for clarity the reflected pulse is magnified by 10^5 times in **figure 6.24 (c)** and by 10^3 times in **figure 6.25(c).** Similar behavior can be observed for velocity responses at two points from transducer face refer **figure 6.26 (c)** and **figure 6.27(c).**

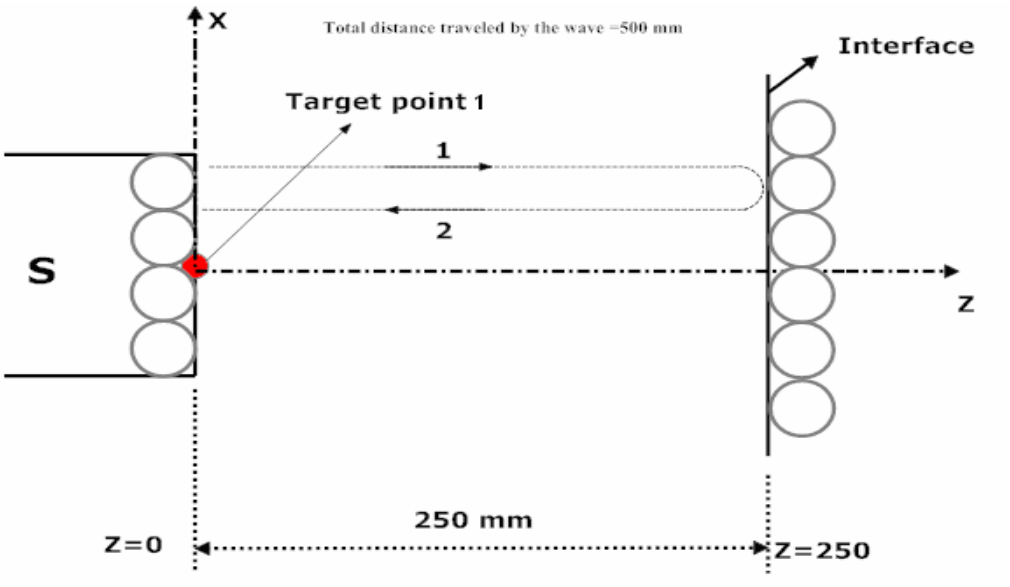

Figure 6.22: Location of Target point 1 where the response of ultrasonic field is observed

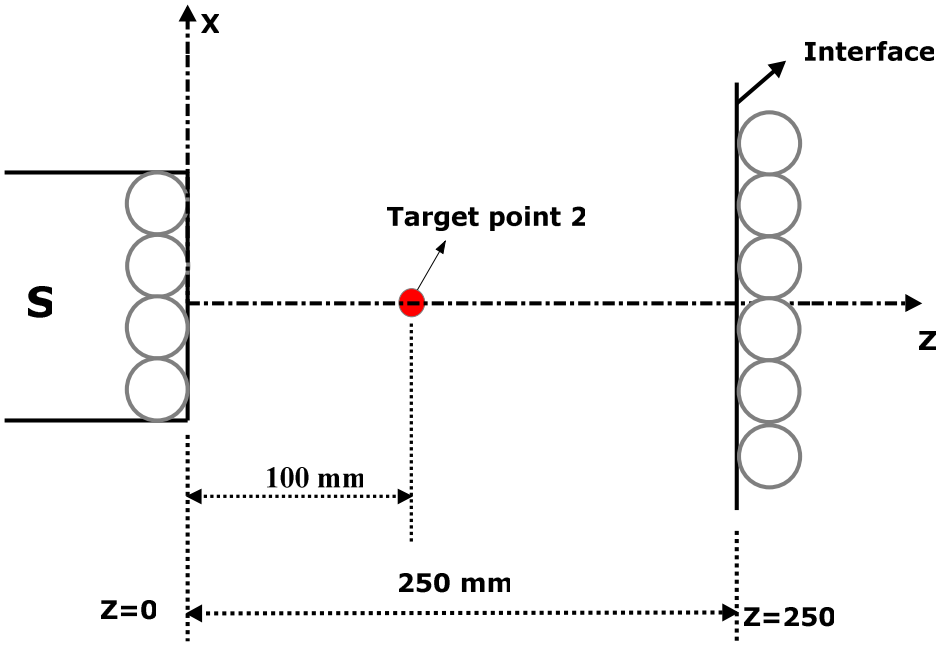

Figure 6.23*:* Location of Target point 2 where the response of ultrasonic field is observed

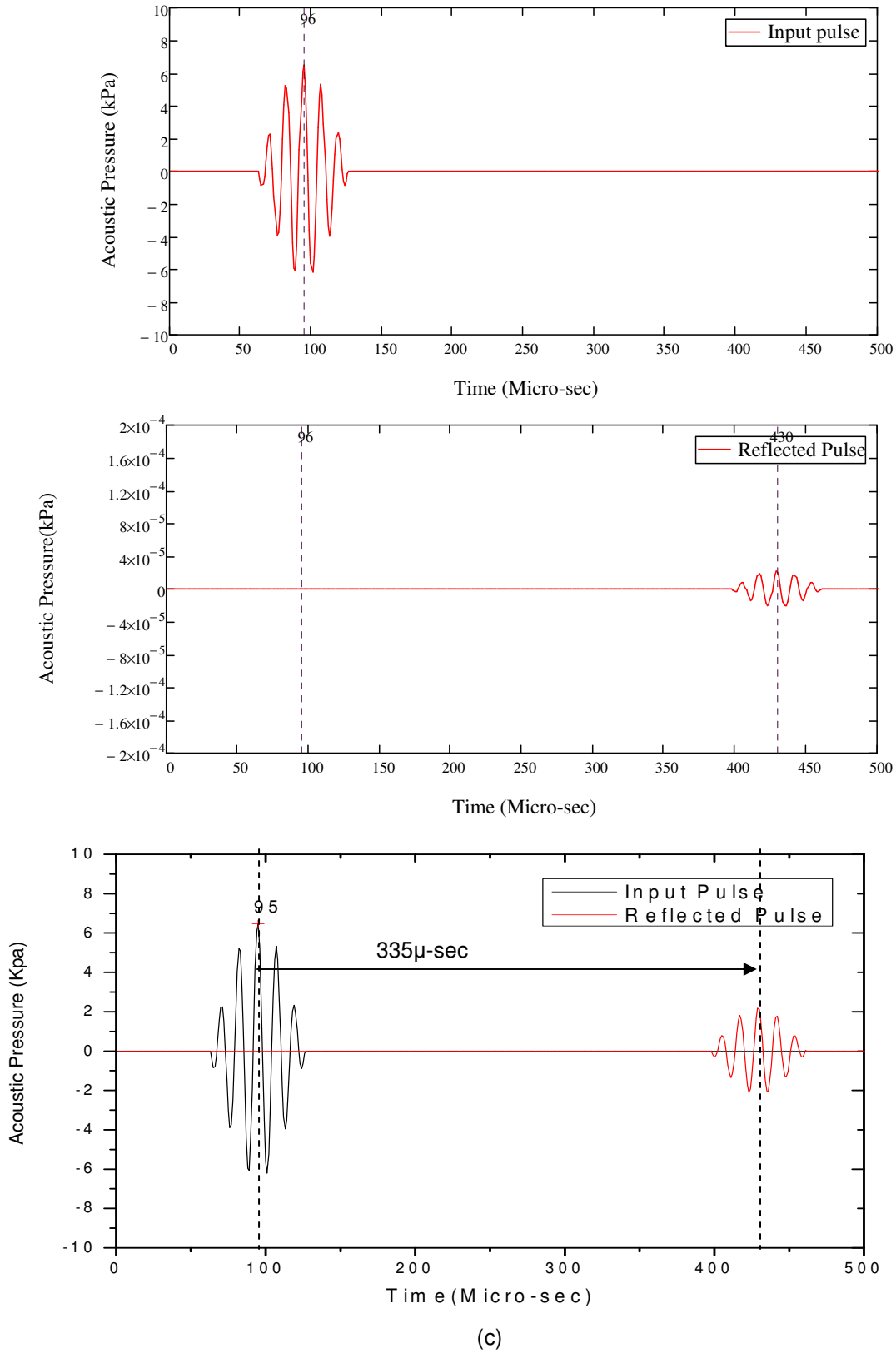

Figure 6.24: Tone Burst Signal -Pressure response at Target point 1(at Z=0mm)

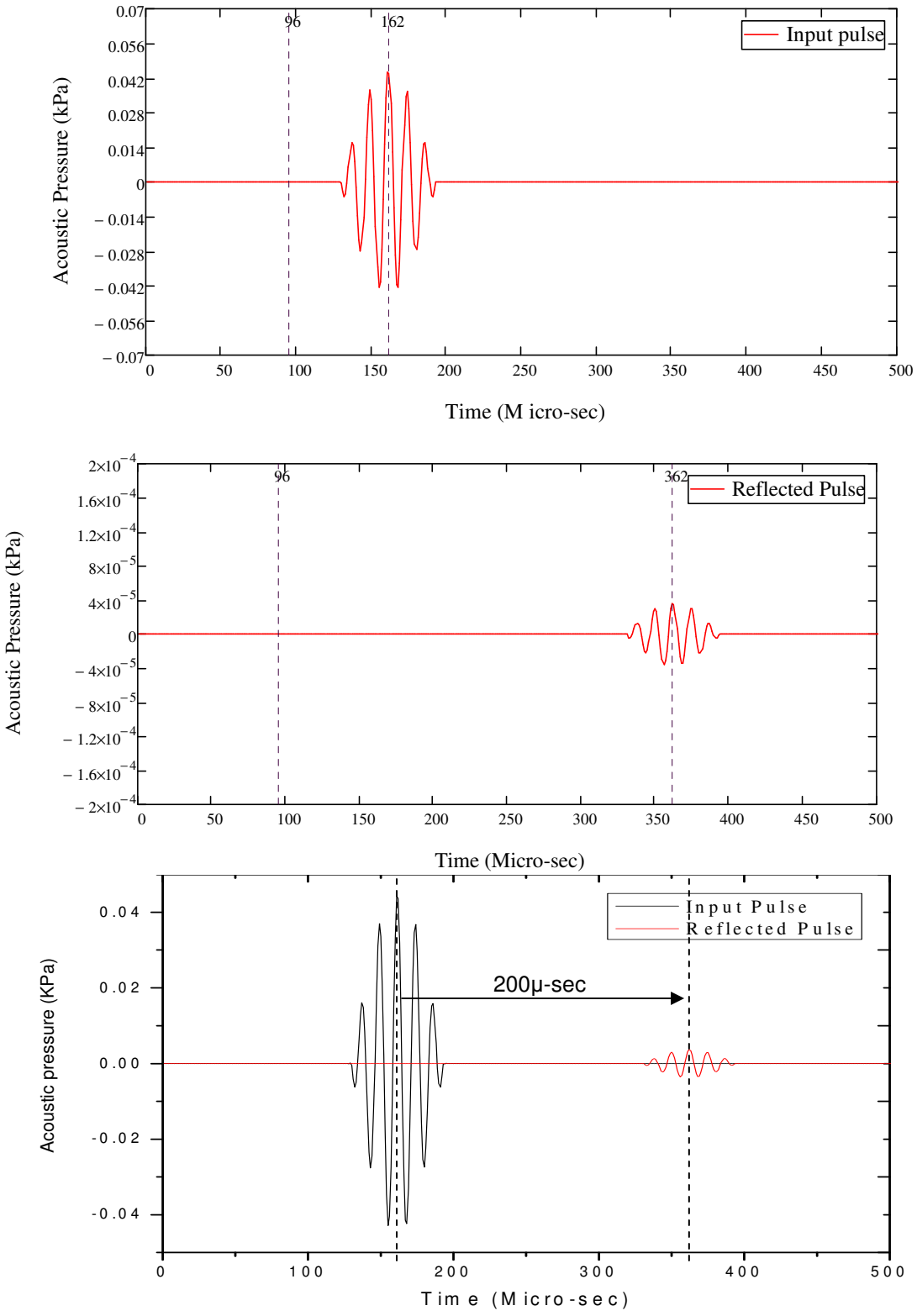

(c)

Figure 6.25*:* Tone Burst Signal -Pressure response at Target point 2(at Z=100mm*)*

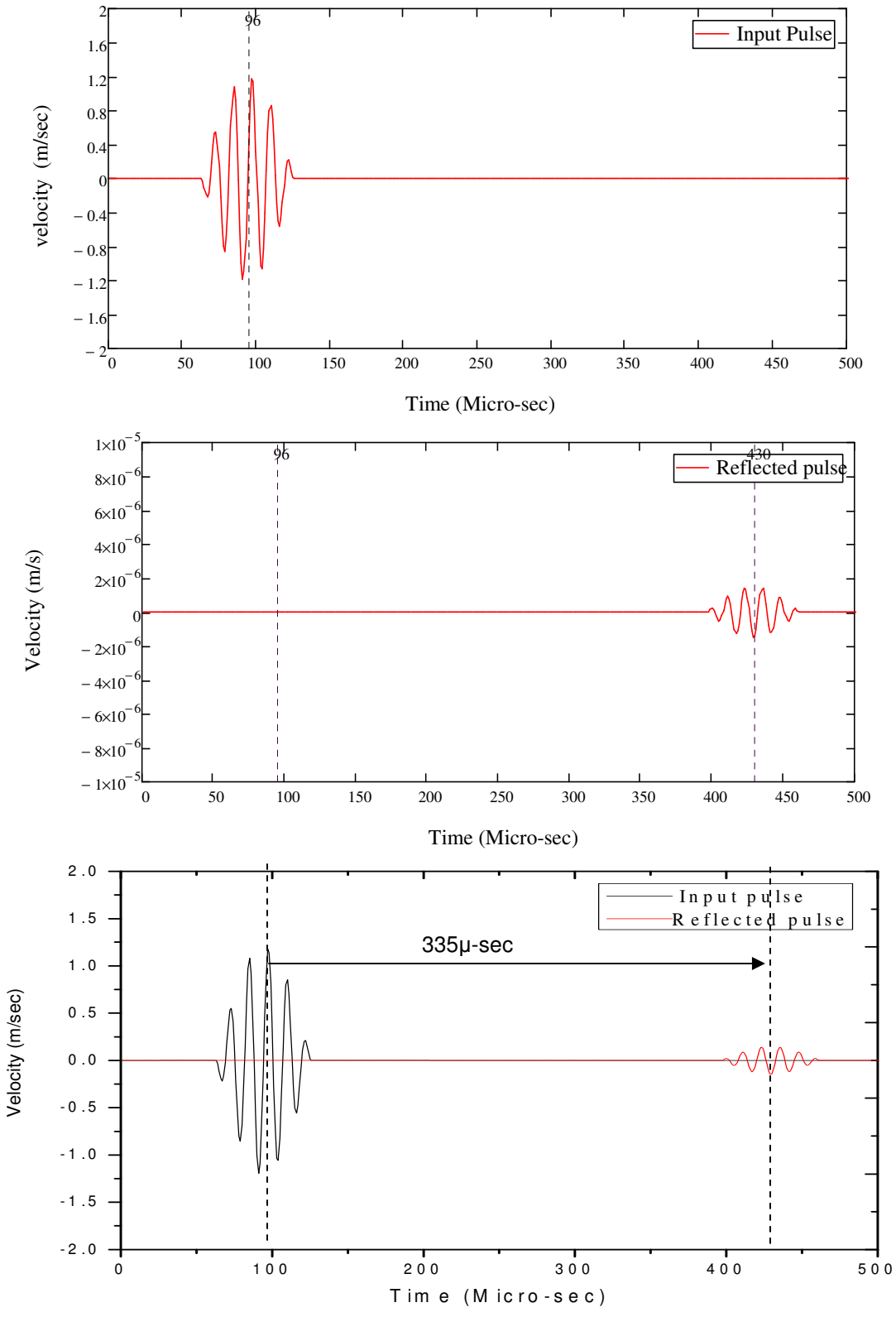

(c)

Figure 6.26: Tone Burst Signal-Velocity response at Target point 1 (at Z=0mm)

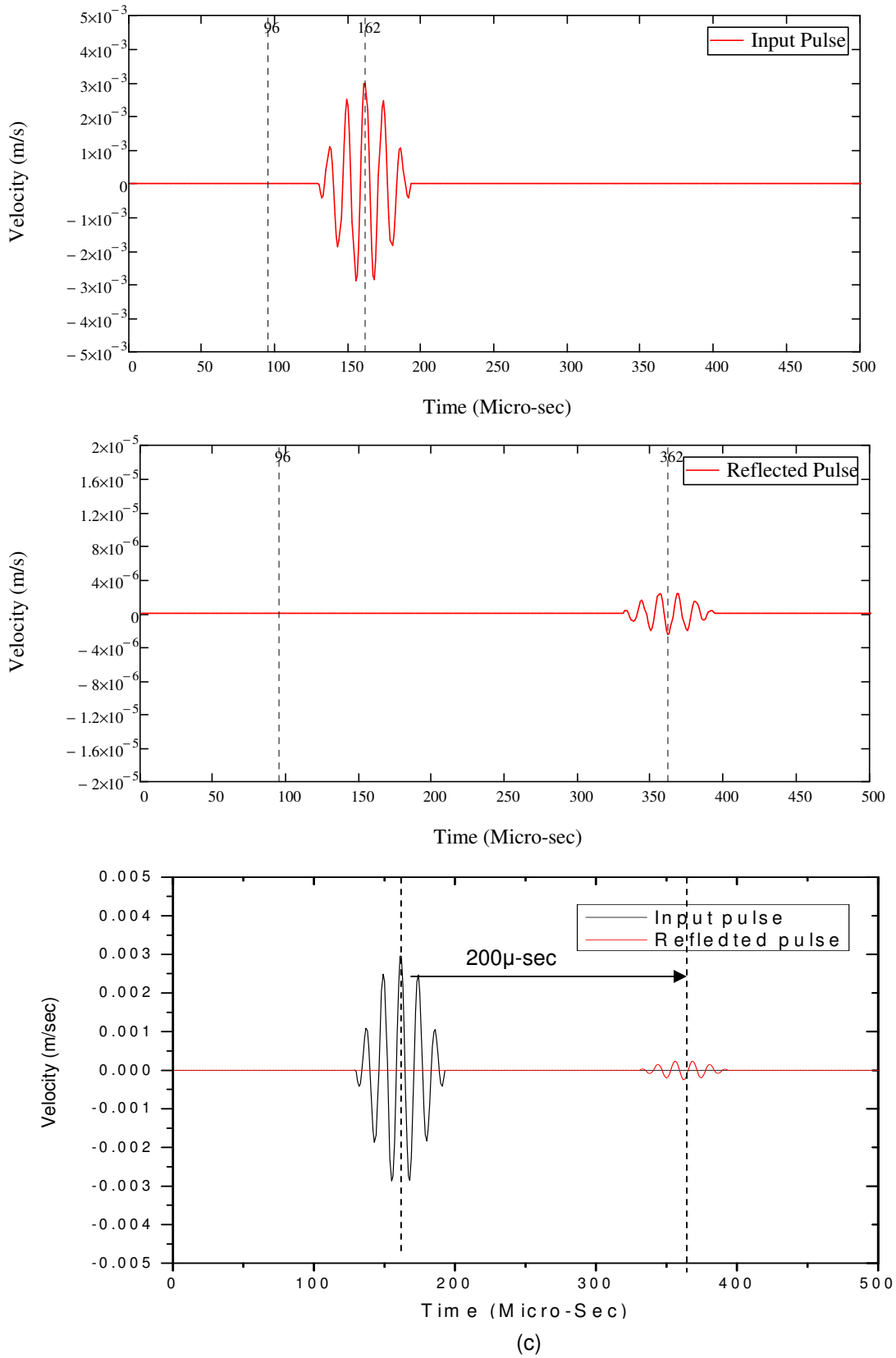

Figure 6.27: Tone Burst Signal-Velocity response at Target point 2 (at Z=100mm)

6.3.3 Acoustic Pressure Distribution with respect to Time

Acoustic pressure contours (tomograms) are plotted at various times interval on X-Z plane as shown in the **figure 6.28** for three types of interfaces. Input velocity pulse at transducer face is again tone burst pulse and having same frequency spread as per **figure. 6.17.** Transducer having diameter 0.1 inch is immersed in water and interface is also kept of same size as 0.1 inch. In the following figures different colors show intensity of pressure obviously red color indicates maximum pressure.

- **Figure 6.29** shows the acoustics pressure tomogram for homogenous at different time instances of infinite boundary.
- **Figure 6.30** shows the acoustic pressure developed in homogenous fluid having a rigid interface. Reflected waves can be seen after 132 μ–sec.
- **Figure 6.31** shows the acoustic pressure developed in case of non-homogenous fluid and in this figure behavior of only one fluid is shown.
- **Figure 6.32** shows acoustic pressure developed due to non-homogenous fluid showing behavior of two fluids.

Rigid interface or free boundary interface are modeled by making second fluid properties ($\rho = 0$) nearly zero for free boundary and ($\rho = 10^5$) for rigid boundary.

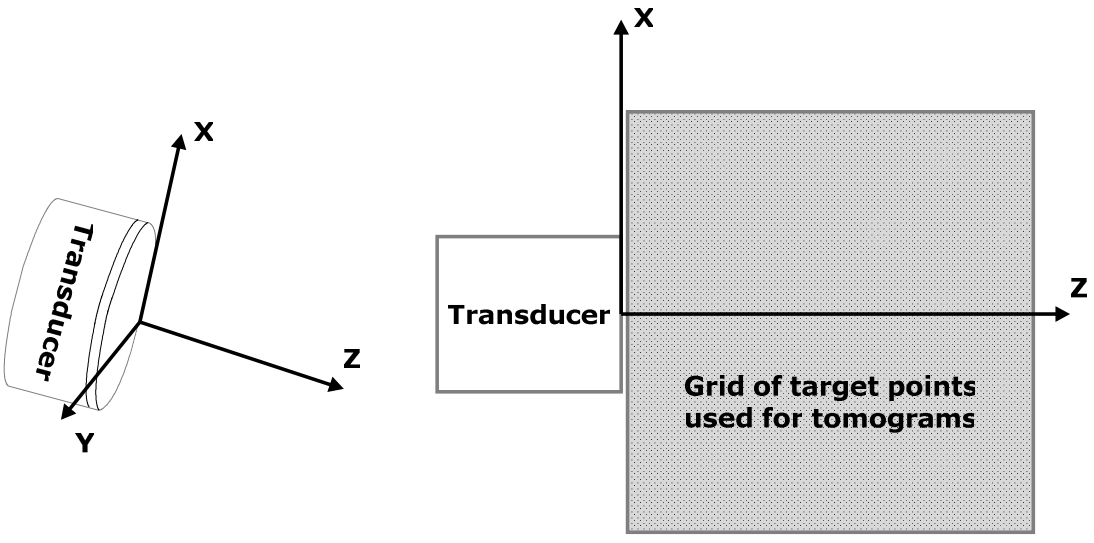

Figure 6.28: Location of X-Z plane and the target point grid used to generate tomo-grams

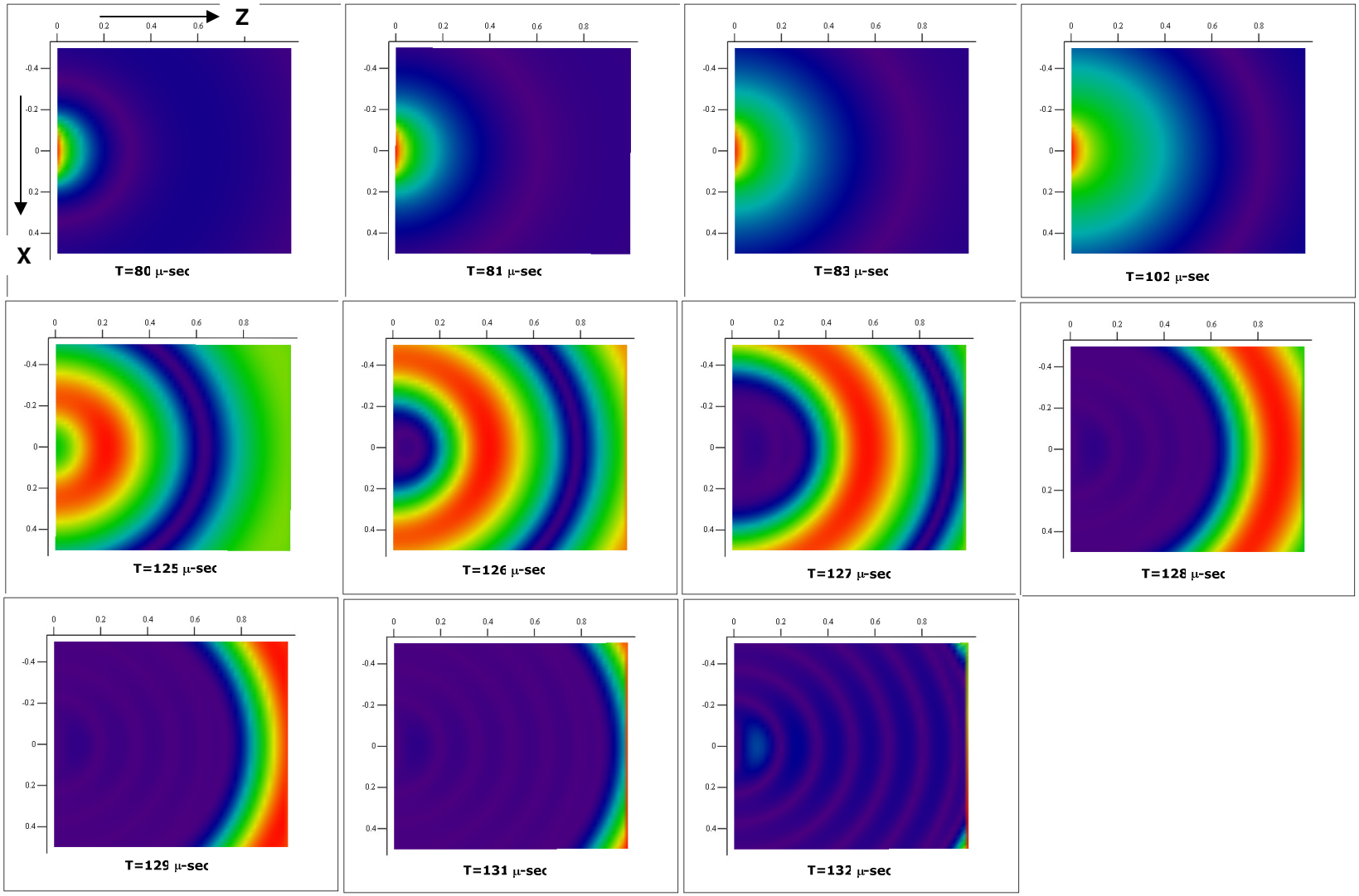

Figure 6.29: Acoustic Pressure Tomograms for Homogenous fluid (infinite boundary)

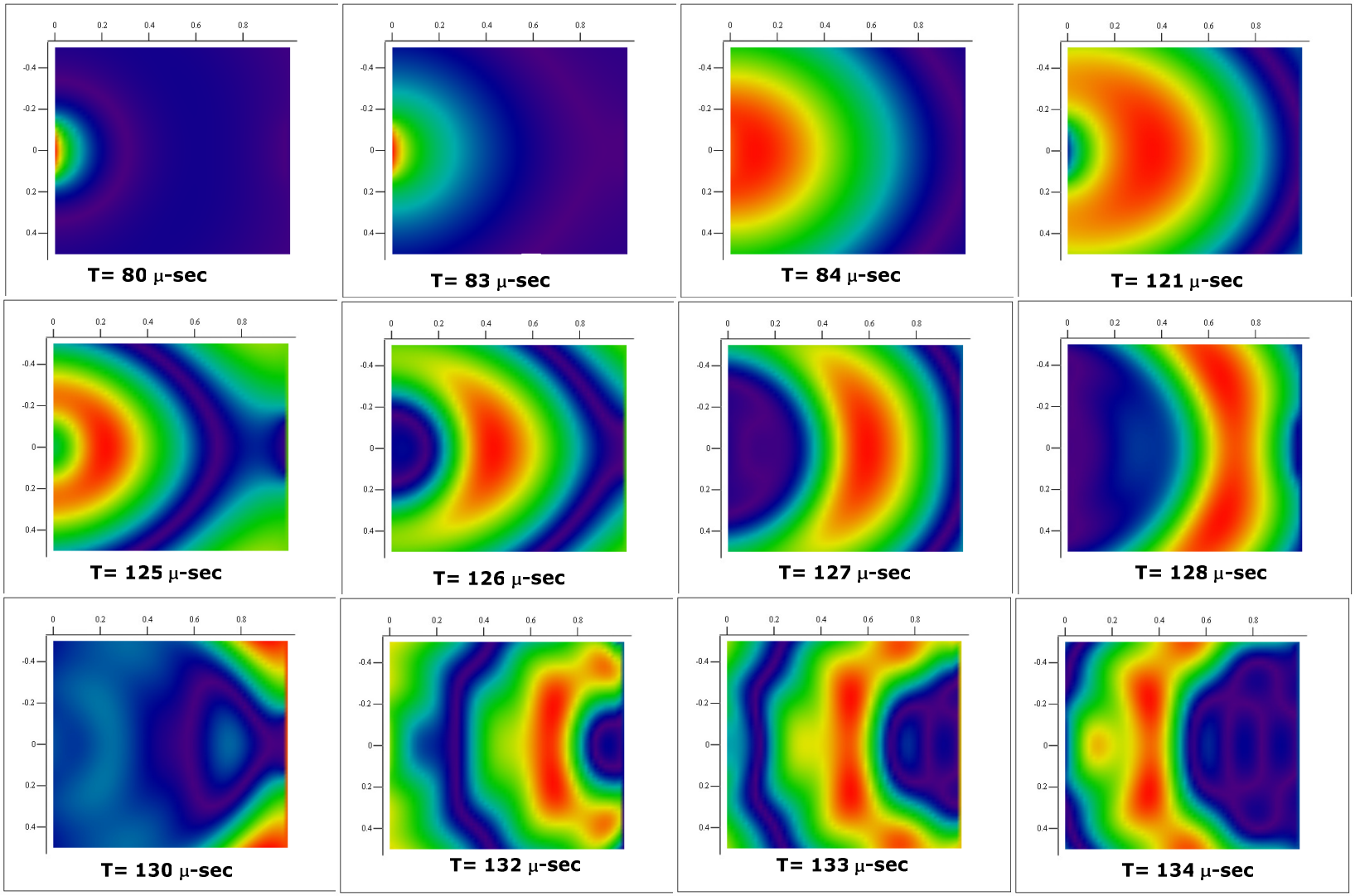

Figure 6.30: Acoustic Pressure Tomo-grams for homogenous fluid (Rigid interface)

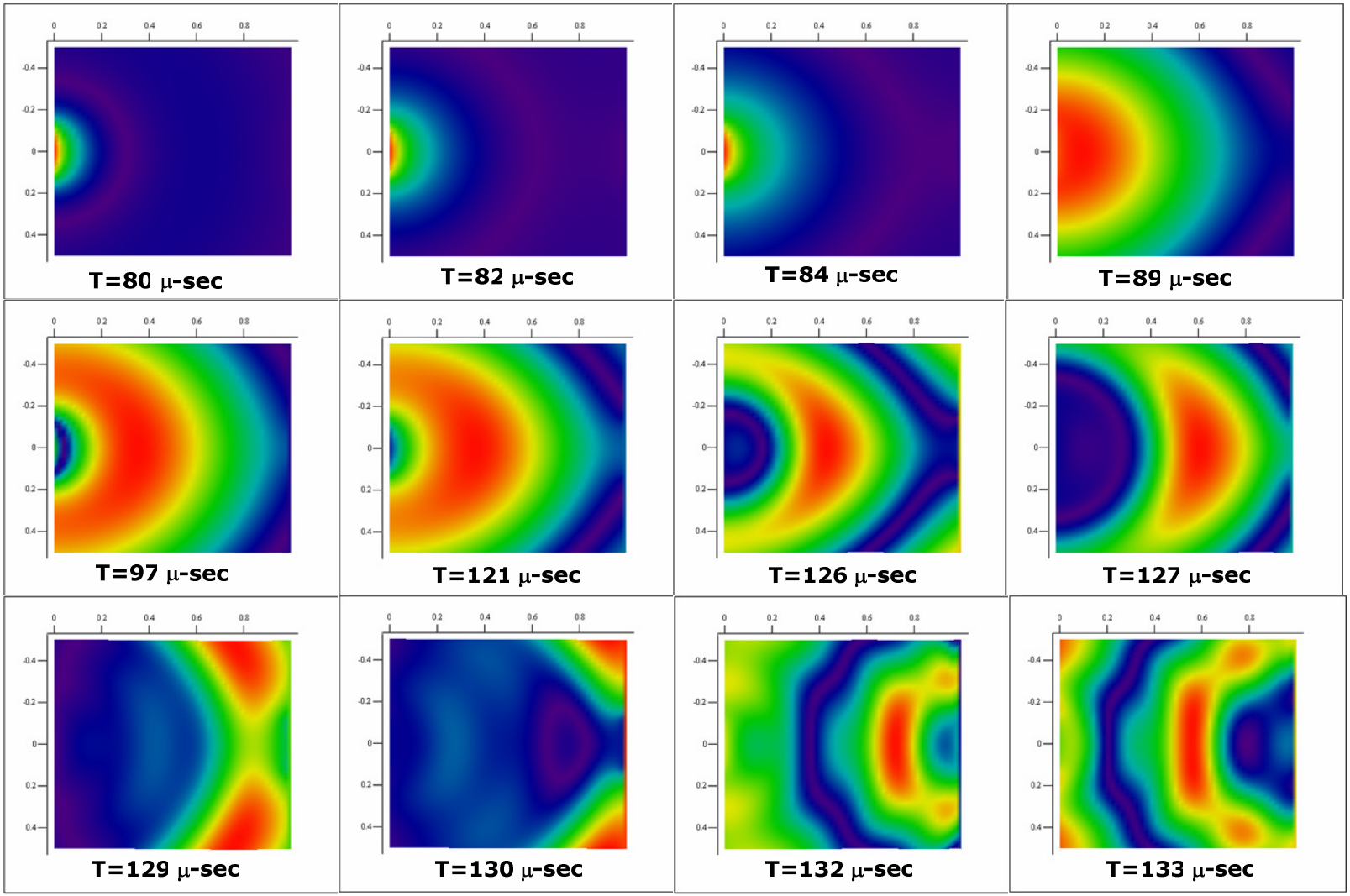

Figure 6.31: Acoustic pressure Tomo-grams for Non-Homogenous Fluid

CHAPTER 7

EXPERIMENTAL VALIDATION

7.1 Experimental Setup:

In the previous chapter numerical results for ultrasonic fields generated in homogenous and non-homogenous media and also their simulation have been presented .In this chapter to validate the numerical results with the experimental results the following setup have been used.

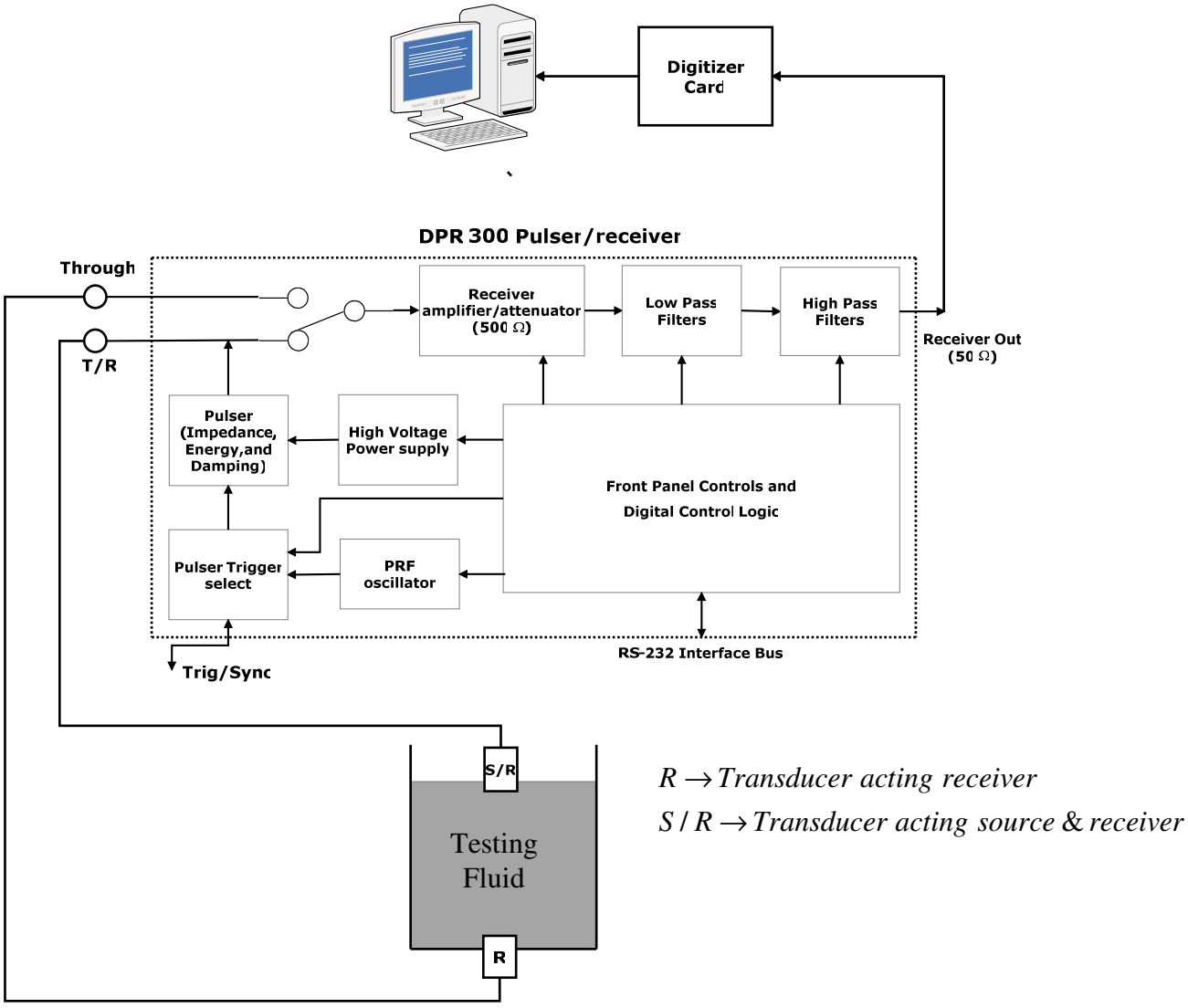

Figure 7.1: Experimental setup used for testing

Following are the salient features of the Pulser/ receiver system used:

PRF Oscillator & Pulser Trigger control: The internal PRF oscillator generates repetitive trigger pulses for the pulser subsystem under the control of the PRF control. Pulser Trigger control selects between the internal PRF oscillator or an external source applied to the Trig/Sync connector as trigger sources for the DPR 300 Pulser.

Pulser (Impedance/Energy/Damping): The pulser generates an excitation pulse upon receiving a trigger event from a selected source. There are four energy and two impedance values, and the single Energy and impedance control adjusts the pulse energy and the pulser impedance.

Receiver amplifier: It controls the amplification or attenuation of signals processed by the DPR300 receiver. The receiver gain can be varied from -13dB to 66 dB.

Low Pass and High Pass filters: Low filters are available for reducing the bandwidth of the DPR300 receiver. High Pass filters are available for eliminating undesirable low frequency energy from the DPR300 receiver signal. High pass filtering can be used as a means of providing faster receiver recovery from strong signals such as the excitation pulse or strong interface echoes.

Digitizer Card: It converts the analog signal which is coming from DPR 300 in to Digital signal and fed to computer.

7.2 Experimental Procedure:

Pulser/receiver system sends a negative spike signal (100 V to 475 V) to the transducer as an input pulse .Depending upon the method (pulse echo or through) the output pulse will be sensed by the respective transducer. The received output pulses are then amplified and filtered by DPR 300 and sends to digitizer card where it converts analog signal to digital form and on computer screen the waveform can be seen with the help of software (Acquiris) and also graphical data can be captured. Thus different waveforms for different types of fluids and interfaces are obtained from experimental setup..

7.3 Verifying the Linearity of the Transducer using DPSM – Technique and Experimental results:

7.3.1 DPSM –technique results:

In the developed MATHCAD code for homogenous fluid different input velocity impulses are inputted and the Acoustic pressures developed at different levels of fluid (100,150,200mm) is observed.

Velocity impulse (in m/s)	Pressure Developed at Z=100mm (in dynes/cm^2)	Pressure Developed at Z=150mm (in dynes/cm^2)	Pressure Developed at Z=200mm ((in dynes/cm^2)
1	114.086	85.263	55.18
2	228.172	170.527	110.365
3	307.449	260.415	203.789
4	409.932	347.22	271.719

Observations:

1. Acoustic pressures vary linearly with respect to input velocity impulses as shown in **figure (7.2).**
2. Acoustic pressure values are decreasing as the level of fluid increases this shows that as the level of fluid is increasing the dissipation of pressure to the surrounding fluid is also increasing.

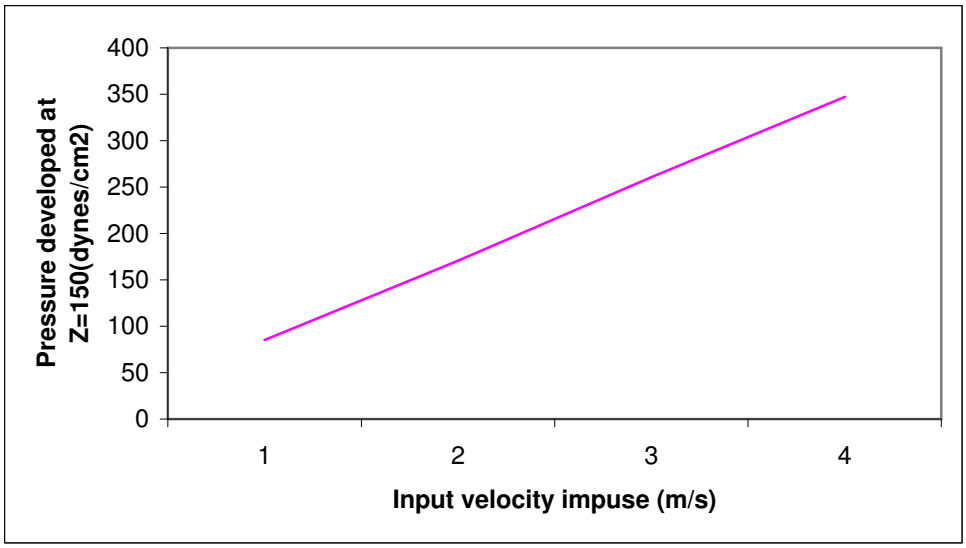

Figure 7.2: Variation of acoustic pressure with respect to input velocity pulse

7.3.2 Experimental Results:

Different input voltages are inputted in steps of 25V (125 to 475 V) from DPR300 and the corresponding output voltages are observed at different levels of water.

Input voltage	Output voltage for 100 mm of water	Output voltage for 150mm of water	Output voltage for 200mm of water
(in volts)	(in volts)	(in volts)	(in volts)
125	0.906	0.668	0.341
150	1.100	0.762	0.416
175	1.280	0.893	0.487
200	1.460	1.010	0.553
225	1.610	1.130	0.625
250	1.780	1.260	0.702
275	1.975	1.370	0.772
300	2.140	1.530	0.845
325	2.360	1.650	0.910
350	2.525	1.770	0.970
375	2.700	1.900	1.040
400	2.880	2.040	1.160
425	3.050	2.156	1.220
450	3.225	2.280	1.280
475	3.410	2.410	1.340

Observations:

1. Output voltages vary linearly with respect to the input voltage as shown in the **figure (7.3).**
2. Output voltage is decreasing as the level of water is increasing this shows that signal is attenuating as the level of water is increasing. (refer to columns 2,3and 4 in the above table)

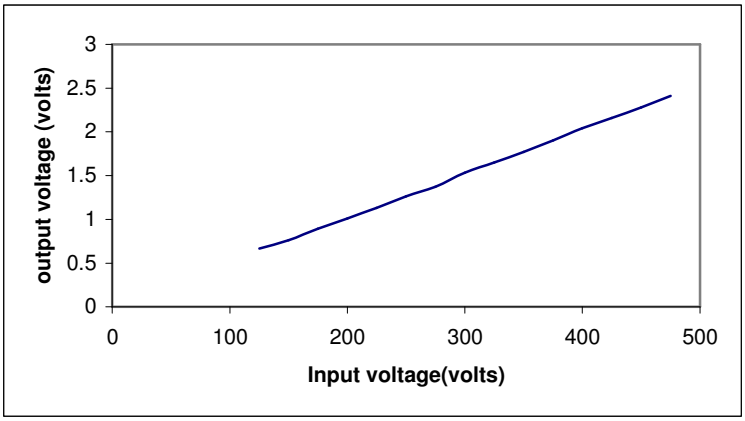

Figure 7.3: Variation of output voltage with respect to input voltage

7.4 Time history Records-DPSM technique Vs Experimental Results:

Experimental setup shown in **figure 7.1** is used for generating experimental results. Different fluids of different levels are tested in the tank using pulse echo method and through transmission methods which are described in chapter 1.Depending upon the method DPR 300 activates respective transducer as shown in table below.

Pulse Echo	Sender and receiver(S/R) transducer is same, signal is send from T/R port of DPR300.
Through transmission	Signal sender is (S) from T/R port and signal receiver (R) is connected to THROUGH port of DPR300

Figure 7.4 and **Figure 7.5** shows the waveforms of reflected pulses which are coming when the wave hits the bottom surface of the glass beaker and touch the transducer face back traveling two times same path as it is a pulse echo method . The tabular form shows how well the experimental times are matching with DPSM time values and also the peak magnitude.

Figure 7.6 shows time domain signal of reflected pulses which are coming both from interface of kerosene oil and water and also from bottom of the glass beaker. In this also the times are matching with DPSM results.

Figure 7.7 shows the reflected pulses which are coming from the stress free boundary by placing the transducer at the bottom of the tank here also pulse echo method is used and the results are well matched with DPSM.

Figure 7.8 shows the incident pulse which is received by the transducer placed at the other end as it is through transmission technique. It takes less time as the target point is near to the interface. Here also experimental results are showing well match with DPSM results.

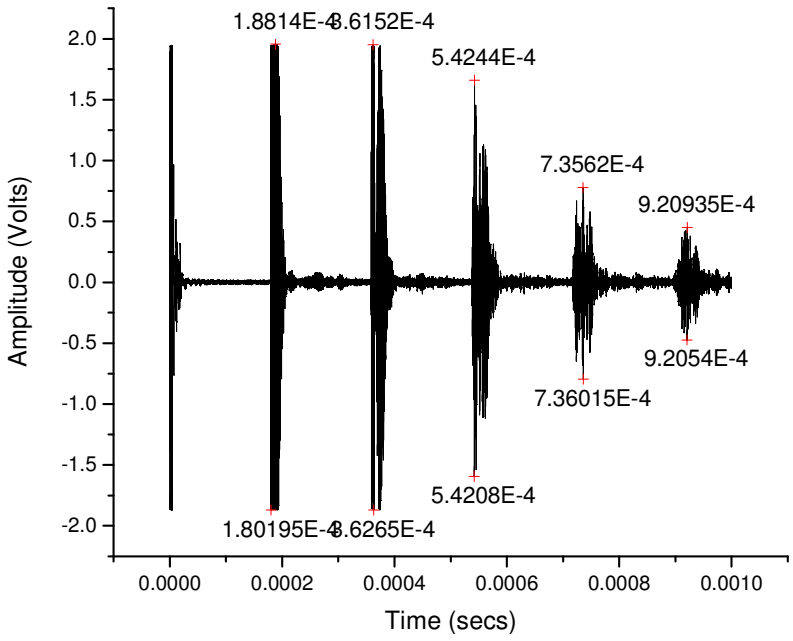

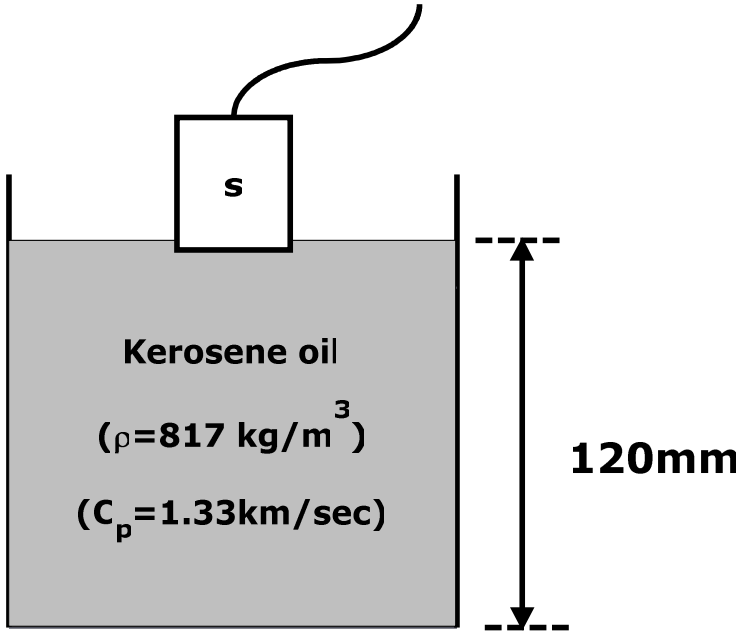

Time(μs)	Ampl(v)	Remarks	DPSM/theoritical(μs)
180	-1.8689	1st from bottom of beaker (120x2)mm	180
363	-1.8689	2nd from bottom of beaker (120x4)mm	361
542	-1.59424	3rd from bottom of beaker (120x6) mm	541

Figure 7.4*:* Variation of Output voltage Vs Time along with peak amplitudes using pulse echo method in kerosene oil. (Homogenous fluid)

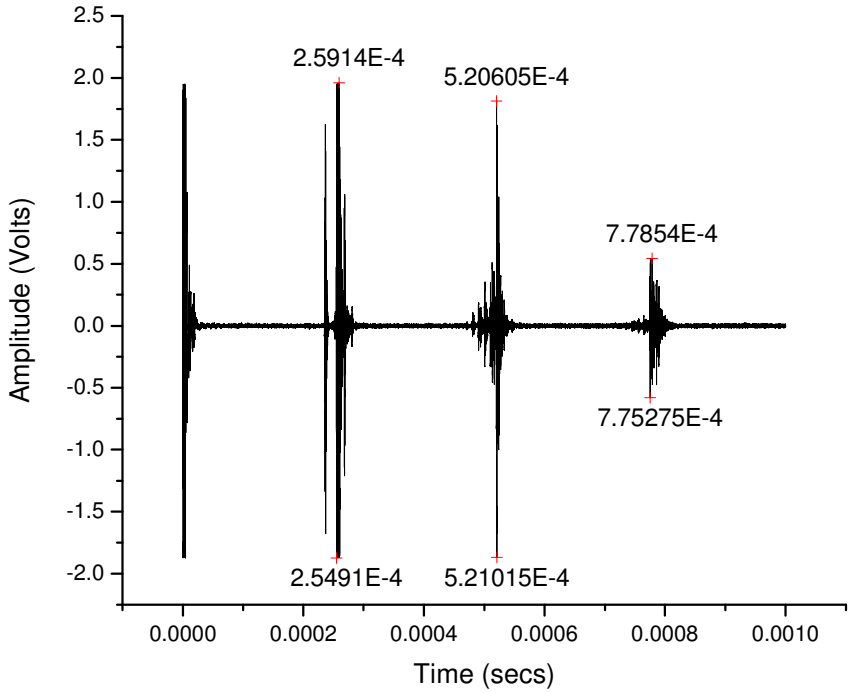

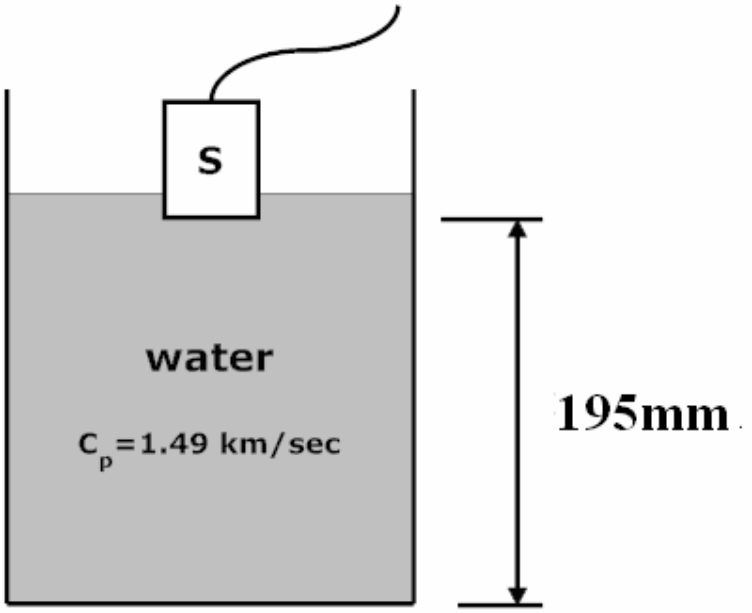

Time(μs)	Ampl(v)	Remarks	DPSM (μs)
260	2.0	1st From bottom of beaker(195x2)mm	261
520	1.8	2nd from bottom of beaker (195x4)mm	523
778	0.5	3rd from bottom of beaker (195x6)mm	785

Figure7.5: Variation of Output voltage Vs Time along with peak amplitudes using pulse echo method in water (homogenous fluid)

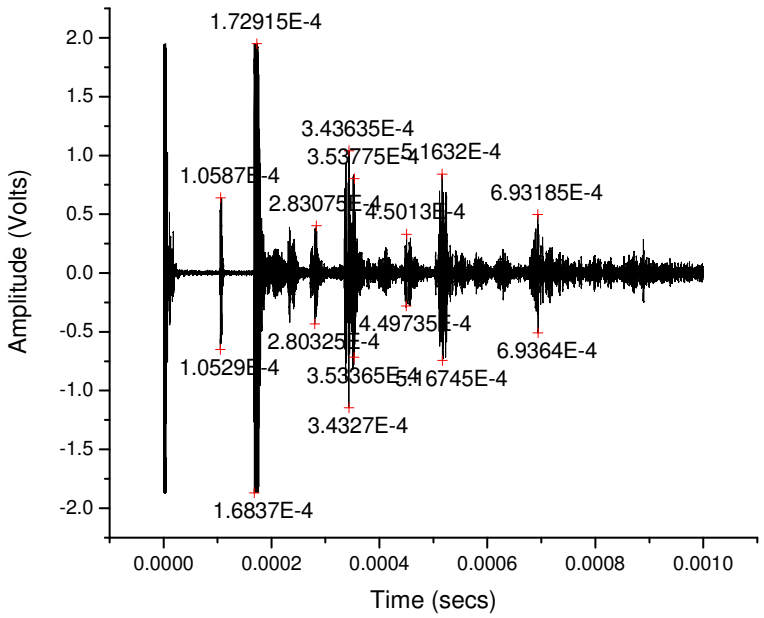

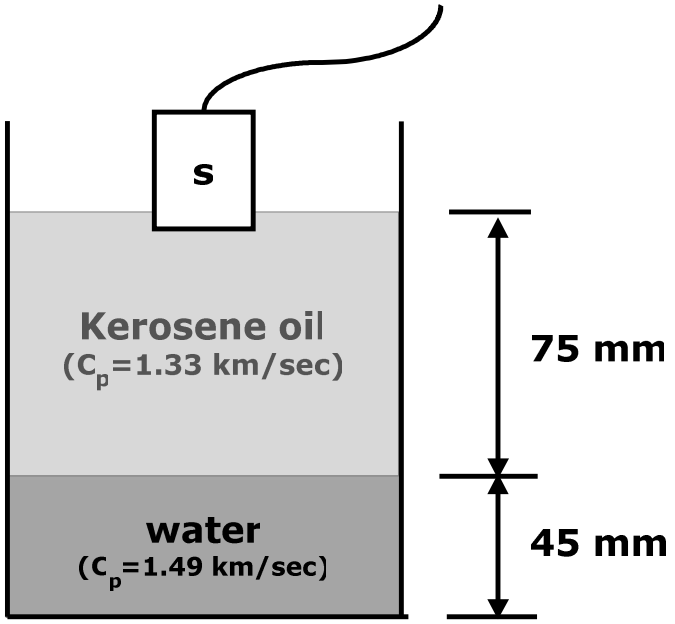

Time(μs)	Ampl(v)	Remarks	DPSM(μs)
105.87	0.64087	From interface (75x2 mm of kerosene)	112
172.92	1.94946	From bottom of beaker (75x2)mm kerosene+ (45x2)mm water	173
283.08	0.40283	2nd from interface (75x4)mm kerosene+ (45x2)mm water	285
343.64	1.04126	2nd from bottom of beaker (75x4)mm kerosene+ (45x4) water	346

Figure7.6: Variation of Output voltage Vs Time along with peak amplitudes using pulse echo method in kerosene and water (non-homogenous case).

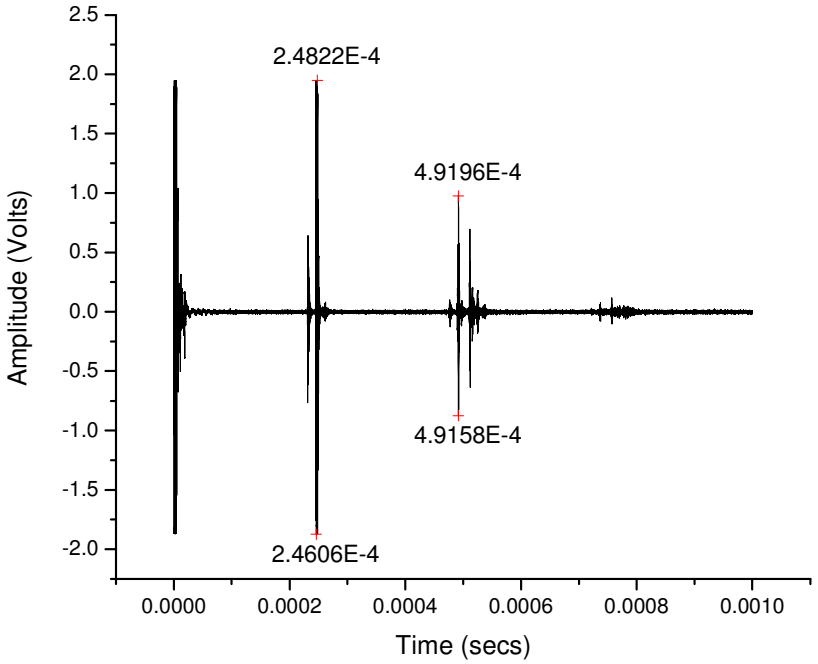

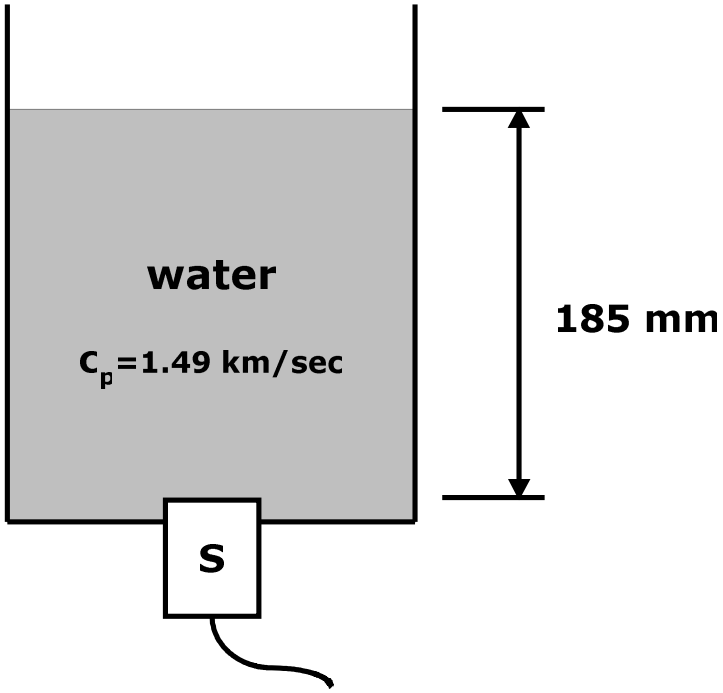

Time(μs)	Ampl(v)	Remarks	DPSM(μs)
248	1.98	From top(185x2 mm of water)	248
491	0.95	Second from top (185x4 mm of water)	496
780	0.1	Third from top (185x6 mm of water)	745

Figure7.7: Variation of Output voltage Vs Time along with peak amplitudes using pulse echo method in water but transducer at bottom.

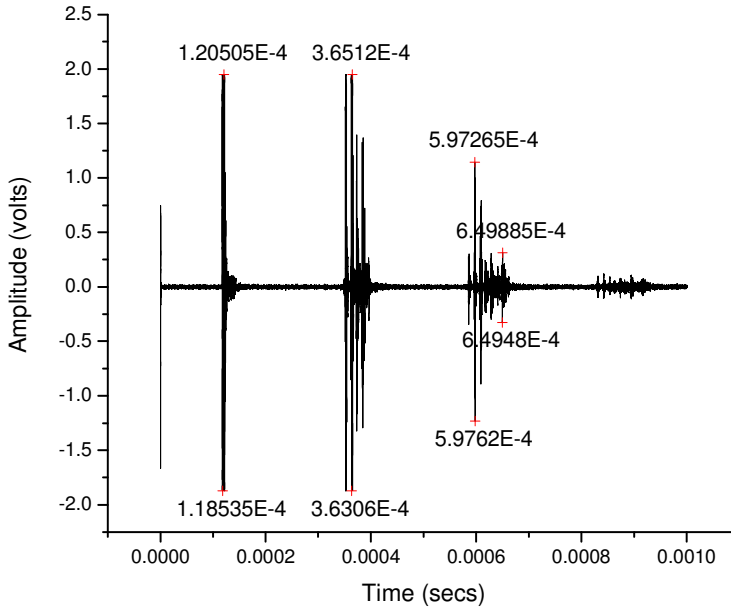

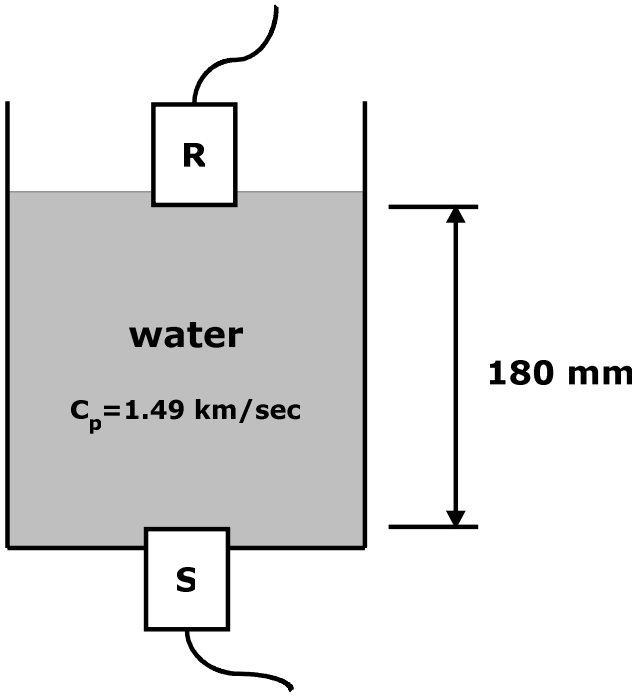

Time(μs)	Ampl(v)	Remarks	DPSM(μs)
120	1.98	Water column 180 mm	120
365	1.95	Water coumn (180 +180x2)	362
650	0.78	Water coumn (180 +180x2 +180x2)	604

Figure7.8: Variation of Output voltage Vs Time along with peak amplitudes using through transmission method in water.

CONCLUSIONS

- In this thesis work DPSM technique has been used to model ultrasonic fields generated by transient wave propagation in homogenous fluid and non homogenous fluid media having single interface.
- It is observed that in the DPSM model as the number of point sources increases the accuracy of the method increases.
- The numerical results show the potential of this semi-analytical method in analyzing wave propagation problems.
- In the acoustic pressure tomo-grams plots presented in this report the transmission, reflection, and different interactions of the ultrasonic beams in various fluids can be visually observed at different time instances.
- The DPSM results are found to be matching with the experimental work and it has been found that experimentally time taken by the wave to hit the interface is matching with the calculated time by DPSM technique.
- This experimental setup can be used on different fluids and interfaces and results can be compared with numerical results by simply changing the properties of fluid in the DPSM model developed.
- The advantage of DPSM method over traditional wave propagation method is that modeling of transducer (source) and discontinuity (interface) is sufficient to know the whole behaviors of wave propagation in fluids.

Scope for Future Work:

- The above developed model can be extended to inclined interface and solid fluid interaction problem. From time taken reflected wave one can determine the location of interface from transducer and the impendence ratio of far end fluid.
- Using multiple transducer and observation points it is also possible to determine the shape of simple interface.
- The developed model can be extended to model the bubble interface also.

REFERENCES

1. Ahmad, R., Kundu, T., Placko, D(2005) "*Modeling of Phased Array Transducers".* Journal of the Acoustical Society of America, Vol. 117, pp. 1762-1776

2. Ahmad, R., Kundu, T., Placko, D(2003) *"Modeling of the Ultrasonic Field of Two Transducers Immersed in a Homogeneous Fluid Using Distributed Point Source Method".* I2M (Instrumentation, Measurement and Metrology) Journal; Vol.3, pp.87-116

3. Abrahams, I. D., Wickham, G. R., (1992), Scattering of elastic waves by a small inclined surface-breaking crack, *Journal of Mech. Phys. Solids*, 40(8), 1707-1733.

4. Banerjee, S., Kundu, T., Placko, D(2005) "*Ultrasonic Field Modelling in Multilayered Fluid Structures Using DPSM Technique",* ASME Journal of Applied Mechanics

5. Banerjee, S., Kundu, T.(2007) "*Ultrasonic field modeling in plates immersed in fluid*", International Journal of solids and Structures,44,6013-6029

6. Banerjee, S., Kundu, T.,Alnuaimi.N,(2007) *"DPSM technique for ultrasonic field modeling near fluid-solid interface",* Journal of ultrasonics ,46,235-250.

7. Banerjee, S., Kundu, T.(2007) "Semi-analytical modeling of ultrasonic fields in solids with internal anomalies immersed in a fluid" ,Journal of Wave Motion.

8. Biwa, S., Yamamoto, S., Kobayashi, F., Ohno, N., (2004), Computational multiple scattering analysis for shear wave propagation in unidirectional composites, *International Journal of Solids and Structures*, 41, 435–457

9. Bruck, H. A(2000) *"A one-dimensional model for designing functionally graded materials to manage stress waves"*, International Journal of solids and Structures, 37, 6383-6395

10. Das,S., Banerjee, S., Kundu, T.(2008) "*Elastic wave scattering in a solid Half –space with a circular cylindrical hole using Distributed point source method*", International Journal of solids and Structures.

11. Das,S., Banerjee, S., Kundu, T.(2007) "*DPSM modeling for studying interaction between bounded ultrasonic beams and corrugated plates with Experimental verification*", IEEE journal,54,No.9,1860-1872

12. Doyle, J. F(1989), *Wave propagation in structures*, Springer, New York

13. Gandhe, D., Mukherjee, A(2006) "*Detection of surface crack by stress wave propagation"* (M.Tech Thesis, IIT Mumbai)

14. Joshi, S., Mukherjee, A., and Schmaudar S (2003) *"Numerical characterization of functionally graded active materials under electrical and thermal fields"*, Smart Materials and Structures, 12, 571-579

15. Kundu, T.,Ed (2003) "*Ultrasonic Nondestructive Evaluation: Engineering and Biological Material Characterization"* (CRC Press, Boca Raton, Florida)

16. Krawczuk, M., Palacz, M., Ostachowicz, W., (2004), Wave propagation in plate structures for crack detection, *Finite Elements in Analysis and Design*, 40, 991–1004

17. Mukherjee ,A.,and Schmauder,.S , Sunilkumar O. Soni (2005)"Stress Waves in Functionally Graded Materials" M.Tech dissertation at IIT Bombay.

18. Mal, A. K., Singh, S. J(1991) "*Deformation of Elastic Solids"* (Prentice Hall: Englewood Cliffs, New Jersey)

19. Samadhiya, R. and Mukherjee,A (2006*)"Functionally graded piezoceramic ultrasonic transducers",* Smart Materials and Structures

20. Schmerr, L. W (1998) "*Fundamental of Ultrasonic Nondestructive Evaluation-A Modeling Approach"* (Plenum Press, New York)

21. Wang, B.L., Mai, Y. W., and Zhang X. H(2004) " *Thermal shock resistance of functionally graded materials"*, *Acta Materialia*, 52, 17, Pages 4961-4972.